DESIGN OPTIMIZATION AND PERFORMANCE SIMULATION OF PERMANENT MAGNET SYNCHRONOUS MOTOR

THESIS

Submitted to the

G.B.PANT UNIVERSITY OF AGRICULTURE & TECHNOLOGY,
PANTNAGAR-263145, UTTARAKHAND, INDIA

By

Deepayan Gope
B.Tech. (Electrical Engineering)

IN PARTIAL FULFILMENT OF THE REQUIREMENTS
FOR THE DEGREE OF

Master of Technology
In
Electrical Engineering
(Electrical Energy Systems)

July, 2018

ACKNOWLEDGEMENT

First of all I bow my head before 'God' who inspired me to face challenges of uneven times. All my sincere gratitude goes to him for the help he has given to me and his unfailing mercies over my life.

The author expresses his deep sense of reverence and heartfelt gratitude to Dr. S K. Goel, Professor, Department of Electrical Engineering, Chairman of Advisory Committee for his invaluable guidance, constant encouragement, abundant counsel and his critical and constructive suggestions throughout the investigation and in the preparation of manuscript. The author is extremely indebted to him and wishes to thank him from the bottom of the heart.

With profound sense of gratitude the author expresses his warmest thanks to the members of the Advisory Committee, Dr. Ajay Srivastava, Professor, Department of Electrical Engineering, Dr Abhishek Yadav, Associate Professor, Department of Electrical Engineering for their inspiring and constructive suggestions at every stage of this study. Author also sincerely thanks Dr. Sudha Arora, Professor & Head of Electrical Engineering Department for her constant encouragement, support and guidance.

The author tenders his sincere thanks to Dr. J. P. Pandey, Dean, College of Post Graduate Studies and Dr. H.C. Sharma, Dean, College of Technology for their keen interest in providing the necessary facilities.

The continuous and tireless effort of Dr. H. S Rawat, Assistant Professor, Electrical Engineering Department without which the accomplishment of the work would not have been possible. The author is grateful to Dr. Rawat for his support and guidance.

This thesis is the outcome of the kind co-operation, help and support in the form of both technical and moral extended by the faculty members of Electrical Engineering Department.

The author owes a very special word of thanks to his parents Mrs. Sanjukta Gope and Dr P. C Gope for their boundless, generosity, everlasting inspiration, blessing abundant love and affection throughout. Appreciations are also extended to my brother Mr Aditya Gope for his encouragement and helping hands at various stage of the work.

This list is obviously incomplete but allow me to submit that the omissions are inadvertent and I once again record my heartfelt gratitude to all those who helped me directly or indirectly in this endeavour.

Deepayan Gope

(Deepayan Gope)
Author

Pantnagar
July 2018

CERTIFICATE

This is to certify that the thesis entitled **"DESIGN OPTIMIZATION AND PERFORMANCE SIMULATION OF PERMANENT MAGNET SYNCHRONOUS MOTOR"** submitted in partial fulfilment of the requirements for the degree of **Master of Technology** in **Electrical Engineering** with major in **Electrical Energy Systems** of the College of Post-Graduate Studies, G. B. Pant University of Agriculture and Technology, Pantnagar, is a record of *bona fide* research carried out by **Mr. Deepayan Gope,** Id. No. **50889** under my supervision and no part of the thesis has been submitted for any other degree or diploma.

The assistance and help received during the course of this investigation and source of literature have been duly acknowledged.

Pantnagar
July, 2018

(S. K. Goel)
Chairman
Advisory Committee

CERTIFICATE

We, the undersigned, members of the Advisory Committee of Mr. **Deepayan Gope,** Id. No. **50889**, a candidate for the degree of **Master of Technology** in **Electrical** Engineering with major in **Electrical Energy Systems**, agree that the thesis entitled **"DESIGN OPTIMIZATION AND PERFORMANCE SIMULATION OF PERMANENT MAGNET SYNCHRONOUS MOTOR"** may be submitted in partial fulfilment of the requirements for the degree.

(S. K. Goel)
Chairman
Advisory Committee

(Ajay Srivastava)
Member

(Abhishek Yadav)
Member

CONTENTS

LIST OF TABLES

LIST OF FIGURES

LIST OF SYMBOLS

Symbols	Description
a	Independent group of samples or treatment
b	Number of measurements in each group or replication
t	magnet thickness
n	Number of observations magnet width (w),
w	Magnet width
S/N	Signal to Noise ratio
Y	Observation vector
E	Error vector
X	Matrix of the design variables at selected points
D1	Diameter for magnet duct
O1	Magnet duct dimension
Rib	Width of the rib at the center of the two adjacent poles to support the bridge
X^T	Transpose of X
y_i	The ith experimental data
$\lvert X^T X \rvert$ Determinant x_{jk}	Measurement in j^{th} row and k^{th} column
$\bar{x}_j$	The mean of measurement in the j^{th} row
$\bar{x}$	Grand mean or overall mean
v	The total variation or sum of the squares of the deviations of each measurement from the grand mean $\bar{x}$
v_w	The variations within factors denoted
v_b	The variation between factors
pf	Power factor

T_{st}	Starting torque
Cu loss	Copper loss
u	Upper limit of x
l	Lower limits of x
THD	Total Harmonic Distortion
V_1	Fundamental component of the waveform
V_2, V_3, V_4, and V_n	Second, third, fourth, and n^{th} order harmonics.
P_{out}	Output power of the DC generator
V_L	Voltage across the lamp loads,
I_L	Current flowing through the load.
P_{arm_Cu}	Armature copper loss
P_{field_Cu}	Field copper loss
$Rot\ loss$	Rotational loss
I_a, I_f	Armature current and field current of the DC motor
E_b	emf generated by the DC motor
V	Applied voltage across the armature of the DC motor
R_a	Armature resistance of the DC motor
R_f	Field resistance of the DC motor

Chapter 1 INTRODUCTION

1.1 Introduction

Electricity is an important parameter for a nation's development. India is the third largest producer as well as third largest consumer of electricity in the world. Agricultural sector is recorded as the highest electrical energy consumption sector (17.89%) in 2015-16 among various other nations. About three fourths of electricity was produced by fossil fuels (mostly coal) in 2017-18. The consumption of electrical energy is increasing at a very fast rate. Efficiency improvements in electrical machines can help in restricting the energy consumption to a large extent. In electrical machines, the efficiency can be improved greatly by development of new materials and the techniques involved in construction of the machines.

An **electrical machine** is a device which converts mechanical energy into electrical energy or vice versa. Electrical machines also include transformers, which do not actually provide conversion between mechanical and electrical form but they convert AC power from one voltage level to another voltage level.

Electric motor converts electrical energy to mechanical energy whereas an electric generator converts mechanical energy to electrical energy. The basic principle of operation used in most of the electric motors is the interaction of a magnetic field created inside the motor and the current flowing in the windings of the motor to produce a force. The interaction of the magnetic fields in the rotor and stator of the electric motor results into a force and thus a torque which rotates the motor shaft. One or both of these magnetic fields must be varying with the motor rotation which is done by either switching the poles sequentially, or the strength of the pole can be varied otherwise.

Electrical machines are broadly classified into two different types of machines:

1. DC Machines
2. AC Machines

D.C. machines are the electro mechanical energy converters which converts DC electrical energy to mechanical energy or mechanical power into a DC electrical energy.

DC machines are a very good option in applications which require a wide range of speeds as the speed control in DC machines is easier as compared to that of AC machines. DC series motor is best suited for applications requiring high starting torque. No reactive power is consumed in case of DC machine and it offers a harmonic free operation also.

Despite so many advantages of DC machines, AC machines have become more popular and are preferred over DC machines. The main reason is the easy generation and transmission of AC power with fewer losses during transmission of power over long distances. The voltage generated by AC machines can be easily stepped up and down to a desired level while transmission and distribution. Moreover, commutation is a serious problem in case of DC machines for which AC machines are more preferred. In industries also AC motors are more preferred over DC motors. AC motors don't need brushes and, hence, lesser maintenance is required.

Industries require different kind of variable torque and speed drives in various applications such as in overhead cranes, conveyer belts, arm of robots, etc. for which DC and AC motor drives are used. However, 70% of the motors used in industries are induction motors. The main reason is the ruggedness and less maintenance requirement of the motor.

Induction motors and synchronous motors are the two main types of AC motor presently used. Inductions motors are further classified into single phase induction motors and three phase induction motors. However in case of Induction motors, a high magnetizing current is required to produce flux, which leads to the copper losses in the motor and, therefore, decreases the efficiency of the motor. Synchronous motors require DC excitation for the rotor windings which is supplied from external sources with the help of collector rings and brushes. This leads to copper losses in the rotor windings of the synchronous motor and increased maintenance of the motor due to brushes. To tackle these problems of existing AC motors, several special machines are designed. One such machine is Permanent Magnet Synchronous Motor (PMSM).

The Permanent Magnet Synchronous Motor (PMSM) is an AC synchronous motor whose field excitation is provided by permanent magnets and has a sinusoidal Back EMF waveform. Permanent magnet synchronous motor has a stator structure similar to that of an induction motor so that a sinusoidal flux density in the

air gap is produced whereas it has permanent magnets in the rotor. In permanent magnet synchronous motor, rotor does not have any field windings which results in a higher power density as compared to induction motors with the same rating, since no stator power is required for magnetic field production in PMSM. PMSM are becoming popular since last three decades due to many advantages over other electrical machines. They have a compact size, high power density, high torque to inertia ratio, better thermal behavior, lower sensitivity to frequency fluctuations and high efficiency which makes them suitable for industrial, domestic as well as transportation applications.

A permanent magnet synchronous motor for starting and operation can be directly connected to power supply which is known as a Line-start permanent magnet synchronous motor (LSPMSM). In applications requiring constant speed and long operation period such as in fans, pumps and compressors, a LSPMSM performs better than an induction motor. Aliabad *et al* (2010) concluded that significant improvement in starting torque, synchronization and steady state performance in Line-Start Permanent-Magnet Motors had been seen.

Permanent magnet machines can be of axial-flux or radial-flux type. Axial flux permanent magnet motors have good efficiency, adjustable air gap, higher torque to weight ratio, better heat removal and balanced rotor stator attractive forces as compared to Radial flux permanent magnet motor. Axial flux permanent magnet motors are mainly preferred in military and transport applications due to machine shape and size.

Several factors influence the performance of an electrical machine and these factors need to be optimized before manufacturing it. In PMSM, permanent magnets (PM) used in rotor to aid in air gap flux density is one such factor. Another main parameter in the design process is the air gap flux density which is influenced by the dimensions of rotor PMs. The machine performance in transient as well as steady state is influenced by the magnets' volume and flux producing areas and, hence, magnet volume needs to be determined. The magnets' volume corresponds to maximum energy production (BH_{max}) of the PMs which intern affects the braking torque and the steady state inductances of PMSM (Kalluf *et al.* 2010, Li *et al.* 2010, Pyrhnen 2010). After determining the magnet volume, magnet specific dimensions are

established. Moreover, the placement of the PM in the rotor influences the air gap flux density in PMSM (Zhao *et al.* 2006, Hung *et al.* 2008, Singh *et al.* 2006).

Magnet is one of the important elements in PMSM and the performance of motor depends on the properties of the magnet used in the rotor. In the earliest days, hardened steel were used as magnet material but as such material can hold very low energy, their use was limited. In recent years many other magnet materials such as Aluminum Nickel and Cobalt alloys (ALNICO), Strontium Ferrite or Barium Ferrite (Ferrite), Samarium Cobalt (SmCo) (First generation rare earth magnet) and Neodymium Iron-Boron (NdFeB) (Second generation rare earth magnet) are used as the permanent magnets in PMSM due to higher flux density levels. From the literature it can be concluded that the selection of magnet material in PMSM design is very important. In most of the studies Ferrite magnet material, SmCo and NdFeB are used as permanent magnet materials in PMSM.

The review work on the advancement of the PMSM systems can be seen in the work of Sebastian *et al.* (1986). Araujo *et al.* in 1997 highlighted the different simulation tools used for visual design and simulation of PMSM machine. Ong (1998), Macbahi *et al.* (2000) explained the need and benefits of powerful computation tools to solve complex models of motor drives and use of MATLAB/SIMULINK software in the analysis of electrical machine models. Many authors have used MATLAB/SIMULINK for design and analysis of PMSM. Finite element method (FEM) is another tool that is used effectively in motor design and performance analysis. The method is more suitable because the performance and the fault can be observed without destroying the machine. Optimum solution can be achieved without laboratory experiment just by changing different machine parameters. These simulation results are more realistic and can be used for machine production.

A considerable amount of work on the electrical motor design optimization has been carried out using Taguchi method in recent years. However, Taguchi method of optimization in the field of motor design optimization of permanent magnet synchronous motor (PMSM) is very limited and unknown. Dr Genichi Taguchi has developed the Taguchi method in 1940s. This method is different than the traditional design of experiment in different ways such as planning of experiments, quality

defining, and signal to noise analysis etc.. Due to various advantages over the traditional design of experiment, Taguchi method is popularly used by researchers in the various fields of engineering, medicines, environmental science, etc.. Use of Taguchi method for the design of Permanent Magnet Synchronous Machine (PMSM) and line start PMSM are also found in the references. The response surface methodology (RSM) is another optimization tool which uses the relationships between several explanatory variables and one or more response variables. The method of RSM was introduced by George E. P. Box and K. B. Wilson in 1951 and used a sequence of designed experiments to obtain an optimal response. Thus, RSM can be used to optimize rotor dimensions to maximize PMSM performance parameters such as efficiency and power factor. Duan and Ionel (2011, 2013) have presented a review on the recent developments in electrical machine design optimization methods of permanent magnet synchronous motor. The paper describes the significant developments in the field of electrical machine design optimization which includes the modeling of electrical machines, direct and stochastic search algorithms for both single- and multi- objective design optimization problems. Response surface optimization of Interior Permanent Magnet (IPM) Synchronous Motor is studied by Jolly, (2005) and Hong (2008) where design of experiment is used and a second order polynomial function is used to create the response surface. 15 design experiments were used.

The most of the research work carried out on the PMSM motor design optimization focused on the single objective functions considering either efficiency or power factor where as in many applications simultaneous optimum performance of several parameters are required. The performance characterization of PMSM is an utmost important task. Due to several constraints in manufacturing of PMSM for specified output requirement, time consuming experimentation and optimum design parameter estimation has drawn the attention of the researchers towards the simulation work of PMSM. The performance simulation using various techniques is used for design of PMSM of any required capacity. The simulation using MATLAB or Finite Element Analysis using ANSYS are frequently used by researchers for the numerical analysis of permanent magnet synchronous machine or in any kind of electric machines. This is the area where maximum attention is required for the successful design and wider application of PMSM in various field of engineering.

Also there is a need of experimental investigations to validate the simulated results obtained using various simulation/mathematical tools.

1.2 Objectives of the work

The main objectives of the proposed work are,

1. To design Line Start Permanent Magnet Synchronous Motor using RMxprt in ANSYS Maxwell software
2. Optimization of magnet size and position in the rotor using optimization tools
3. Performance evaluation of optimized Line Start Permanent Magnet Synchronous Motor
4. Design of drive system of Permanent Magnet Synchronous Motor using ANSYS Simplorer
5. Validation and comparison using experimental data

1.3 Organisation of the Thesis

The thesis consists of five chapters including this introductory chapter. In chapter 1, the evolution of PMSM, its need, and objectives of the work are outlined. The relevant review of literature is dealt in Chapter 2. In Chapter 3, design of PMSM using ANSYS Maxwell software is discussed and optimization methods such as Taguchi method and Response Surface Method for optimal design of PMSM are also discussed. Design of drive system for PMSM using ANSYS Simplorer software is also presented in this chapter. In Chapter 4, the results obtained after co-simulating the optimally designed PMSM in ANSYS Maxwell software and ANSYS Simplorer software are discussed. The experimental investigation and analysis of PMSM are also presented in this chapter of the thesis. A comparison of the results obtained after simulation with those obtained experimentally is also shown in Chapter 4. Chapter 5 summarizes and concludes the work done in the thesis. The scope of further work is also discussed in Chapter 5.

Chapter 2 REVIEW OF LITERATURE

2.1 Introduction

This chapter presents the brief review on the works carried out by various researchers for the performance analysis of PMSM. The various methods of optimization used by researchers for optimal design of PMSM are also reviewed. A brief review on the magnet shape and dimensions is also included in this chapter.

2.2 Review of Literature

In PMSM there are no field windings which results in no field copper losses in the machine. Instead, permanent magnets are used in place of field windings. **Aydin (2004)** discussed the importance of selection of permanent magnet material for good performance of the machine. Earlier, hardened steel was used as the permanent magnet material in PMSM due to its ease in magnetizing. However, the flux density is far too low as compared to the new magnetic materials used nowadays. Moreover, it easily demagnetizes and its flux density degrades with aging. Nowadays, Samarium Cobalt (First Generation Rare Earth magnet), Aluminum Nickel and Cobalt alloys (ALNICO), Strontium Ferrite or Barium Ferrite and Neodymium Iron Boron (Second Generation Rare Earth magnets) are used as permanent magnets in PMSM. Although Samarium Cobalt (SmCo) magnets have higher flux density as compared to Neodymium Iron Boron (NdFeB) magnets but they are expensive also which makes Neodymium Iron Boron magnets more popular and suitable magnetic material in PMSM.

Ilya Petrov and Juha Pyrhonen (2013) have discussed the cost effectiveness, easy availability and almost negligible eddy current losses are prime factors for many PMSM manufacturers to prefer ferrites in low frequency applications as the case in motor drives. However Ferrites have much lower energy product (BH_{max}) than modern magnets used.

Sigrid Jacobs *et al.* (2009) have studied on the Magnetic material optimization for hybrid vehicle PMSM drives. They have studied the effectiveness of different grades of steel materials based on the efficiency of the machine using finite

element (FE) simulations. N020, M235-35A, M250-50A, M330-50A, M330P-50A, M600-50A, M310-65A and M800-100A materials are used in simulation out of which N020 and M235-35A are recommended as the optimum grades for highest efficiency.

Peter Seker´ak *et al.* (2012) have designed PMSM with ferrites because of its popularity due to their low cost and cost increasing of NdFeB. Due to increase in ferrite properties in the last decade, this material is mostly used in high power applications by many manufacturers of PMSM.

Lee *et al.* (2009) have investigated two permanent magnet synchronous motors of interior magnet type with ferrite magnets and NdFeB magnets. In both the cases the permanent magnets have been totally embedded in the rotors. The results of the work conducted by Lee e*t al.* reveals that the rated efficiency of the ferrite motor has been about 1% lower than the efficiency in the motor with NdFeB magnets and the volume of ferrites was about five times higher than the volume of NdFeB magnet.

Richter E. and Neumann T. (1984) have investigated with SmCo magnets and ferrites. It is reported that the efficiency of the Ferrite motor is about 0.5 % lower at the same output power than SmCo. The weight of Ferrite is also found to be about 2.5 times than the weight of SmCo. In a similar study by **Chaudhari and Fernandez (1999)** with ferrites and damper winding with new rotor design shows 4% improvement in efficiency as compared to constant ferrite PM volume.

Peter Sergeant and Alex Van den Bossche (2013) have investigated the effect of the mass of the magnet for several soft magnetic material, rare earth (NdFeB) magnets and ferrite magnets on the efficiency of PMSM with concentrated windings. In their investigation the power, volume and mechanical air gap thickness were kept constant. The study reveals that the amount of permanent magnet material can vary in a wide range with a minor influence on the efficiency, torque density, and torque ripple and with a limited demagnetization risk. Similar effects of reducing the amount of magnets can be found in the work of **Sergeant and Bossche (2012)**.

The effect of two magnet materials SmCo and ferrite magnets on optimal design of a high speed synchronous machine for different rotor speeds was investigated by **Martin *et al.* (2015)**. In order to decrease the iron losses, the magnetic flux density tends to be lowered in case of high speed electrical machines. Thus, in

the optimal design of surface mounted permanent magnet synchronous machines, ferrite magnets should lead to similar performances as rare earth magnets. It was concluded that although SmCo offers higher specific power, but both magnets show some similar performances. The magnetic air gap in case of ferrite magnet synchronous machine is smaller which results in a thinner flux weakening range as compared to that of rare earth magnet synchronous machines. This makes rare earth magnet synchronous machines more suitable for variable speed applications. However, if the application demands a constant speed operation then ferrite magnet synchronous machine is a better choice due to its cost effectiveness. The machine performance is also affected by the magnet temperature limit especially when the machine is operated at high speed. Hence, a good cooling system for bearings and air gap is must in order to counter the effect of air friction and bearing losses in situation of high temperature during the operation of the machine.

Dinh (2017) used NdFeB35 as magnet material to design a Line Start Permanent Magnet Synchronous Motor by Genetic Algorithm due to its good thermal stability and remanent flux density (~1.3T) which allows it to use the machine even at a temperature of about 180 ^{0}C.

From the above literature it can be concluded that the selection of magnet material in PMSM design is very important. In most of the studies Ferrite magnet material, SmCo and NdFeB are used as permanent magnet materials in PMSM. SmCo and NdFeB are costlier as compared to Ferrite magnet material as they are rare earth magnets. Moreover, SmCo has higher flux density than NdFeB magnets but expensive which makes NdFeB the most appropriate magnet material in PMSM design. Although, Ferrite magnet synchronous machine have negligible eddy current losses but the air gap flux density remains low and the volume of magnet for the same power rating increases as compared to that of a rare earth magnet synchronous machine. For variable speed applications rare earth magnet materials are unavoidable as Ferrite magnet synchronous machine has thinner flux weakening range. However for constant speed application Ferrite magnet material can be used.

When designing the rotor of a permanent magnet synchronous motor (PMSM), one key part is to fix the size of the permanent magnets (PM) in the rotor to produce the required air-gap flux density. Several investigators have optimized the

size of magnet through different techniques. One of the main parameters for designing a PMSM is the air gap flux density. The air gap flux density is very much dependent on the rotor permanent magnet sizing dimensions.

Sorgdrager and Grobler (2013) studied the effect on the air-gap flux density of four radial flux PMSM rotor topologies. The study was performed using the static finite element model simulations. It was concluded that there is a direct relation between flux producing magnet area and magnet size. It was concluded that the flux producing magnet area can be calculated once the minimum magnet volume is determined. This methodology is suitable for designing of line-start PMSM rotors where the rotor area is limited.

Kim *et al.* (2012) have investigated that by modification in the shape of permanent magnets used in PMSM, high torque density can be achieved. Different models were compared by varying the width and thickness of the permanent magnet so as to increase the torque density. Torque characteristics based on amount of permanent magnets used and different shapes of magnet were analyzed. It was concluded that increasing the width of permanent magnets was much more effective than increasing the thickness and about 70% less permanent magnet material is required when the width is increased and thickness is reduced for a given load torque.

Todorov and Stoev (2015) discussed an analytical model for sizing the magnets of PMSM. A simple iterative procedure and analytical model using finite element analysis for determining magnet dimensions to satisfy the required characteristics of a PMSM was presented. The presented iterative procedure changes the magnet dimensions at each step and analysis of the model was performed to obtain an operating point to achieve the required motor characteristics. It is concluded that the parameters and characteristics of PMSM is highly influenced by the magnet size.

Chaudhari, Fernandes and Pillai (1998) studied the effect of magnet width, inclination angle and magnet material on the air gap flux density in a line start permanent magnet synchronous motor. Finite element modeling and analysis was carried out for the same. The air gap flux density for four combinations of magnet position where faces of four magnets were kept parallel to the shaft and four magnets inclined to the shaft had been studied. It was observed that the flux density remained within the saturating limits for all combinations. The design with bonded rare earth

magnet material shows insignificant improvement in average air gap flux density whereas PMSM with ferrite magnet higher flux density shows almost 30% higher flux density compared to conventional circumferentially magnetized rotor for same magnet volume.

Dinh (2017) investigated different parameters such as the magnet size, geometry parameters of rotors and stators and copper loss for minimization of cost and copper loss of a line start permanent magnet synchronous motor using Genetic Algorithm. The geometry parameters of stator and rotor obtained by an analytical model were validated by finite element simulation.

It is reported in the work of **Ilhan Tairimer (2011)** that the efficiency of PMSM is greatly influenced by the permanent magnet configuration. It was mentioned that the highest efficiency is obtained by using V-shape permanent magnet. It is also mentioned that manufacturing possibilities, cost of production are some of the other criterion to decide the permanent magnet position. Some of the permanent magnet configurations such as T shape, L shape, V shape and U shape are used by many researchers. By considering the manufacturing aspect, cost effectiveness and high flux density in air gap, four I-shape permanent magnet positions with width and thickness as 60 and 8 mm were used by **Dinh (2017)** in PMSM design.

Lee *et al.* (2005) proposed the effects of permanent magnet shape on the performance of motor especially in obtaining a sinusoidal induced EMF. The configuration of permanent magnet is very critical in designing a PMSM. A sinusoidal current is necessary for minimizing the torque ripples which requires analysis of different magnet configurations and optimizing it. Finite element method was used to design various models for comparison of emf waveform, torque characteristics and harmonics between conventional and designed models. The different models designed were lateral magnet, V-shape magnet, modified V-shape magnet and C-shape magnet. The C-shape magnet configuration showed an increment of 21.6% in the peak induced emf value as compared to lateral magnet configuration and thus reduction in torque ripple and improvement of output power density.

Cogging torque is one of the main causes of torque ripples and pulsation. In the work of **Chabchoub *et al.* (2012)** different rotor magnet shapes were designed using Finite Element method and the simulated results were used in order to minimize

the cogging torque. Different controlling parameters such as angle of the magnets and angle between the magnets were kept as 89.12° and 0.44° respectively in the first three cases whereas in the fourth case these values were kept as 89.82° and 0.09° respectively. The thickness of the magnet was kept constant at 5 mm.

Chikouche *et al.* (2015) also studied different magnet shapes using Finite Element method to minimize the cogging torque and established an analytical solution of magnetic field distribution as a function of magnet shape, irregular thickness of air gap and semi closed stator slots.

Zheng *et al.* (2007) used magnetic pole embrace, magnetic bridge and magnetic pole eccentricity as the aspects for optimizing the rotor and achieving better air gap magnetic field distribution and torque curves using Finite Element Method. Air gap magnetic field amplitude and distribution in the air gap are greatly affected by the magnetic pole embrace which in turn affects the average torque and torque ripple. Magnetic pole embrace of 0.82 gives the lowest torque ripples but the magnetic-pole embrace of 0.85 is considered to be optimum as the average-torque increases by 1.44% and the torque-ripple decreases of 4.07% as compared to the magnetic-pole embrace of 0.82. The magnetic bridge allows a path for the leakage flux and hence, its shape and size are crucial in designing for better torque and speed characteristics. The study showed that width of magnetic bridge is more important as compared to length and lesser the width, better the performance of machine. Magnetic pole eccentricity was also optimized and a value of 0.5 mm gave the best results with an air gap magnetic field very close to sinusoidal wave and reduction in cogging torque also.

There are several issues in the design stage of permanent magnet synchronous motor. These are high efficiency, low noise, low cost, high starting torque, low power losses, high torque output, etc.. It is very difficult to meet all the challenges at a time. Different design parameters behave differently for each selected objective. Thus, if the number of objectives increases, the design optimization becomes more complicated. The design optimization of PMSM is a multi-variable, non-linear and constrained optimization procedure. Some of the methods frequently used by many researchers for optimization of different performance parameters and optimum design of PMSM are Taguchi method, surface response methodology, Genetic Algorithm, particle swarm optimization etc.. The response surface methodology (RSM) approach

uses the relationships between several explanatory variables and one or more response variables. RSM is used to maximize the PMSM performance parameters such as efficiency and power factor by optimizing the rotor dimensions by many investigators. A considerable amount of work on the electrical motor design optimization has been carried out using Taguchi method in recent years. However, Taguchi method of optimization in the field of motor design optimization of permanent magnet synchronous motor (PMSM) is very limited and unknown. Taguchi method has various advantages over the traditional design of experiment such as planning of experiments, quality defining and signal to noise analysis etc..

Uğur Demir and Mustafa Caner Aküner (2017) used Taguchi method and conventional method to optimize the critical rotor pole data of line-start permanent magnet synchronous motor with an objective function of maximization of efficiency and power factor based on the data obtained from Maxwell 3D and RMxprt.

Jikai Si *et al.* (2017) used Taguchi method and surface response methods for optimization of peak value of cogging torque, ratio of average torque and weight of permanent magnet, torque ripple and total harmonic distortion in back emf. Optimal objective function is established using the least-squares method and resolution of the optimization objective function is performed using Response Surface Methodology. Taguchi and RSM are used in combination to optimize the design of surface-mounted permanent magnet (SPM) and interior permanent magnet (IPM) synchronous motor. Taguchi method is used to filter out the structural parameters such as peak value of cogging torque, torque ripple, ratio of average torque and permanent magnet weight and total harmonic distortion in back emf. RSM is used to optimize SIPMSM after reduction of scope of design variables. In the above work author uses central composite design method and Finite Element experiments.

Fujishima *et al.* (2002) minimized the area of magnet material of an outer rotor PMSM subject to the constraints T_{max}=7490 Nm and open circuit induced voltage E_o=1500V. The constraints were included in the total objective function as weighted penalty factors. The combination of GA and FEM results in more CPU time and for this reason RSM is combined along with GA and FEM for optimization purpose and CPU time is reduced significantly.

Cvetkovski and Petkovska (2008) have studied the topology optimization for optimal design of a permanent magnet synchronous motor based on the efficiency maximization using Genetic Algorithm. 2D finite element method is used for magnetic field computation and analysis of PMSM. Comparative results of the motor efficiency with optimized motor parameters and the basic model and the results of the 2D FEM magnetic field are presented. It was shown that the efficiency has improved to a significant level with the optimized motor parameters.

Response surface optimization of PMSM is studied in **[Jolly and Jabber (2005), Fang *et al.* (2008), Jolly *et al.* (2006), Park *et al.* (2006)]** where design of experiment is used and a second order polynomial function is used to create the response surface. Different number of design experiments is used by the researchers to find an optimal solution.

Manko *et al.* (2017) have used the simplest design of experiments (DoE) by applying Taguchi method and optimized the design of PMSM. Two different optimization goals are used by the authors. These goals are the reduction of the motor volume and maximization of the efficiency. In the optimization process limits of some parameters are fixed at the initial stage. These parameters are: maximum continuous torque, peak torque, base speed, maximum speed and DC-link voltage. Optimization of the geometry parameters were made in two stage process. In the first stage different factors of geometrical parameters are considered. In this investigation air gap flux density, number of pole pairs, saturation, diameter to length ratio, lamination quality, magnet quality, cooling intensity, working temperature, safety factor, production technology are considered as different factors A to K and factors are varied on three levels. The responses considered in the investigation are volume of the machine and efficiency. The numbers of experiments were determined using Taguchi orthogonal array approach. In the second stage of optimization only the most significant factors (2 to 6) were selected and data were taken as five levels. It was shown that two stage optimization procedure as proposed in their investigation gives significantly better results as optimization in one step.

The research work carried out on the PMSM motor design optimization focused on the single objective functions considering either the efficiency or power factor where as in many applications simultaneous optimum performance of several parameters are required.

The manufacturing cost of PMSM is quite high as compared to other electrical machine. The performance characteristic studies under steady state and transient condition is of prime importance in PMSM. The experimental dynamic analysis of PMSM is very complicated and time consuming. The determination of the exact motor parameters for a specified output or response is a complicated task. Therefore, performance simulation using various techniques is used for design of PMSM of any required capacity. The simulation using MATLAB or Finite Element Analysis using ANSYS are frequently used by researchers for the numerical analysis of permanent magnet synchronous machine or in general electric machines.

Petkovska, and Cvetkovski (2006) studied the transient performance characteristics of surface mounted PMSM using software package FEMM **[Meeker (2005)]**. Both steady state and dynamic performance characteristics of the machines are studied. Finite element approach is used to compute the flux linkage and reactance and stator winding parameters. The simulation studies are performed at rated supply condition and no load start-up condition. Authors compared the simulated results with the experimental results and found a very good agreement.

Wang *et al.* (2015) used finite element analysis to analyze the torque of Permanent Magnet Synchronous Motor (PMSM) of an electric vehicle using a 2D model. Field lines and flux density distribution on no load condition were used to verify the accuracy of model. Further they analyzed the torque fluctuation curve to test the stability under rated load condition. The relation between motor torque and current amplitude was found to be non linear with the help of various current simulations. The results presented are useful in optimal design of a PMSM in electric vehicle.

Lv *et al.* (2013) controlled a three phase AC motor using FPGA device EP1C3T144C8. DDS technique was also introduced aiming at the flexibility of the variable frequency system based on SPWM. Based on the SPWM signal inverter switch device generated a tunable frequency for the speed adjustment of AC motor fed by three phase ac supply. Fast switching, high frequency resolution and stable SPWM signal was achieved using DDS technique.AC-DC-AC variable frequency speed control technique is used in SPWM that adjusts the frequency and voltage of sine wave in three phase AC motor.

Chapter 3 MATERIALS AND METHODS

3.1 Introduction

This chapter describes design procedure of Permanent Magnet Synchronous Motor (PMSM) using RMxprt of ANSYS Maxwell software. The chapter also explains about the equipments and procedures used for experimental analysis. The principle of operation involved is also included in this chapter. Neodymium Iron Boron (NdFeB) was used as the magnetic material in the designing as it is the most frequently used material. The size of the magnet and rotor dimensions for a 1.07 kW PMSM were optimized using Taguchi method and Surface Response Method (SRM). Multi-objective functions along with few constraints of dimensions were used for minimization or maximization of the required responses. The complete drive system was designed using ANSYS Simplorer for performance analysis of the optimally designed PMSM in RMxprt. Experiments were conducted on a 1.07 kW PMSM and results were analyzed and compared with those obtained by the simulation of the PMSM model.

3.2 Permanent Magnet Synchronous Motor

A Permanent Magnet Synchronous Motor (PMSM) is quite similar to other electrical AC machines having a stator, rotor, windings put in the stator for 3 phase or single phase supply, and a shaft to load the motor. The only thing that makes the PMSM different from other electrical AC machines is its rotor containing the permanent magnets on its surface or embedded inside it. The permanent magnets produce the rotor flux which in case of other electrical AC machines is produced by external supply for which rotor windings are required. A typical constructional view of PMSM is shown in Fig. 3.1.

Permanent Magnet Synchronous Motors require inverter for starting, which is not economical in view of single speed applications such as in fans, pumps, compressors, etc.. Permanent magnet motors equipped with a cage like structure are therefore designed which is known as Line Start Permanent Magnet Synchronous Motor (LSPMSM). It can start and accelerate when they are directly connected to line voltage without the need of an inverter and operate at synchronous speed. LSPMSM

are used in applications requiring frequent starts and stops as Permanent Magnet (PM) motors have low inertia. LSPMSM is an alternative to Induction Motors (IM) in applications which require high efficiency. The introduction of high energy density magnets and reduction in its price has led to the use of LSPMSM instead of IM in several applications. In induction motors, the torque is developed due to the slip between stator rotating magnetic field and rotor bars, and for production of the magnetic flux, some magnetizing current is required which adds to further losses in the machine. However, in case of LSPMSM, no magnetizing current is required for production of the magnetic flux as permanent magnets are used in this case. In this way, an LSPMSM is more efficient as compared to an induction motor. The design of stator of an LSPMSM remains the same as that of an induction machine and hence retains the simplicity and ruggedness of the machine. A 3-dimensional view of PMSM modeled in ANSYS Maxwell software is shown in Fig. 3.2.

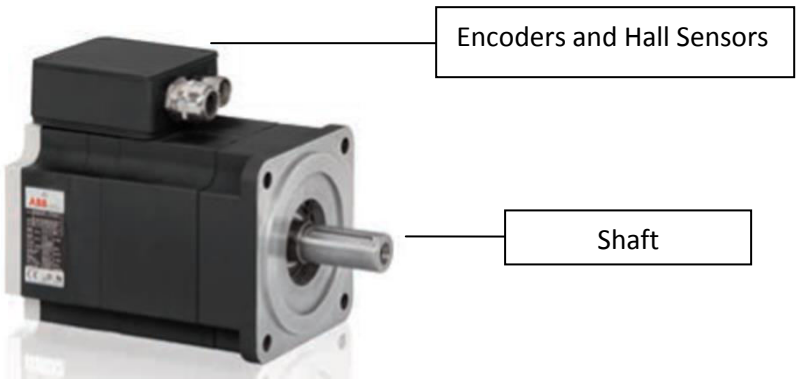

Fig. 3.1 Permanent Magnet Synchronous Motor

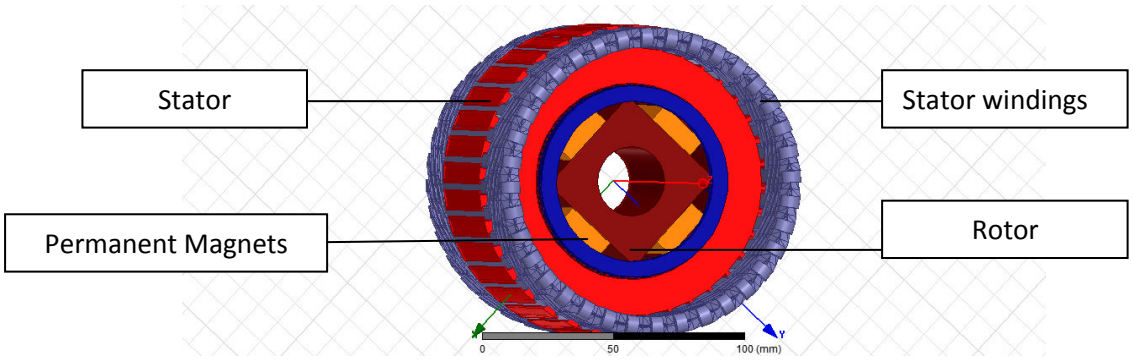

Fig. 3.2 Permanent Magnet Synchronous Motor modeled in ANSYS Maxwell

3.3 Material Used in Design

For the design of stator, one of the objectives to be considered is to minimize the stator copper losses as much as possible so as to have a good efficiency but at the same time the economic viability is also to be considered. Cobalt-irons and Nickel-irons are generally used for designing the stator, however they are expensive. Silicon iron materials are widely used because they are cost effective and exhibit excellent magnetic performance. Cobalt iron alloys are often used in manufacturing the stator and rotor cores. However, annealing of cobalt iron alloys is done for building of magnetic circuits in rotating electrical machines as it changes the magnetic properties of the cobalt iron alloy greatly. In the present work, the stator is made up of iron. The rotor is made up of cobalt. Damper bars are made up of aluminum. Material used for permanent magnets is Neodymium Iron Boron (NdFeB). The mechanical and electrical properties of the stator are presented in Table 3.1.

Table 3.1 Materials of different components of PMSM

Sl. No	Component	Material
1	Stator	Iron
2	Rotor	Cobalt
3	Permanent Magnet	Neodymium Iron Boron (NdFeB).
4	Damper	Aluminum

3.4 Design of PMSM Using ANSYS Maxwell

ANSYS Maxwell software is used to design the PMSM. Finite Element Method (FEM) approach is used in the ANSYS Maxwell software. The model for the machine was developed in RMxprt which requires data related to the stator, the stator windings, the stator slots, the rotor and the poles. The rotor can be designed with or without dampers. In this work, dampers were used which facilitate the PMSM to start like an IM.

The steps used in designing a PMSM in RMxprt are described below. Initially the capacity and speed of operation for the PMSM are to be specified for designing a

PMSM. The capacity and speed of operation mainly depend on the type of application. Some of the applications are presented in Table 3.2.

Table 3.2: Different applications and required power capacity (Product Manual, Toshiba, Jing Wang *et al.,* 2017, Guo Hong *et al*., 2015)

Sl No	Application	Power rating (kW)	Used in
1.	Hybrid Electric Vehicle	15	Motor cycles, trucks, buses, Formula 1, etc.
2.	Aerospace applications	0.2	Boeing
3	Railways	120 - 200	Tokyo Metro, subway trains, etc.
4	Robotics applications	1.1 - 7.5	AC servo drives (Industrial robot)
5	Industrial applications	5 - 10	Cutters and grinders

In the present work, 1.07 kW capacity motor having 4 poles with a rated speed of 4000 rpm has been selected, and magnet size and position, rotor with embedded magnets, damper windings for the rotor and a stator is designed using RMxprt. The different steps for design of PMSM are described below.

Step 1: ANSYS Maxwell software was used and the Graphical User Interface (GUI) that appeared after software was opened is shown in Fig. 3.3.

Step 2: Three options are available in ANSYS Maxwell software for designing various electrical machines. These are “Insert Maxwell 3D Design”, “Insert Maxwell 2D Design”, and “Insert RMxprt Design”. In the present work “Insert RMxprt Design” icon was selected. The window which appeared after selecting above stated icon is shown in Fig. 3.4 and “Line Start Permanent Magnet Synchronous Motor” option was selected out of the different options available.

Step 3: Once LSPMSM is selected under Insert RMxprt design, a new project opens up and four options *viz.*, “Machine”, “Analysis”, “Optimetrics”, and “Results” are available.

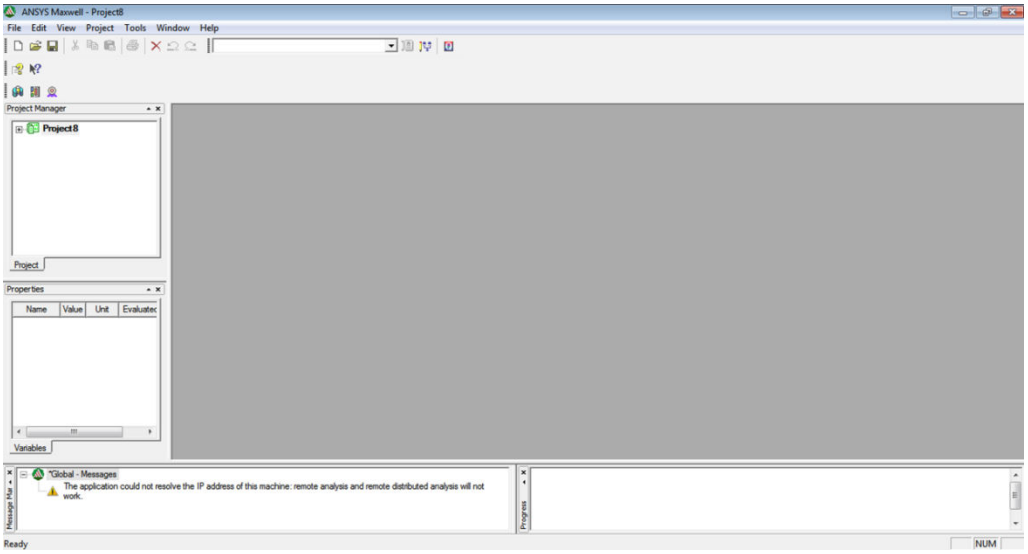

Fig. 3.3 Graphical User Interface (GUI) of ANSYS Maxwell software

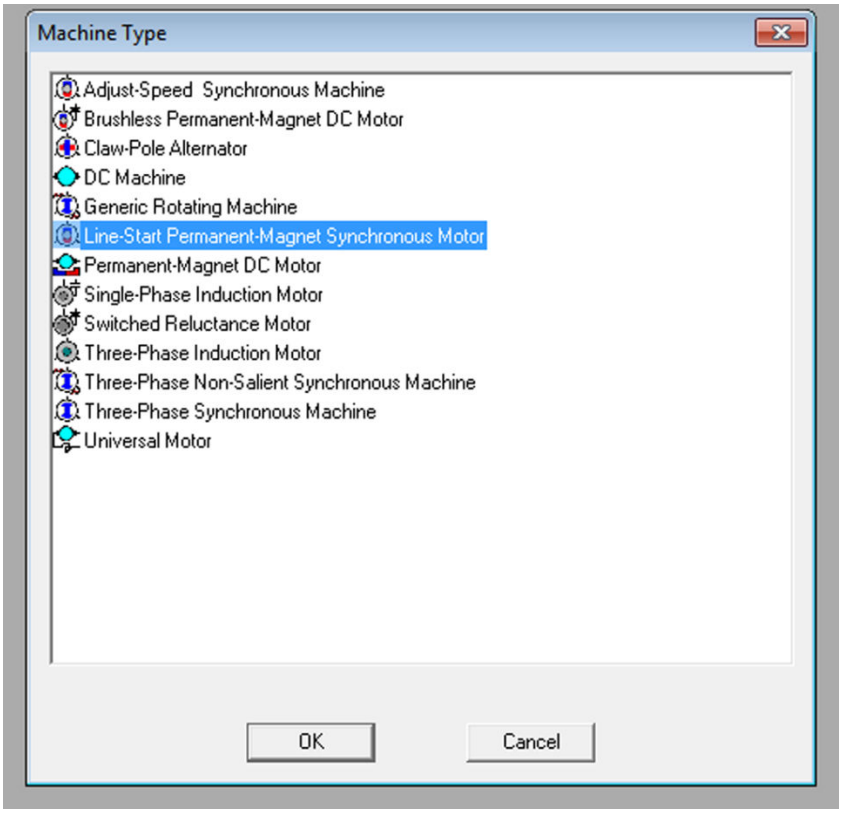

Fig. 3.4 Selection window of LSPMSM

For starting the design of LSPMSM, "Machine" option was selected and different parameters such as number of poles, frictional losses, windage losses, and a reference speed was entered as shown in Fig. 3.5. The parametric values were selected based on the previous work and experimental investigation done.

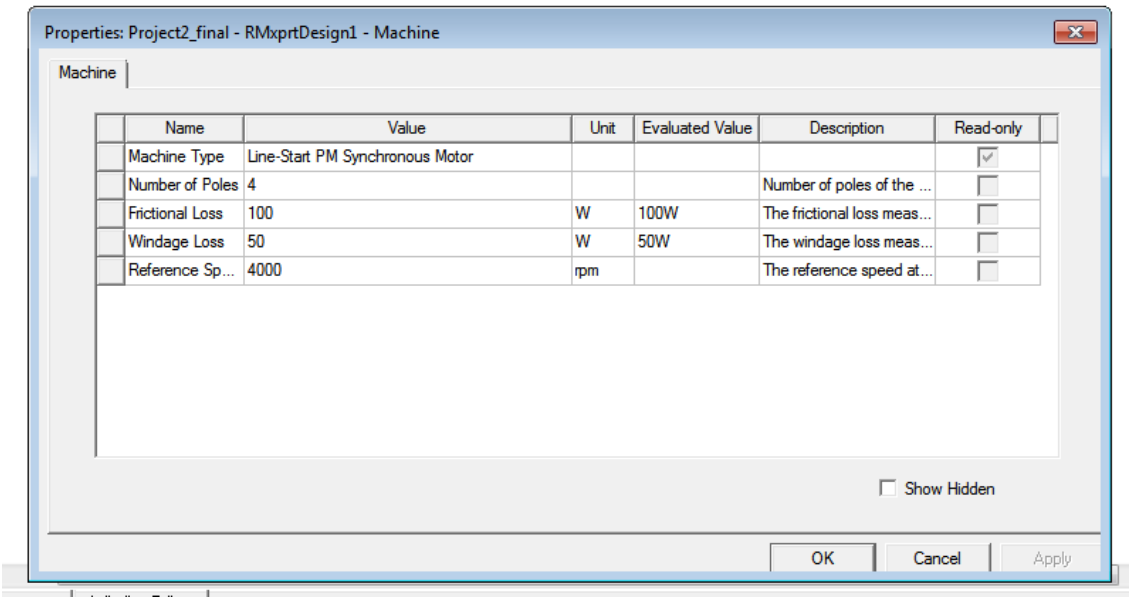

Fig. 3.5 Entering machine properties for design

Keeping in view the previous work done, the stator data were selected so as to make a compact and valid design. This took several trials and the final dimensions are shown in Fig. 3.6.

Step 4: Once the stator is designed, the dimensions for the slots were given as shown in Fig. 3.7. This was done by various trials such that the slots fit best into the stator.

The winding details were then entered as shown in Fig. 3.8, and with this the design of stator is completed.

Different wire diameters were tried in the design. Nine wire diameters taken in this investigation were selected between 0.381 mm to 11.69 mm. Based on the analysis of the efficiency, power factor, starting torque, losses etc. minimum volume optimization was conducted and based on the results, 0.965 mm wire diameter was taken for an LSPMSM design. The results are discussed in the "Result and Discussion" chapter.

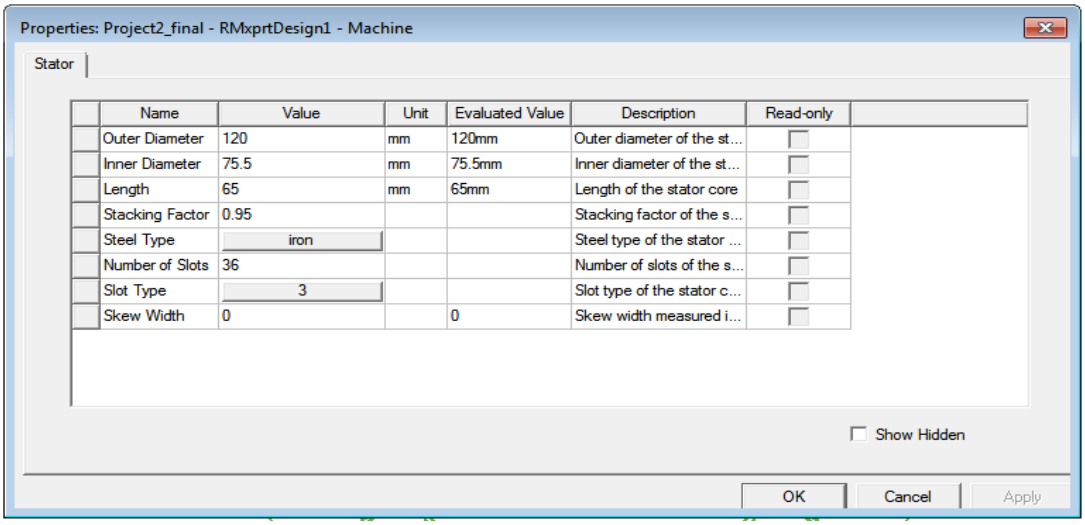

Fig. 3.6 Stator design parameters

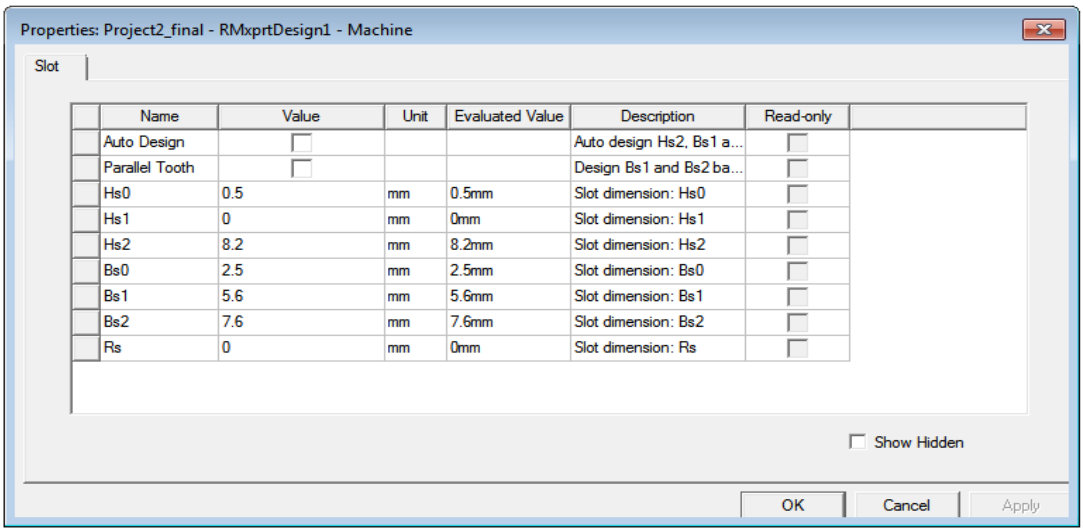

Fig. 3.7 Stator slot parameters

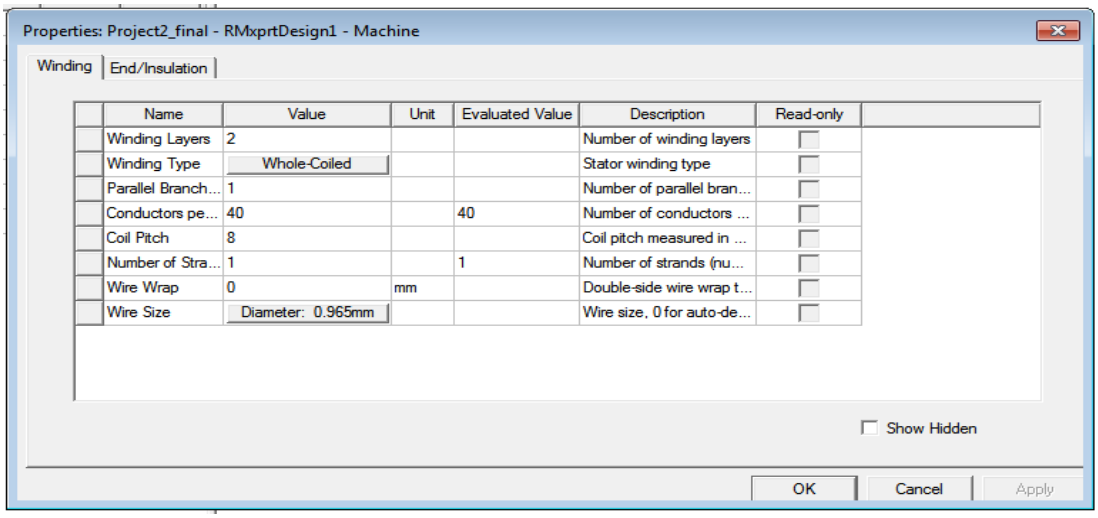

Fig. 3.8 Stator winding parameters

The rotor was now designed by giving inputs as shown in Fig. 3.9. Once the rotor structure was created, the pole type of permanent magnets was selected. Eight such designs for pole structures are available in RMxprt. One of such designs (Fig. 3.10) was selected and then the data for pole was entered as shown in Fig. 3.11. The dimensions and position of the permanent magnets inside the rotor greatly affects the efficiency, power factor, and various other output responses. So, optimization of the pole data is required. The data entered for pole can be optimized using various techniques. The techniques used in the present work are Taguchi and Surface Response Method. The details of the methods are discussed in subsequent section of this chapter. The results are discussed in "Results and Discussion" chapter. This completes the design of rotor of the PMSM.

The outer diameter of the rotor was taken as 74.5 mm so as to keep an air gap of 0.5 mm. The inner diameter was taken as 26.5 mm as shown in Fig. 3.9 and the permanent magnets are to be placed inside the rotor periphery left.

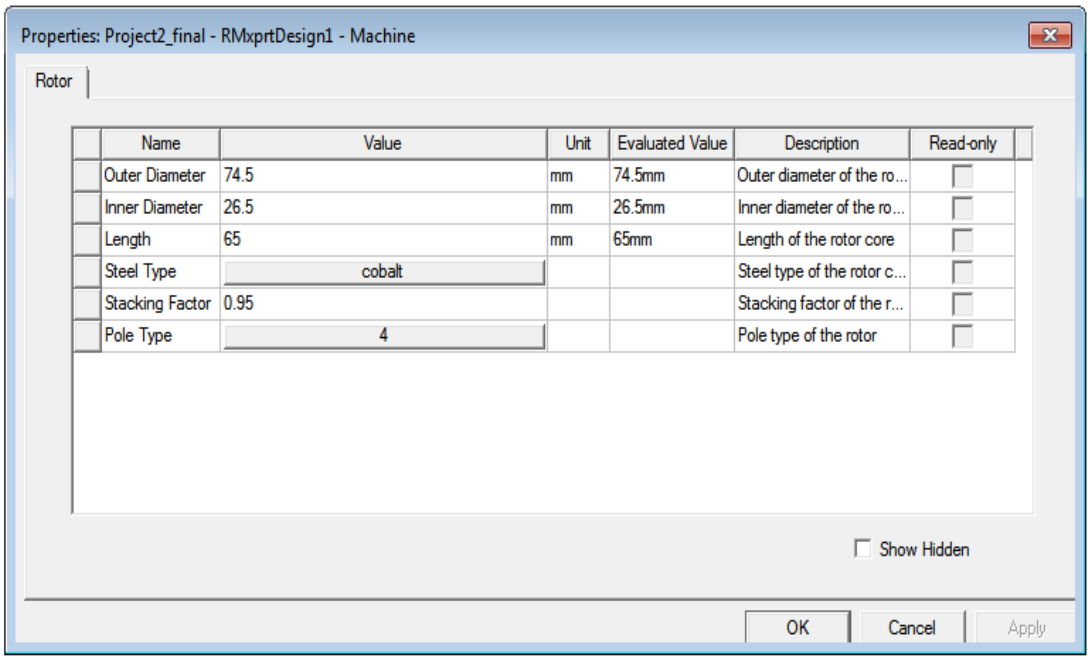

Fig. 3.9 Rotor parameters

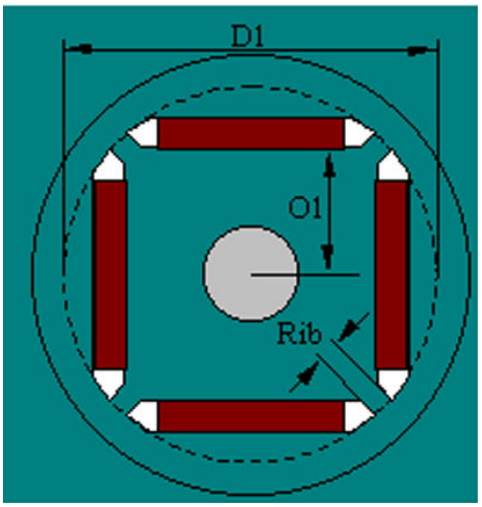

Fig. 3.10 Permanent Magnet placement inside the rotor structure

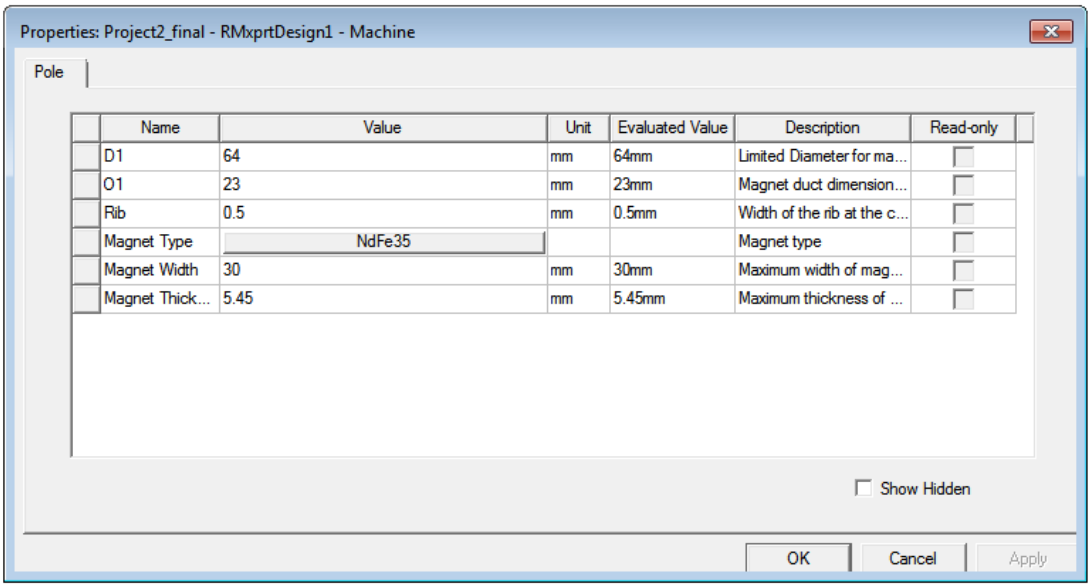

Fig. 3.11 Rotor pole parameters

The various parameters shown above such as D1, O1, Rib, magnet width, and magnet thickness were optimized so that maximum efficiency and power factor were achieved. Dampers were added to the design of rotor, and various data were entered for the damper as shown in Fig. 3.12. 12 damper slots per pole were used for this design as it gave a good starting torque. Next, the damper slots were designed and the data was given on trial and error basis as shown in Fig. 3.13.

This completes the design of PMSM using RMxprt as shown in Fig. 3.14 which was checked and validated by the software by selecting the "RMxprt" option in

the menu bar and clicking on the "Validation Check" option. Different components are shown in Fig. 3.15- Fig. 3.19.

Now, for the analysis purpose a solution setup was created in which we need to specify the load type, rated output power, rated voltage, rated speed, and the operating temperature. Finally, the PMSM was simulated on the basis of its design and solution setup added. The various results were achieved in tabular as well as graphical form and discussed in the "Results and Discussion" chapter.

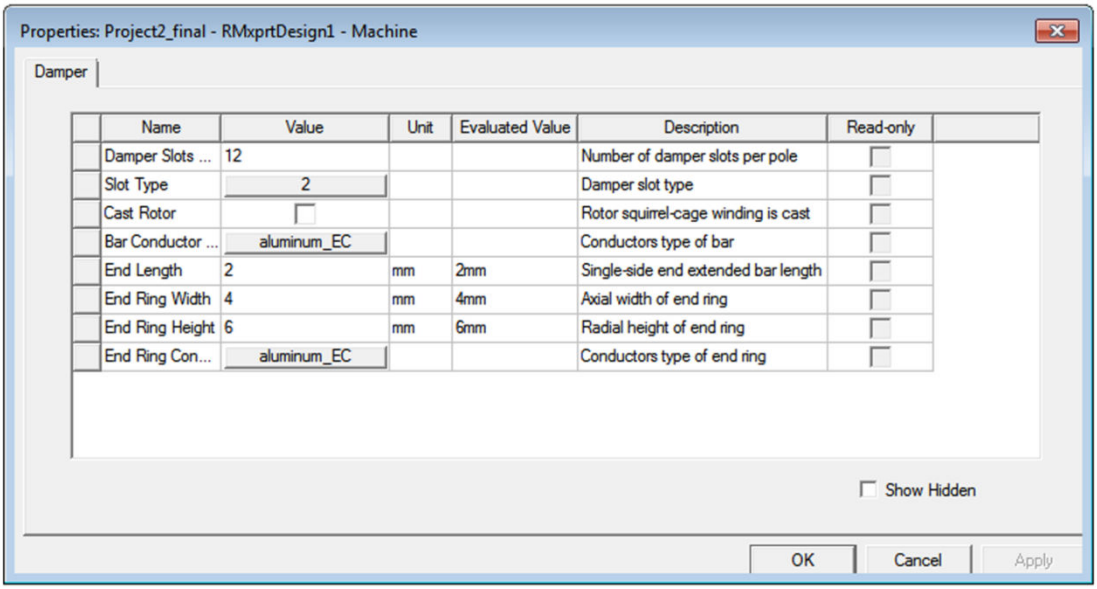

Fig. 3.12 Rotor damper properties

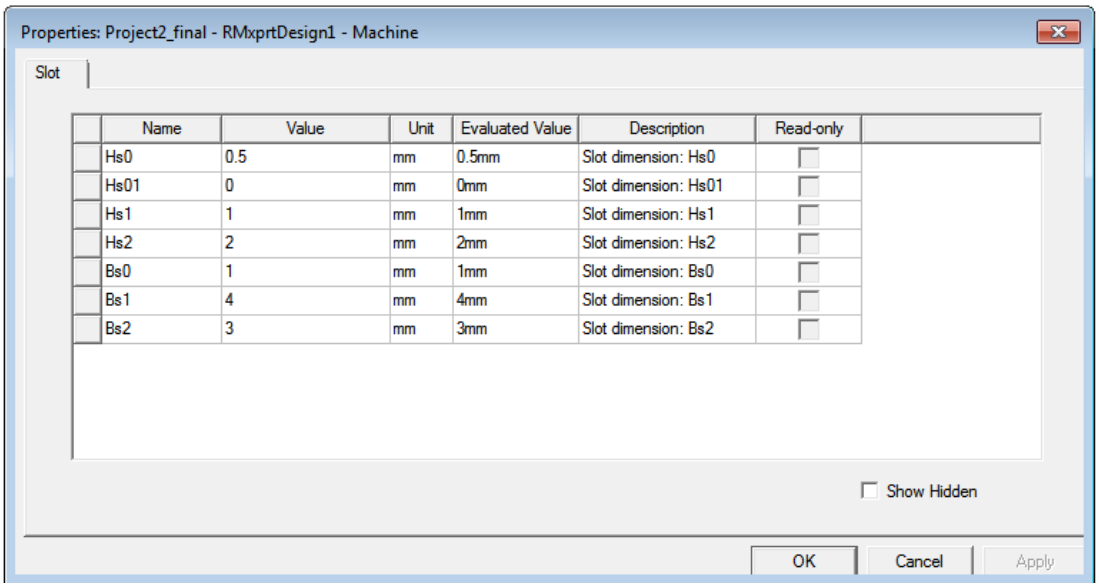

Fig. 3.13 Rotor damper slot parameters for design

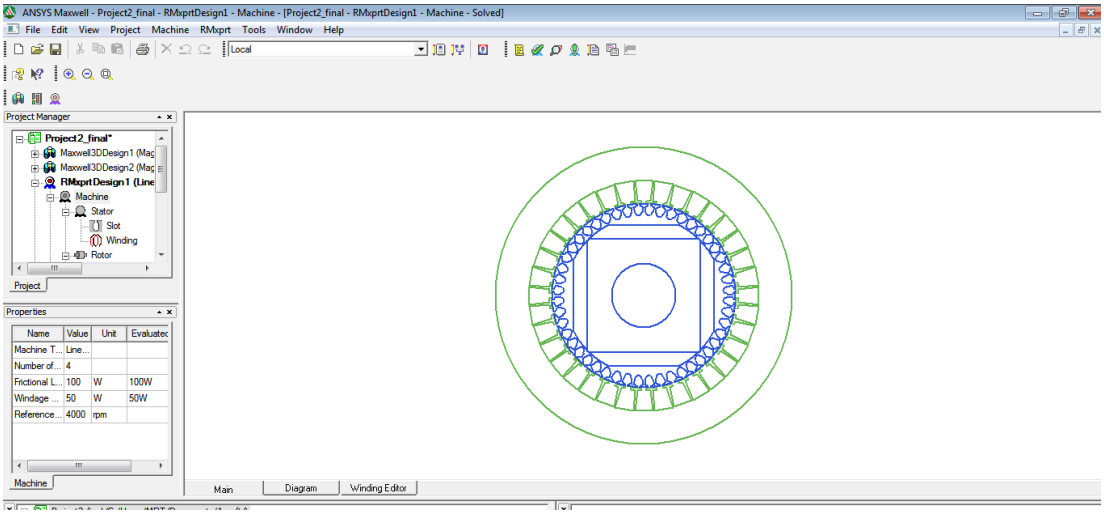

Fig. 3.14 LSPMSM design in RMxprt.

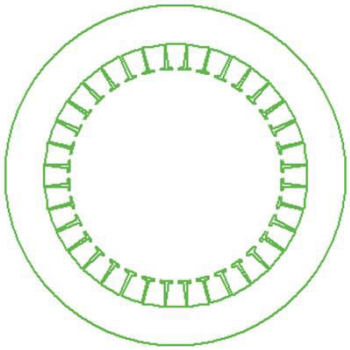

Fig. 3.15 Stator structure

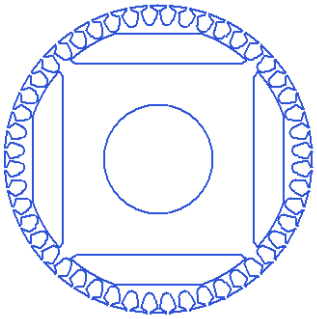

Fig. 3.16 Rotor structure with damper windings

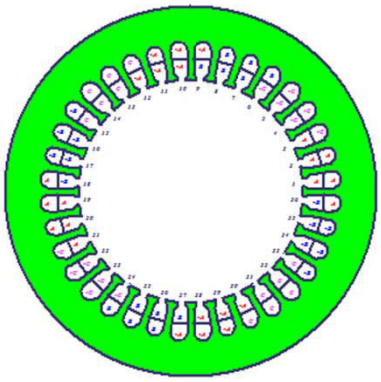

Fig. 3.17 Winding structure

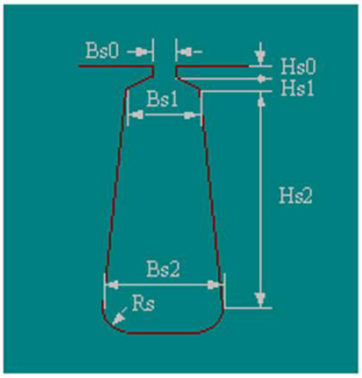

Fig. 3.18 Type of slot used in PMSM design

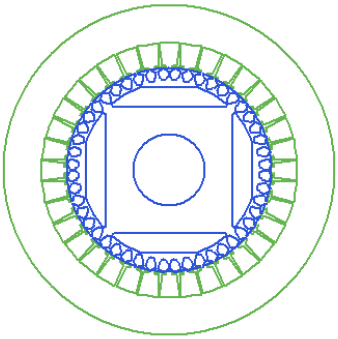

Fig. 3.19 Final design of PMSM

The final specifications of PMSM are given in Tables 3.3 and 3.4.

Table 3.3: Specification of the PMSM motor

Rated Power, kW	1.07
Rated voltage, V	300
Number of poles	4
Number of stator slots	36
Outer diameter of stator, mm	120
Inner diameter of stator, mm	75
Inner diameter of rotor, mm	26.5
Length of rotor, mm	65
Air gap, mm	0.5
Magnet material	NdFeB
Rotor material	Steel
Winding connection	Star

Table 3.4: Dimensions of stator slot

Hs0, mm	0.5
Hs1, mm	0
Hs2, mm	8.2
Bs0, mm	2.5
Bs1, mm	5.6
Bs2, mm	7.6

3.5 Design Optimization

Taguchi method and Surface Response Method (Montgomery, 2009) are widely used in optimal design of the PMSM. Two kinds of parameters mostly affect the performance of a PMSM. One kind is the controllable parameters such as magnet size, its position, and rotor data. The uncontrollable parameters kept under noise parameters are air gap error caused by machining operation. Cogging torque also plays an important role in the machine noise and vibration. Similarly, torque ripple is also to be minimized for smooth operation of the machine. So, in optimization, all or few of the above can be taken as design parameters whereas performance characteristics such as efficiency, power factor, losses, etc. can be taken as responses. In the design optimization of PMSM, the optimization was done based on the steady-state performance of the motor.

3.5.1 Taguchi design methodology

In Taguchi optimization method (Montgomery, 2009) different factors were selected with different levels to study the effect of the factors on the performance. Design of Experiment (DoE) is used to find the possible combination of different design factors, operational conditions, etc. in order to get the best results. DoE may be full factorial design or randomized block design known as fractional design of experiment. Taguchi method is based on the fractional factorial design concept and it significantly reduces the total number of experiments. The DoE in Taguchi method uses specially created Orthogonal Arrays (OA) which allows reducing the number of

experiments and time in conducting the experiments. The OA used in Taguchi method is presented in Table 3.5 which can be used to aid in selecting an OA for up to 15 parameters and 2 to 4 number of levels.

Table 3.5: Taguchi's parameter design orthogonal array selection map

		Number of parameters													
Number of levels		2	3	4	5	6	7	8	9	10	11	12	13	14	15
	2	L4	L4	L8	L8	L8	L8	L12	L12	L12	L12	L16	L16	L16	L16
	3	L9	L9	L9	L18	L18	L18	L18	L27	L27	L27	L27	L27	L36	L36
	4	**L16**	**L16**	**L16**	L16	L32	L32	L32	L32	L32					

Table 3.5 shows the relation between number of parameters and number of levels used in the design optimization. In the present investigation for optimum magnet size four thickness and four width combinations were taken. Thus, it creates 16 experiments in full factorial design.

3.5.1.1 Selection of factors and levels

Two types of variables are used to perform experiments in the field of DoE. These are responses and factors. The response gives information about the investigated system and the factors are used to manipulate it. Normal factors have a set of two or more values. The first step in the Taguchi method of optimization and analysis is the selection of factors and levels. In the present investigation, the magnet dimension such as width and thickness were taken as main factors with 4 levels. The minimum and maximum dimensions (levels) were selected on the basis of several trial designs in the RMxprt design software. The levels and the associated parameters are presented in Table 3.6. The responses taken in this study are power factor, efficiency, and starting torque.

In the optimization of magnet size, there were two control factors i.e., width and thickness, and each at four levels. Full factorial experiment with 2 factors and 4 levels require $4^2 = 16$ number of experiments (Montgomery, 2009). Hence, L16 array is selected (Table 3.7) and the details of the factors and responses are presented in Table 3.8.

Table 3.6: Design parameters and their levels

Parameters	Levels			
	1	2	3	4
Magnet Width (mm)	4	8	15	20
Magnet Thickness (mm)	4	6	7.3	7.38

Table 3.7: L16 Orthogonal Array

Expt. No	Width	Thickness
1	1	1
2	1	2
3	1	3
4	1	4
5	2	1
6	2	2
7	2	3
8	2	4
9	3	1
10	3	2
11	3	3
12	3	4
13	4	1
14	4	2
15	4	3
16	4	4

Table 3.8: Details of the factors and responses

Expt No	width, mm	thickness, mm	efficiency, %	power factor	Starting Torque, Nm	Cu loss, W
1	4	4.00	73.427	0.512	31.421	330.091
2	4	6.00	82.439	0.640	31.102	246.615
3	4	7.30	83.687	0.666	30.864	177.486
4	4	7.38	83.746	0.667	30.843	150.344
5	8	4.00	79.341	0.591	31.422	194.397
6	8	6.00	84.118	0.675	31.104	167.72
7	8	7.30	85.147	0.701	30.867	132.895
8	8	7.38	85.181	0.702	30.846	113.04
9	15	4.00	83.493	0.661	31.424	174.52
10	15	6.00	86.410	0.738	31.108	151.908
11	15	7.30	87.282	0.768	30.871	120.143
12	15	7.38	87.278	0.768	30.851	101.217
13	20	4.00	85.242	0.703	31.426	173.601
14	20	6.00	87.775	0.787	31.110	151.385
15	20	7.30	88.610	0.824	30.874	12.198
16	20	7.38	88.582	0.823	30.854	101.586

3.5.1.2 Analysis of response data

In Taguchi method, a loss function is used to calculate the deviation between the experimental and the desired values. The Signal to Noise ratio (S/N) is obtained from the loss function. Three types of quality characteristics of S/N ratio are used in the analysis. These are: the lower the better, the higher the better, and the nominal the best. In the analysis, S/N ratio for each response is calculated as per response characteristics. In the present investigation, the motor efficiency, power factor, and

starting torque were taken for maximization whereas armature copper loss was taken for minimization. Hence, for the first three responses, higher the better and for last response lower the better criteria were used. Equation 3.1 and 3.2 describe the quality characteristics.

The higher the better

$$\frac{S}{N} = -10log\left[\frac{1}{n}\sum_{i=1}^{n}\frac{1}{y_i^2}\right] \quad (3.1)$$

The lower the better

$$\frac{S}{N} = -10log\left[\frac{1}{n}\sum_{i=1}^{n}y_i^2\right] \quad (3.2)$$

y_i is the ith experimental data and n is the number of observations.

The selection of the array depends on the number of control factors and desired levels. The performance in terms of efficiency, power factor, starting torque, etc. of PMSM depends on the several design parameters. Magnet size is one of the factors which affect the performance of PMSM significantly. The effect of magnet volume on the PMSM performance parameters is presented in "Results and Discussion" chapter of the thesis.

Using the S/N ratio values for all the 16 experiments for efficiency, power factor and Cu loss as responses, Analysis of Variances (ANOVA) was performed to identify the contribution of each of the factors to the variability in performance of the product.

In addition to magnet dimension, its position in the rotor is also important. The magnet position parameters were also optimized using Taguchi method. The different parameters selected for such studies are presented in Table 3.9.

In rotor position optimization, there are five control factors, two at 4 levels and three at 2 levels. Mixed full factorial experiment with 2 factors at 4 levels and 3 factors at 2 levels require $4^2 \times 2^3 = 128$ number of experiments which can be reduced to one-eighth of 128 which is equal to 16. Hence, L16 array was selected and the details of the factors are presented in Table 3.10.

Table 3.9: Rotor design parameters and their levels

Parameters	Levels			
	1	2	3	4
Magnet Width, w (mm)	4	8	15	20
Magnet Thickness, t (mm)	4	6	7.3	7.38
D1 (mm)	63	64	-	-
O1 (mm)	21	23	-	-
Rib (mm)	0.5	4	-	-

Table 3.10: L16 array of magnet and position data

w	t	D1	O1	Rib
1	1	1	1	1
1	2	1	1	1
1	3	2	2	2
1	4	2	2	2
2	1	1	2	2
2	2	1	2	2
2	3	2	1	1
2	4	2	1	1
3	1	2	1	2
3	2	2	1	2
3	3	1	2	1
3	4	1	2	1
4	1	2	2	1
4	2	2	2	1
4	3	1	1	2
4	4	1	1	2

In Table 3.10, 1, 2, 3, and 4 are the different levels of the parameters used in optimization process as shown in Table 3.9.

L16 Orthogonal Array (OA) was used in Taguchi method and the results of S/N ratio for power factor and efficiency are discussed in the "Results and Discussion" chapter.

3.5.2 Response Surface Methodology (RSM)

Response Surface Methodology (RSM) is an empirical modeling tool based on the various mathematical and statistical techniques. The main objective of RSM is to optimize single or multiple objective responses which are influenced by several independent variables. In RSM, the total experiments, known as run, are designed in order to identify the reasons for difference or changes in the output response.

There are many geometry parameters in a rotor of PMSM, but optimization of all parameters is not required as it leads to the objective functions and constraints for the optimization of PMSM design very complex and impractical. The main rotor parameters to be optimized are magnet size and its position. Hence, the critical design parameters and the most required responses are to be considered in the design optimization of PMSM. The RSM and multiple objective function optimization approach are used in such cases. In this work, to limit the objective functions, variables, and constraints to a certain range, the other parameters in the optimization were considered as constant. In RSM, the careful design of experiments (DoE) optimizes a response (output variable) which is influenced by several independent variables with minimum number of runs. Generally, the structure of the relationship between the response and the independent variables is unknown. The first step in RSM is to find a suitable approximation to the true relationship. The most common forms are low-order polynomials (first- or second-order). Factorial designs are used for fitting a model. A first-order polynomial may be used initially, and if it shows a lack of fitting, then a second-order polynomial model can be used to improve the optimization process. A second-order model is defined as

$$y = a_0 + \sum_{i=1}^{n} a_i x_i + \sum_{i=1}^{n} a_{ii} x_i^2 + \sum_{i=1}^{n} \sum_{\substack{j=1 \\ j \neq i}}^{n} a_{ij} x_i x_j \qquad (3.3)$$

where *x's* are input parameters and *a's* are the constants to be optimized.

The RSM uses statistical tools to find the functional relationship between the input and output variables. It means that, it relates the responses with the design parameters. In case of electrical machine design, the main responses are efficiency, power factor, cost, and material. In PMSM, the main design components are design dimensions of the magnet and magnet duct. In the present investigation, width and thickness of the magnet and its positional parameters (duct dimensions) were taken as input variables. The lower and upper bounds of these parameters were defined. When the dimensional parameters are defined at only the lower and upper bounds (two levels), the resulting design is known as 2^nfactorial design. However, to improve the results, the mid points are also included and the resulting design is 3^n full factorial design which is shown in Fig. 3.20.

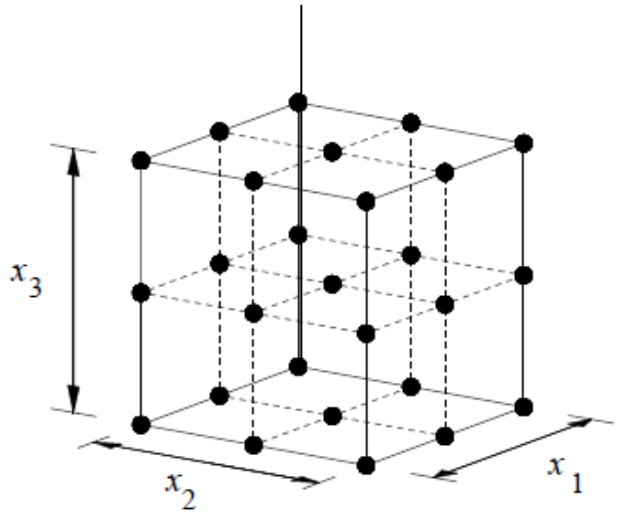

Fig. 3.20 A 3^3 (27) full factorial design

Fig. 3.20 shows a 3 factor full factorial design at 3 levels. It requires total of 27 number of experiments. Fig. 3.21 shows a central composite design for 3 variables at 2 levels. In this design, one data is taken at center of each face and other data points are located at the corners of a cube. In general, the design involves 2*n* factorial points, 2*n* axial points, and one central point. It is generally used for fitting second order models as the number of runs reduces to a large extent. Thus, number of runs required in a central composite design with 3 variables with central points are 13 instead of 27 as required in full factorial design. In this design, there was one central point and four

axial points as shown in Fig. 3.21. The central composite design for 3 design variables at 2 levels in 2D is shown in Fig. 3.22.

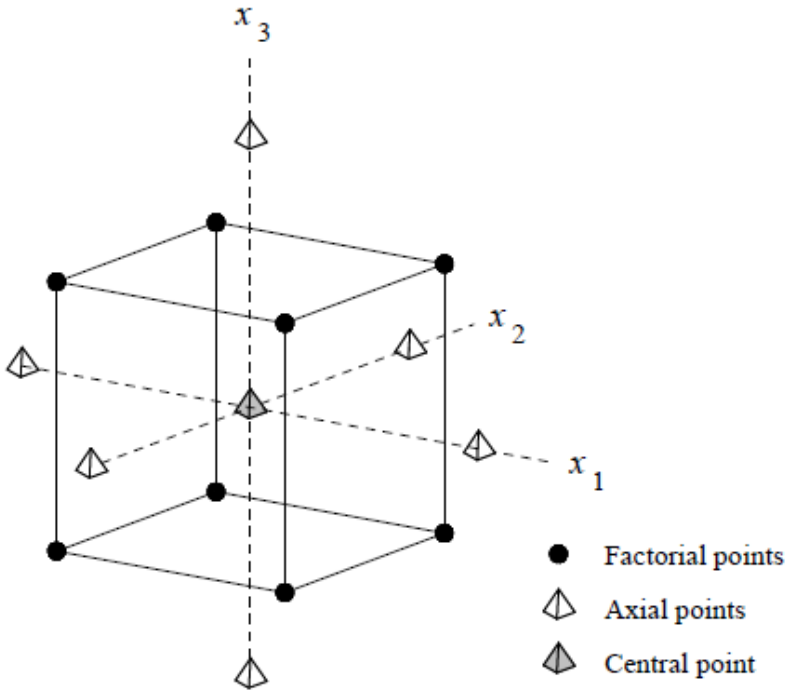

Fig. 3.21 Central composite design for 3 design variables at 2 levels

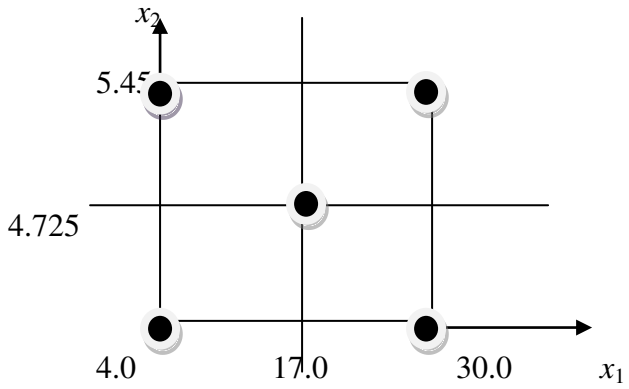

Fig. 3.22 Full factorial design

3.5.2.1 D-optimal designs

The D-optimality criterion is a more efficient way of a quadratic model generation. The objective is to select *P* design points from a larger set of candidate points.

Equation (3.3) can be expressed in matrix notation as:

$$Y = X \times A + E \qquad (3.4)$$

where Y is the observation vector, E is the error vector, X is the matrix of the design variables at selected points and A is the vector of tuning parameters. Using least square method A can be estimated from Equation 3.5.

$$A = (X^T X)^{-1} X^T Y \tag{3.5}$$

The D-optimality criterion states that the best set of points in the experiment maximizes the determinant $|X^T X|$. D stands for the determinant of the $X^T X$ matrix associated with the model. From a statistical point of view, a D-optimal design leads to response surface models for which the maximum variance of the predicted responses is minimized. This means that the points of the experiment will minimize the error in the estimated coefficients of the response model. In the present investigation, this criterion was used.

3.5.2.2 Design of experiment for RSM

The detailed dimensions and response values used in RSM are given in Table 3.11. There are 52 runs for five parameters and two responses. Different parameters were critically selected according to the method described in previous sections. The ranges of different parameters are mentioned below in Equation 3.6.

$$4 \leq w \leq 30 \text{ (mm)}$$

$$4 \leq t \leq 7.38 \text{ (mm)}$$

$$63 \leq D1 \leq 64 \text{ (mm)}$$

$$21 \leq O1 \leq 23 \text{ (mm)}$$

$$0.5 \leq Rib \leq 4 \text{ (mm)} \tag{3.6}$$

where “w” is the width of the magnet, “t” is the thickness of the magnet, “D1” is the limited diameter for magnet ducts, “O1” is the magnet duct dimension and, “Rib” is the width of the rib at the center of the two adjacent poles to support the bridge.

Table 3.11: Details of the rotor factors and responses

Expt No.	w (mm)	t (mm)	D1 (mm)	O1 (mm)	Rib (mm)	Efficiency, %	Power Factor
1	17	4.000	64	23	0.5	85.292	0.705
2	30	4.725	64	23	0.5	89.261	0.857
3	4	5.450	64	23	0.5	82.200	0.635
4	30	4.000	64	23	0.5	88.583	0.823
5	17	4.725	64	23	0.5	86.114	0.729
6	30	5.450	64	23	0.5	89.902	0.857
7	4	4.725	64	23	0.5	80.939	0.614
8	17	5.450	64	23	0.5	86.830	0.752
9	17	4.725	64	23	0.5	86.114	0.729
10	17	4.725	64	23	0.5	86.114	0.729
11	17	4.725	64	23	0.5	86.114	0.729
12	4	4.000	64	23	0.5	78.584	0.581
13	17	4.725	64	23	0.5	86.114	0.729
14	4	4.000	63	21	0.5	63.251	0.283
15	4	6.000	63	21	0.5	71.720	0.407
16	4	7.300	64	23	4.0	83.690	0.666
17	4	7.380	64	23	4.0	83.746	0.667
18	8	4.000	63	23	4.0	71.277	0.386
19	8	6.000	63	23	4.0	74.162	0.508
20	8	7.300	64	21	0.5	84.186	0.677
21	8	7.380	64	21	0.5	84.249	0.678
22	15	4.000	64	21	4.0	72.155	0.395
23	15	6.000	64	21	4.0	83.984	0.672
24	15	7.300	63	23	0.5	84.015	0.673
25	15	7.380	63	23	0.5	83.900	0.670

26	20	4.000	64	23	0.5	86.174	0.731
27	20	6.000	64	23	0.5	88.053	0.799
28	20	7.300	63	21	4.0	81.244	0.619
29	20	7.380	63	21	4.0	81.665	0.626
30	4	4.000	63	23	4.0	73.427	0.512
31	4	6.000	63	23	4.0	82.439	0.640
32	4	7.300	63	23	4.0	83.687	0.666
33	4	7.380	63	23	4.0	83.746	0.667
34	8	4.000	63	23	4.0	79.341	0.591
35	8	6.000	63	23	4.0	84.118	0.675
36	8	7.300	63	23	4.0	85.147	0.701
37	8	7.380	63	23	4.0	85.181	0.702
38	15	4.000	63	23	4.0	83.493	0.661
39	15	6.000	63	23	4.0	86.410	0.738
40	15	7.300	63	23	4.0	87.282	0.768
41	15	7.380	63	23	4.0	87.278	0.768
42	20	4.000	63	23	4.0	85.242	0.703
43	20	6.000	63	23	4.0	87.775	0.787
44	20	7.300	63	23	4.0	88.610	0.824
45	20	7.380	63	23	4.0	88.582	0.823
46	20	7.380	64	23	0.5	88.792	0.833
47	20	7.300	64	23	0.5	88.753	0.831
48	8	7.380	64	20	4.0	81.942	0.631
48	8	7.300	64	20	4.0	81.735	0.627
50	30	5.450	64	23	0.5	89.902	0.985
51	28.67	5.450	64	23	0.5	89.639	0.879
52	28.54	5.450	64	23	0.5	89.611	0.877

The results of RSM are discussed in the "Results and Discussion" chapter. ANOVA was conducted to find out the effect of different design parameters w, t, D1, O1, and Rib and their interaction on efficiency and power factor. The result of ANOVA was discussed in "Results and Discussion" chapter. The coefficients of regression equations for power factor and efficiency were also statistically analyzed and the results are discussed in subsequent chapter. Method of ANOVA is briefly summarized in Table 3.12.

Table 3.12: Method of ANOVA

Variation	Degree of Freedom	Mean Square	F
Between Factors $v_b = b\sum_j (\bar{x}_j - \bar{x})^2$	$a-1$	$\widehat{s_b}^2 = \frac{v_b}{a-1}$	$\frac{\widehat{s_b}^2}{\widehat{s_w}^2}$ with $a-1$, $a(b-1)$ degrees of freedom
Within Factors $v_w = v - v_b$	$a(b-1)$	$\widehat{s_w}^2 = \frac{v_w}{a(b-1)}$	
Total $v = v_b + v_w$ $= \sum_{j,k}(x_{jk} - \overline{x})^2$	$ab-1$		

where

$a =$ independent group of samples

$b =$ number of measurements in each group

"a" can be considered as treatments, each treatment having "b" repetitions.

Representation in tabular form will give a rows and b columns. Here, x_{jk} denotes the measurement in j^{th} row and k^{th} column where j = 1,2,…, a and k = 1,2,…, b.

The mean of measurement in the j^{th} row is denoted by $\bar{x}_j$ known as group mean or treatment mean and is given as

$$\bar{x}_j = \frac{1}{b}\sum_{k=1}^{b} x_{jk} \qquad (3.7)$$

The mean of all the measurements in all the groups is known as grand mean or overall mean and is denoted by $\bar{x}$, *i.e.,*

$$\bar{x} = \frac{1}{ab}\sum_{j=1}^{a} \sum_{k=1}^{b} x_{jk} \quad (3.8)$$

The total variation is denoted by v and is defined as the sum of the squares of the deviations of each measurement from the grand mean $\bar{x}$, *i.e.,*

$$\text{Total variation} = v = \sum_{j,k} (x_{jk} - \bar{x})^2 \quad (3.9)$$

The variations within factors denoted by v_w is given as

$$v_w = \sum_{j,k} (x_{jk} - \bar{x}_j)^2 \quad (3.10)$$

The variation between factors is denoted by v_b is given as

$$v_b = b\sum_{j} (\bar{x}_j - \bar{x})^2 \quad (3.11)$$

3.6 Design of Drive Circuit

The high cost of PM motor drives calls for a need of modeling and simulating PM drives rather than building system prototypes for the performance analysis of the drive. The design of drive circuit is essential for the complete analysis of the PMSM and to study the real time response of transient state as well as steady state. It will also help in finding out the various losses in the machine that would have been found if the drive were actually run. This saves not only the cost of building prototype but also a lot of time. ANSYS Simplorer software was used to design the drive circuit for PMSM. The LSPMSM was already designed in RMxprt tool of ANSYS Maxwell. After designing the drive circuit in ANSYS Simplorer, the complete analysis is performed and the results were then obtained by co-simulating the ANSYS Simplorer software and the ANSYS Maxwell software.

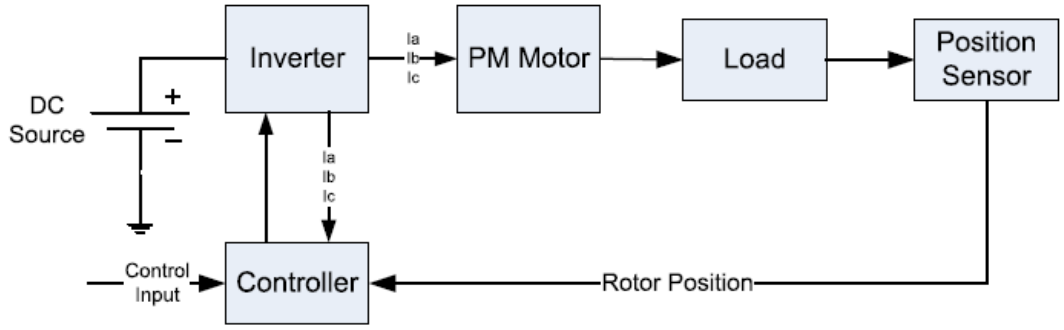

Fig. 3.23 Electrical drive system

For designing the drive system for PMSM, three phase voltage source inverter was first designed. A voltage source inverter converts a DC voltage into an AC voltage having variable magnitude and frequency. In a three-phase inverter, there are 3 legs, each leg containing two power switches and therefore six power switches in total. Table 3.13 shows the various switching devices along with their power handling capacity and switching speed. Appropriate switching device can be selected based on the requirements of operation and application. The switching devices also contain anti-parallel diodes for inductive motor current path when the switch is turned off.

The high input impedance of IGBT turns on the device with a very small amount of energy. Moreover, IGBTs have large voltage blocking capability which makes them suitable for high voltage applications. For this reason IGBTs are more preferable in case of motor drives and were also used in the present work.

Table 3.13 Devices power and switching capabilities

Device	Power Capacity	Switching Speed
BJT	Medium	Medium
GTO	High	Low
IGBT	Medium	Medium
MOSFET	Low	High
THYRISTOR	High	Low

The steps involved in the design process using ANSYS Simplorer software is as follows,

Step 1: When ANSYS Simplorer was opened, a Graphical User Interface (GUI) appeared as shown in Fig. 3.24.

The "Component Manager" toolbar on the right side of the screen contains all the elements and tools required for designing the drive circuit of PMSM.

The basic structure of a three phase inverter consists of a DC source and six switches (IGBTs) along with an anti-parallel diode for each switch as shown in Fig. 3.25.

Step 2: Under the "Basic Elements" option, "Circuit" option was expanded and then "Semiconductor System Level" option was selected. The various semiconductor switches were then displayed, out of which "IGBT: IGBT" and "D: Diode" were chosen. Under the "Sources" option, "E: Voltage Source" option was chosen for DC voltage source.

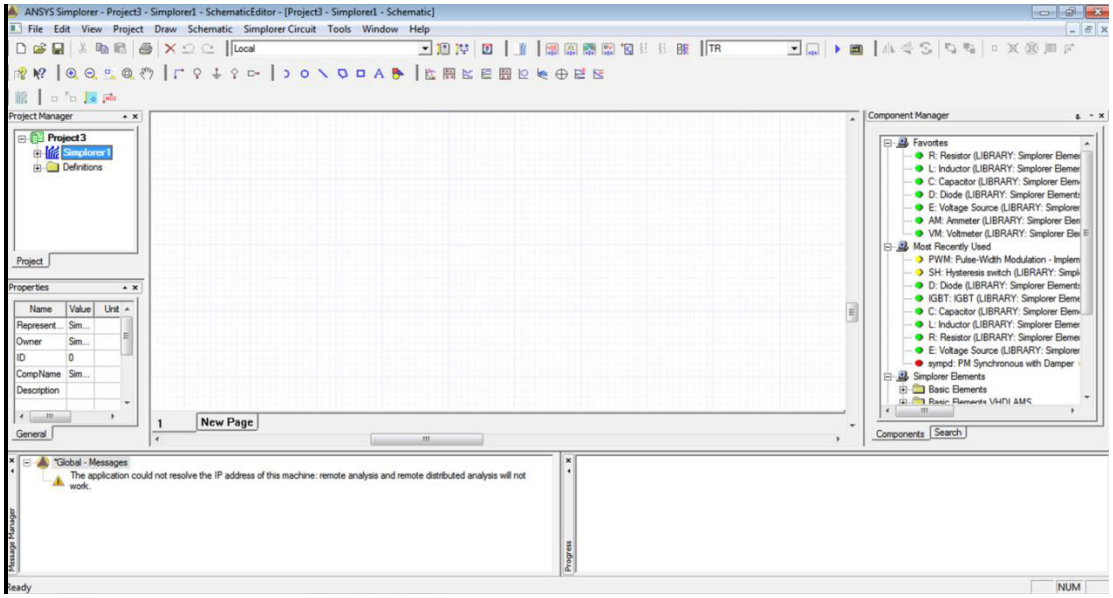

Fig. 3.24 The GUI of ANSYS Simplorer software

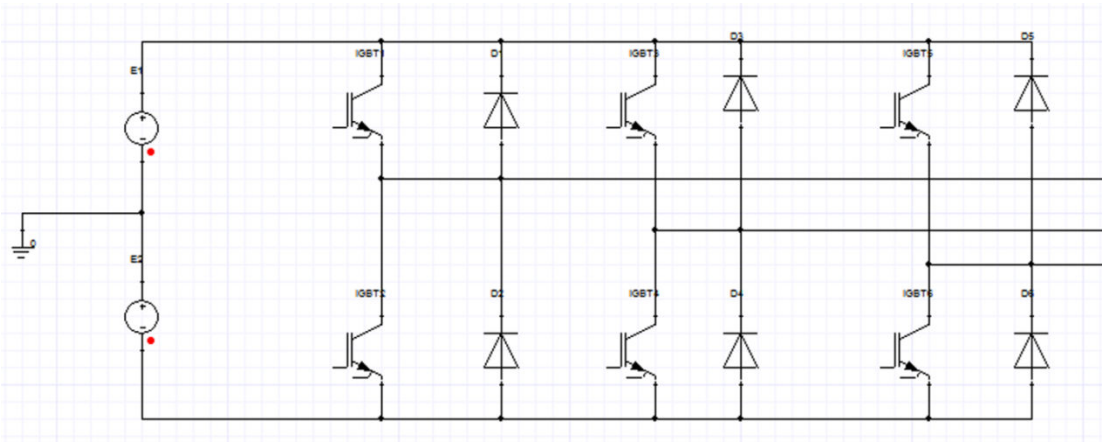

Fig. 3.25: Three phase inverter circuit in ANSYS Simplorer

For switching the IGBTs, a Pulse Width Modulation (PWM) current controller is designed. The PWM current controller provides a control signal to the IGBTs to switch them ON. The basic idea of PWM current controller is to compare a triangular carrier wave of desired switching frequency with the three sinusoidal reference waves phase delayed by 120^{o} each. If the amplitude of sinusoidal wave is greater than the

amplitude of triangular carrier wave, the upper IGBT is switched on otherwise the lower IGBT is switched on.

Step 3: For designing the PWM generator for firing the IGBTs in ANSYS Simplorer, "Tools" option under the "Components Manager" toolbar was expanded. After this, "Time Functions" option was expanded, and "TRIANG" option was then selected to produce a triangular carrier wave. And "SINE" option was also selected and dropped on the Simplorer page thrice for three different sinusoidal modulating waves with a phase lag of 120° representing the three phases. The amplitude and frequency for triangular wave were set to 1 and 10 kHz respectively. The amplitude and frequency of sinusoidal waves were kept as 1 and 50 Hz, respectively. These values were selected based on the previous work.

For designing the PWM generator, "Basic Elements" option in the "Components Manager" toolbar was expanded. Then "States" option was expanded, and "STATE_11: State 11" option was chosen. The different IGBTs to be triggered were then defined in the states accordingly. "TRANS" option was selected for transition of the control signals and the condition for transition was entered. The PWM generator is shown in Fig. 3.26.

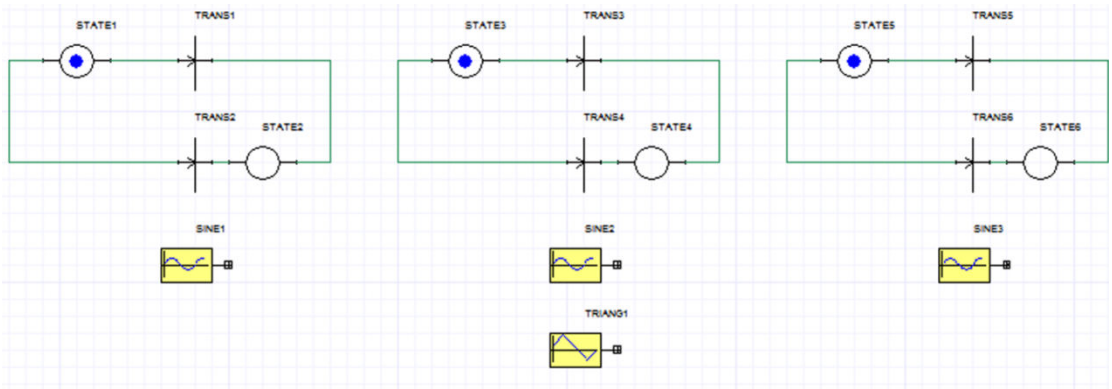

Fig. 3.26 PWM generator circuitry for three phase inverter circuit

Step 4: Maxwell 2D model for PMSM designed earlier was invoked in ANSYS Simplorer as shown in Fig. 3.27 for complete analysis of the machine. The three phase input terminals of the designed motor 2D model were then connected to the three legs of the inverter through a resistance. An ideal mechanical velocity source was connected to the 2D model of the motor which supplied the defined velocity for an arbitrary torque.

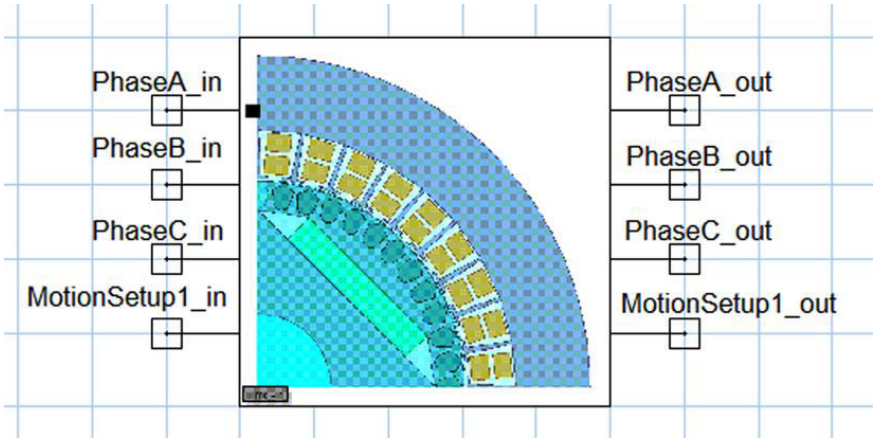

Fig. 3.27 ANSYS Maxwell 2D model with various pins after invoking in ANSYS Simplorer

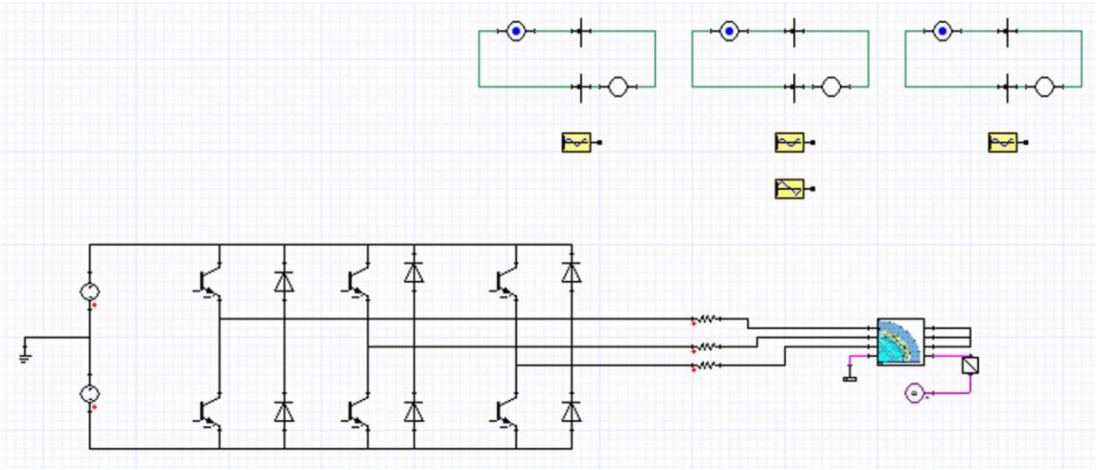

Fig. 3.28 Drive system of Permanent Magnet Synchronous Motor in ANSYS Simplorer

The final design of the PMSM drive system is shown in Fig. 3.28. The co-simulation was done by setting up a transient-transient link between the ANSYS Maxwell software and the ANSYS Simplorer software, and the results obtained from the simulation are presented in "Results and Discussion" chapter.

3.7 Experimental Setup

A 1.07 kW PMSM having a rated speed of 4000 rpm is mechanically coupled to a DC generator. Vector control technique is used in controlling the speed and current of the motor as shown in Fig. 3.29. A Field Programmable Gate Array (FPGA) controller was used for speed and current control of the PMSM. The PMSM is fed through a three-phase Voltage Source Inverter (VSI). A three-phase diode

rectifier converts the AC supply from a single phase variac to a DC voltage. The DC voltage is then applied to the VSI and was fixed at 300 V. Hall sensors and digital encoders mounted on the rotor of the PMSM give the information about the rotor position through a feedback from the motor to the FPGA control board. The VSI consists of six IGBTs and six anti-parallel diodes. The firing of IGBTs is controlled by the FPGA control board on the basis of PWM technique. A PWM pulse is generated by the FPGA controller for switching of inverter. The experimental setup is shown in Fig. 3.30.

The speed control using an FPGA controller ensures a fast processing operation, and the steady-state speed is achieved quickly after the speed command is given. It makes the system more user-friendly by allowing the user to give various commands such as speed command through a PC connected to it.

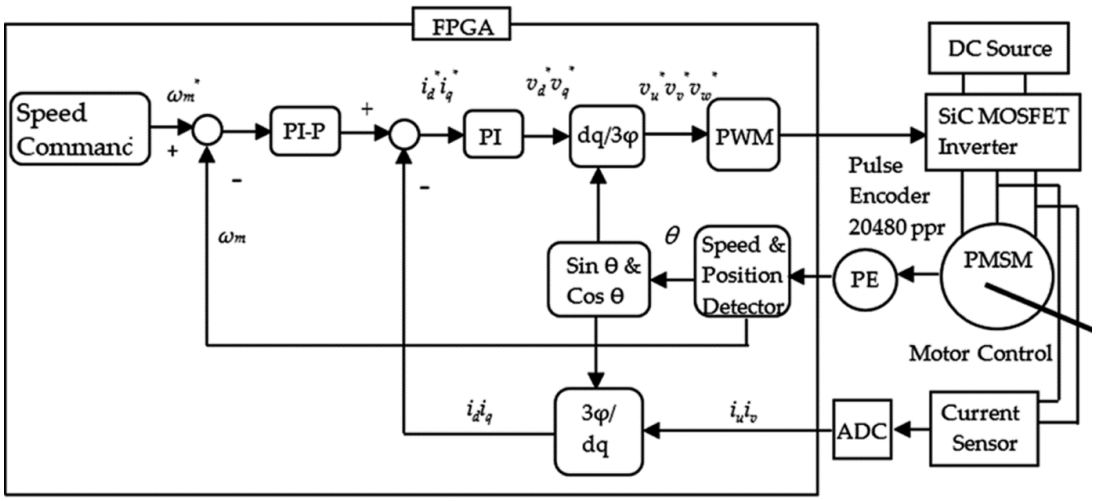

Fig. 3.29 Speed control of PMSM using FPGA controller

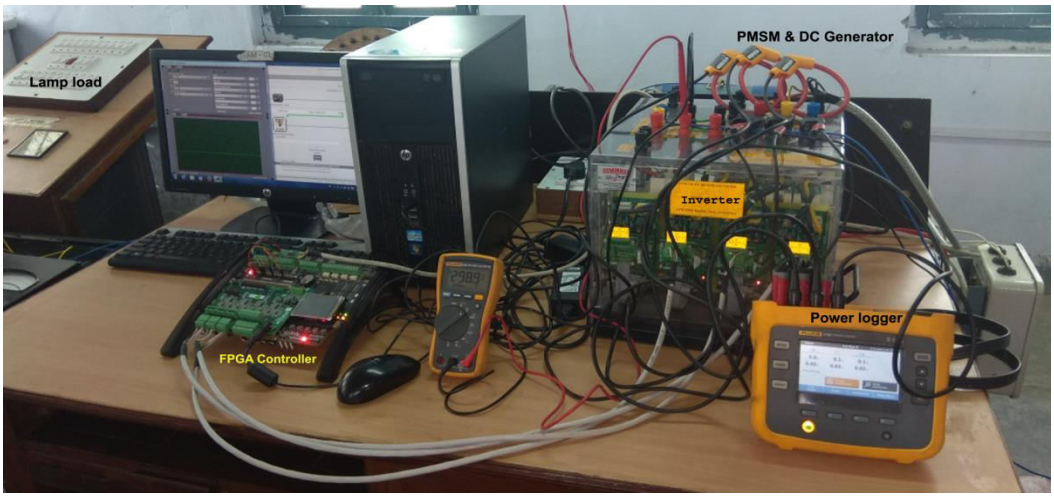

Fig. 3.30 A view of experimental setup

3.7.1 Experimental Procedure

The PMSM was run at different speeds *viz.,* 2700 rpm, 3000 rpm, and 3300 rpm (Appendix G). It was coupled with a 1 hp DC generator having a rated speed of 3000 rpm as shown in Fig. 3.31. Lamp loads were connected to the DC generator for indirect electrical loading of the PMSM. The lamp loads used in the experiment is shown in Fig 3.32. The PMSM was loaded in steps of 25 %, 50 %, 75 %, 100 %, and 110 % loading at different speeds of 2700 rpm, 3000 rpm, and 3300 rpm. The DC link voltage for the inverter was held constant at 300V. The input line voltage and input line current to the PMSM were measured using FLUKE 1738 Power Logger. The armature voltage developed across the DC generator and current to the load were also recorded with the help of a voltmeter and an ammeter. The no load losses of the DC generator at three different speeds of 2700 rpm, 3000 rpm, and 3300 rpm were measured by decoupling the PMSM and running the DC generator alone by supplying 220 V DC across its field (Appendix A). A view of decoupled DC generator for conducting the no load test is shown in Fig. 3.33. These losses act as a load to the PMSM while calculating the efficiency of the PMSM. The efficiency and load torque were calculated for different load levels at different speeds (Appendix B).

Fig. 3.31 Mechanically coupled PMSM and DC machine

Fig. 3.32 Lamp loads

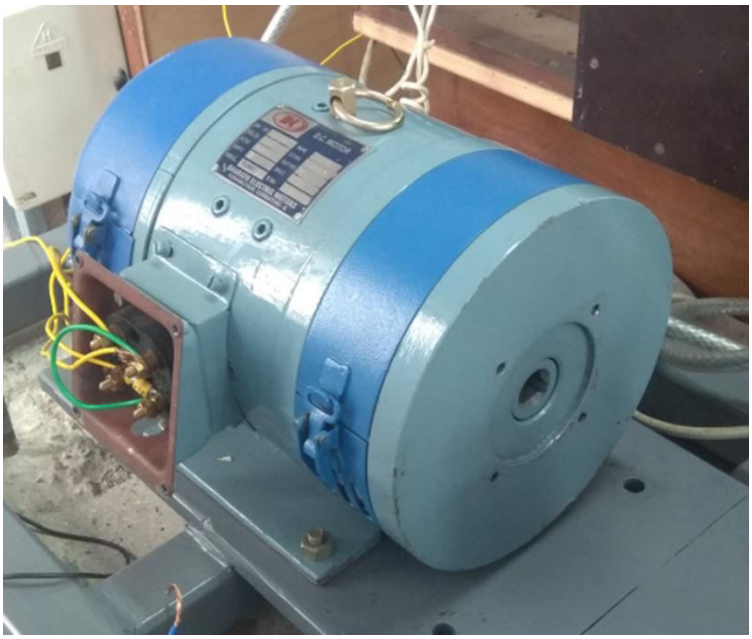

Fig. 3.33 A view of decoupled DC machine

The PMSM performance results obtained after co-simulation of ANSYS Maxwell and ANSYS Simplorer were then compared with the results obtained during experimental investigation and analysis. A comparative study of input line currents, load torque, and efficiency for full load condition at three different speeds *viz.,* 2700 rpm, 3000 rpm, and 3300 rpm was made. A good agreement between the simulated and experimental results was found in the comparative study. The comparative analysis is presented in brief in the "Results and Discussion" chapter.

4.1 Introduction

In this chapter, the optimal design of PMSM using Taguchi method and Response Surface Method (RSM) with multi-objective functions is done. The simulation and experimental results of PMSM are discussed. The performance of the optimally designed PMSM is compared and validated with the experimental results. The line current, load torque, and efficiency at full load for different speeds are validated by conducting the experiments on 1.07 kW PMSM.

4.2. PMSM Design using RMxprt

1.07 kW capacity PMSM was designed using RMxprt. The detailed specifications are given in Table 4.1.

Table 4.1: Specifications of designed PMSM

Rated Power, kW	1.07
Rated voltage, V	300
Number of poles	4
Number of stator slots	36
Outer diameter of stator, mm	120.0
Inner diameter of stator, mm	75.0
Inner diameter of rotor, mm	26.5
Length of rotor, mm	65.0
Air gap, mm	0.5
Magnet material	NdFeB
Rotor material	Steel
Winding connection	Star

The PMSM designed with these specifications was simulated in RMxprt for steady state results. The results of the performance of PMSM having magnet width = 20 mm, thickness = 7.3 mm, and wire diameter = 0.965 mm are shown in Figs. 4.1-4.5.

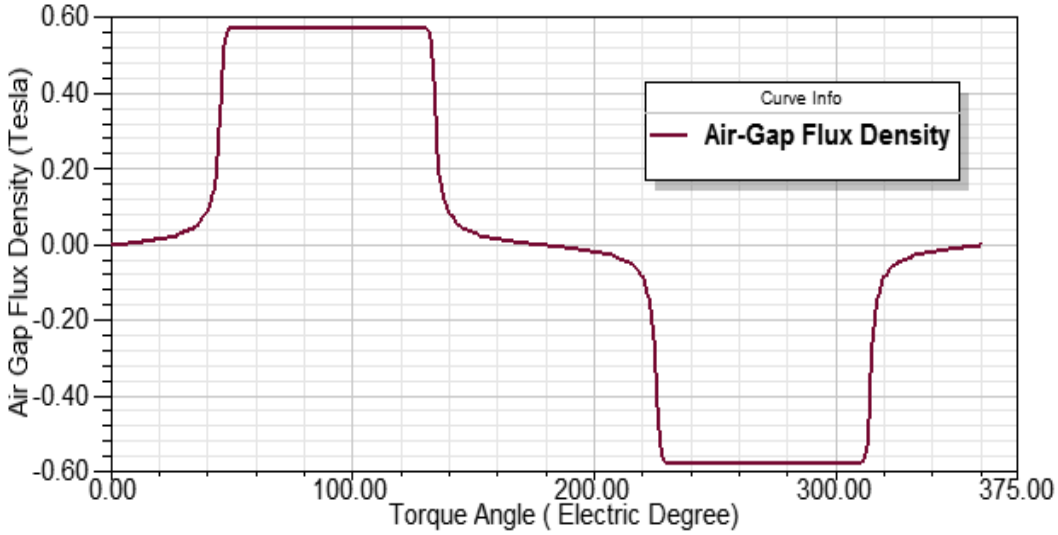

Fig. 4.1: Air gap flux density vs. torque angle for magnet thickness 7.3 mm and width 20 mm

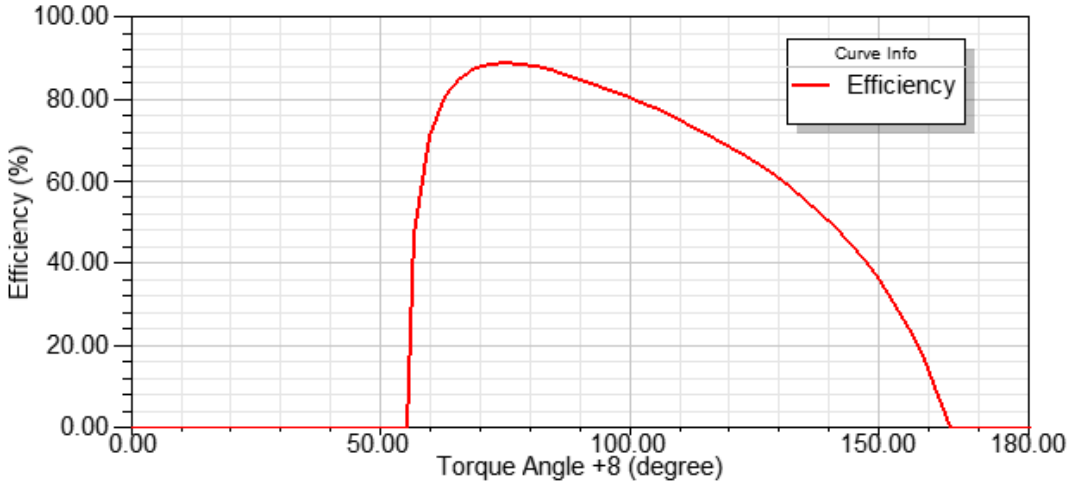

Fig. 4.2: Efficiency vs. torque angle for magnet thickness 7.3 mm and width 20 mm for a rated speed of 4000 rpm with friction and windage losses of 150 W

The air gap flux density (in tesla) vs. torque angle (in electrical degree) is shown in Fig. 4.1 for magnet width of 20 mm and a thickness of 7.3 mm. It is seen that in this design, the air gap flux density is 0.57 tesla for a torque angle ranging from 40 electrical degree to 115 electrical degree and the power factor reaches 0.88 which is high enough for LSPMSM. The full load line current is 3.78 A which is also suitable for LSPMSM.

Fig. 4.2 shows the efficiency curve with torque angle. Optimum efficiency of 88.61% was obtained at a torque angle of 64.45 degree and full load line current of 3.78 A when the friction and windage losses are 100 W and 50 W respectively. But the previous work done on PMSM and the experimental results show that friction and windage losses for a 1.07 kW PMSM are within a range of 20 W to 35 W (Appendix H). The efficiency curve with friction and windage losses of 35 W for a rated speed of 4000 rpm is shown in Fig. 4.3. The maximum efficiency in this case was 91.27 %.

Fig. 4.4 shows the torque vs speed curve having a starting torque of around 31 N-m. The induction torque shown in Fig. 4.4 is due to the damper bars introduced in the design of PMSM. The damper bars help the motor in starting and gives a high starting torque. The total torque shown in figure is the resultant torque due to induction torque and magnet generated torque.

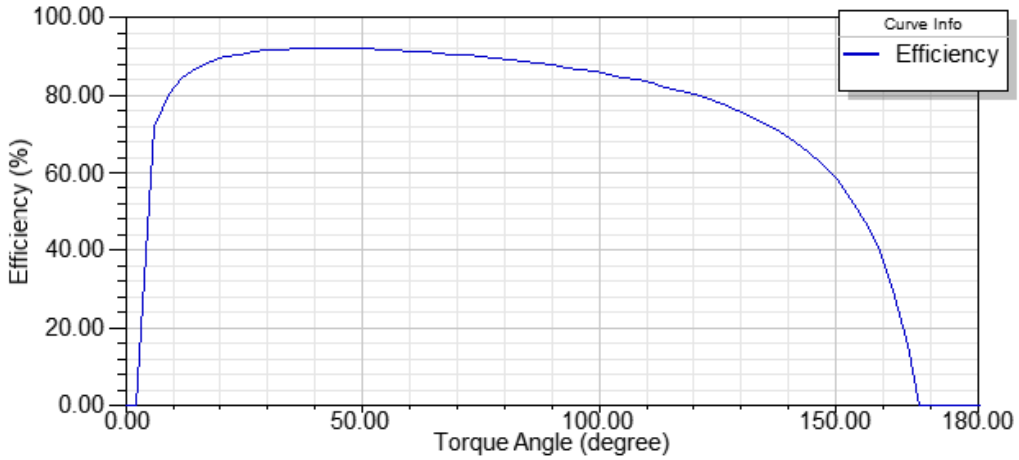

Fig. 4.3: Efficiency vs. torque angle for magnet thickness 7.3 mm and width 20 mm at 4000 rpm for frictional and windage losses of 35 W

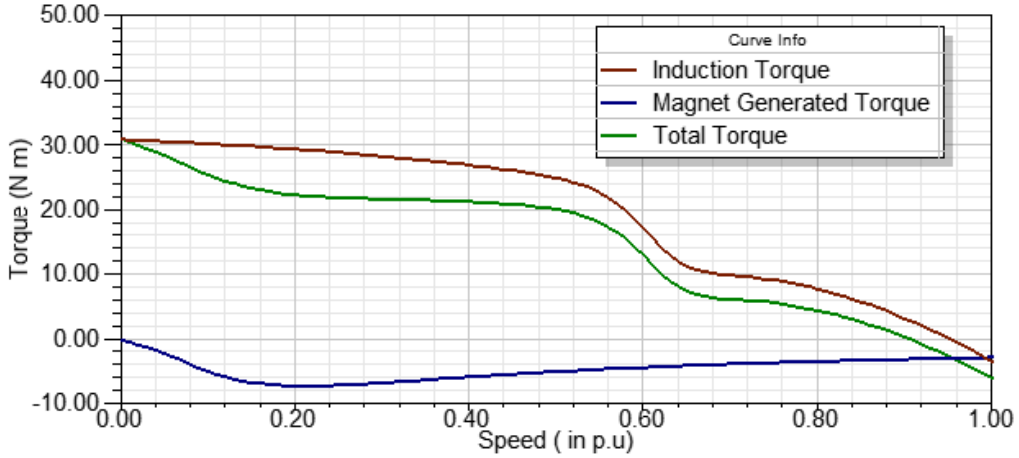

Fig. 4.4: Torque vs speed characteristics for magnet width 20 mm and thickness 7.3 mm for a rated speed of 4000 rpm

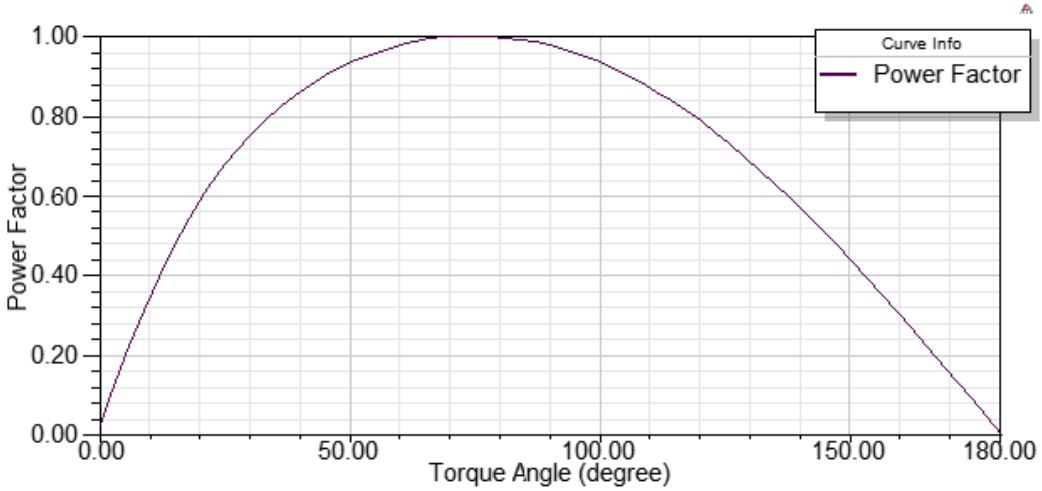

Fig. 4.5 Power factor vs torque angle for magnet width 20 mm and thickness 7.3 mm

Fig. 4.5 shows the variation of power factor with torque angle. The maximum power factor was obtained at around 80 to 85 degree. However, the operation of machine at such a torque angle is not advisable due to stability issues.

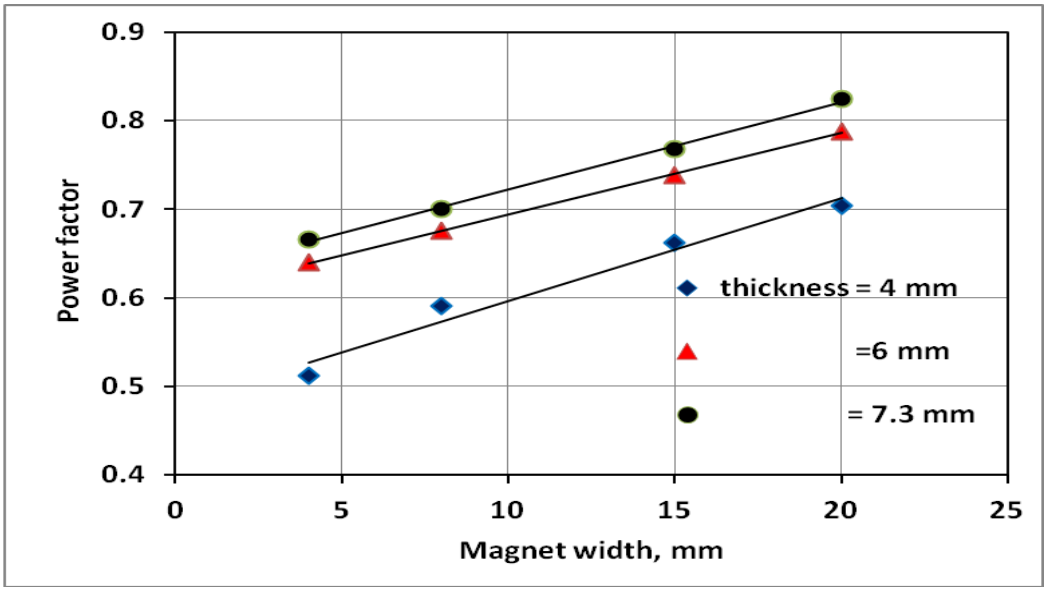

Fig. 4.6 Effect of magnet dimensions on the power factor of PMSM

Fig. 4.6 to Fig. 4.8 show the effect of magnet width, thickness, and volume on motor power factor and efficiency. A non-linear relation exists for magnet of thickness$\leq$ 4 mm whereas the variation is of linear type for thickness $>$ 4 mm.

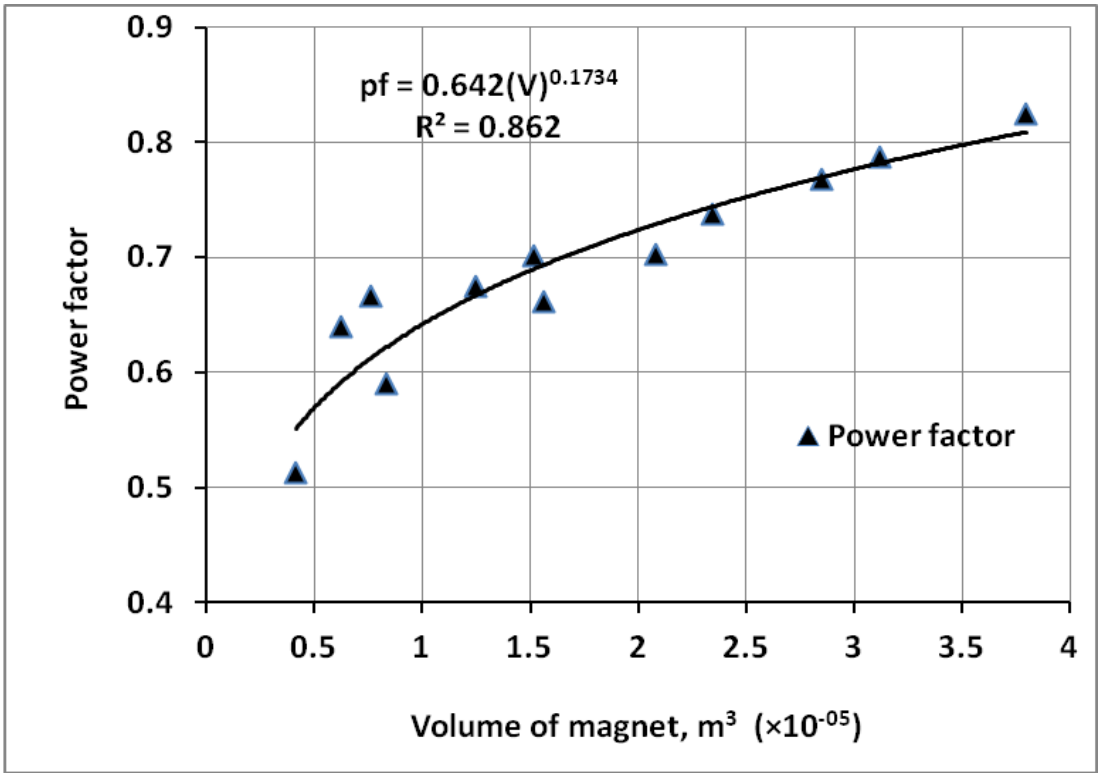

Fig. 4.7 Power factor as a function of magnet volume

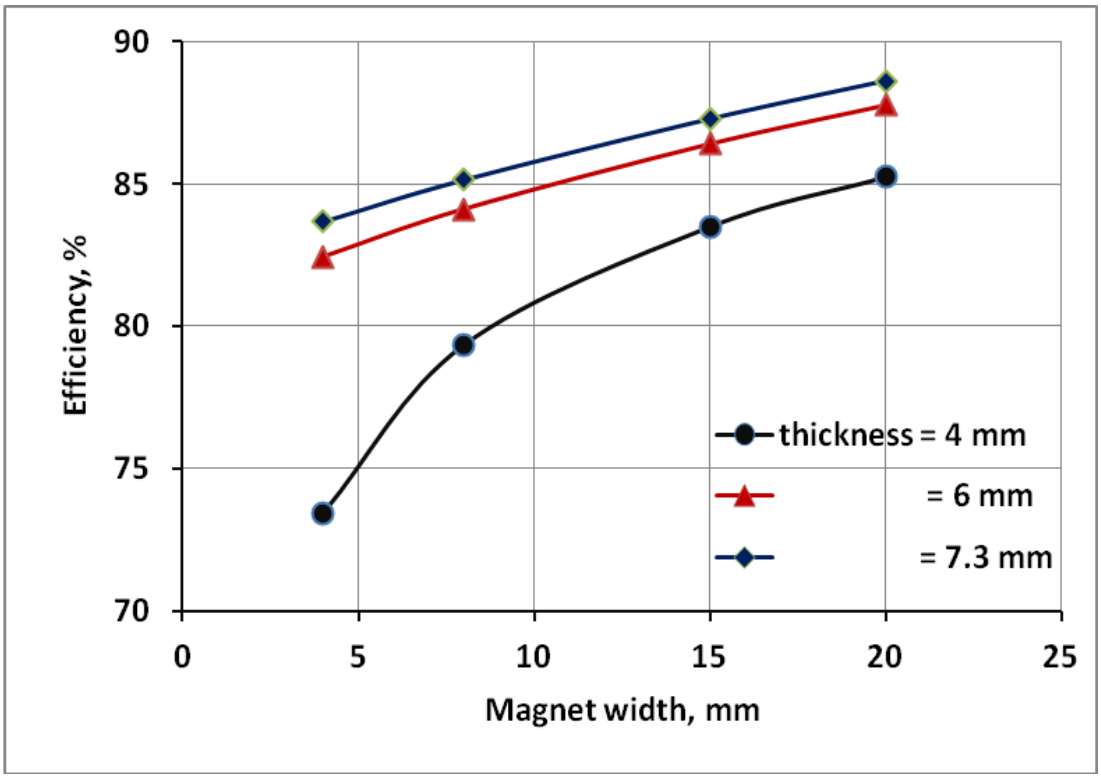

Fig. 4.8 Effect of magnet dimensions on the efficiency of PMSM

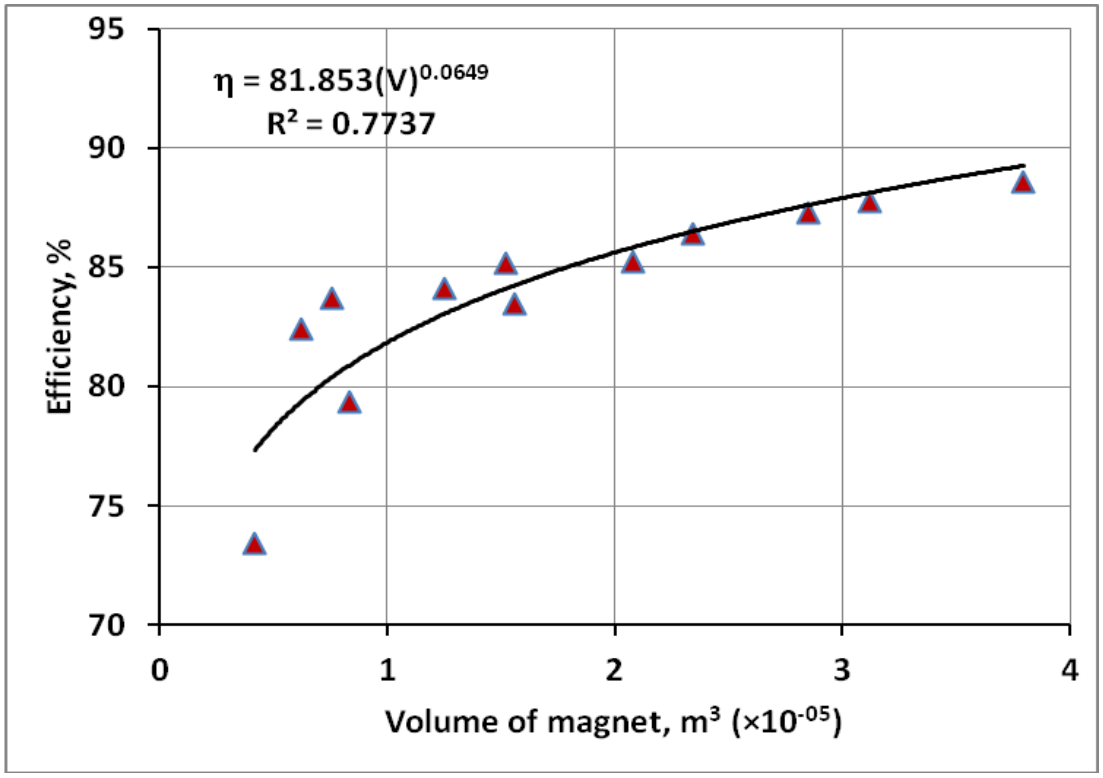

Fig. 4.9 Efficiency as a function of volume of the magnet

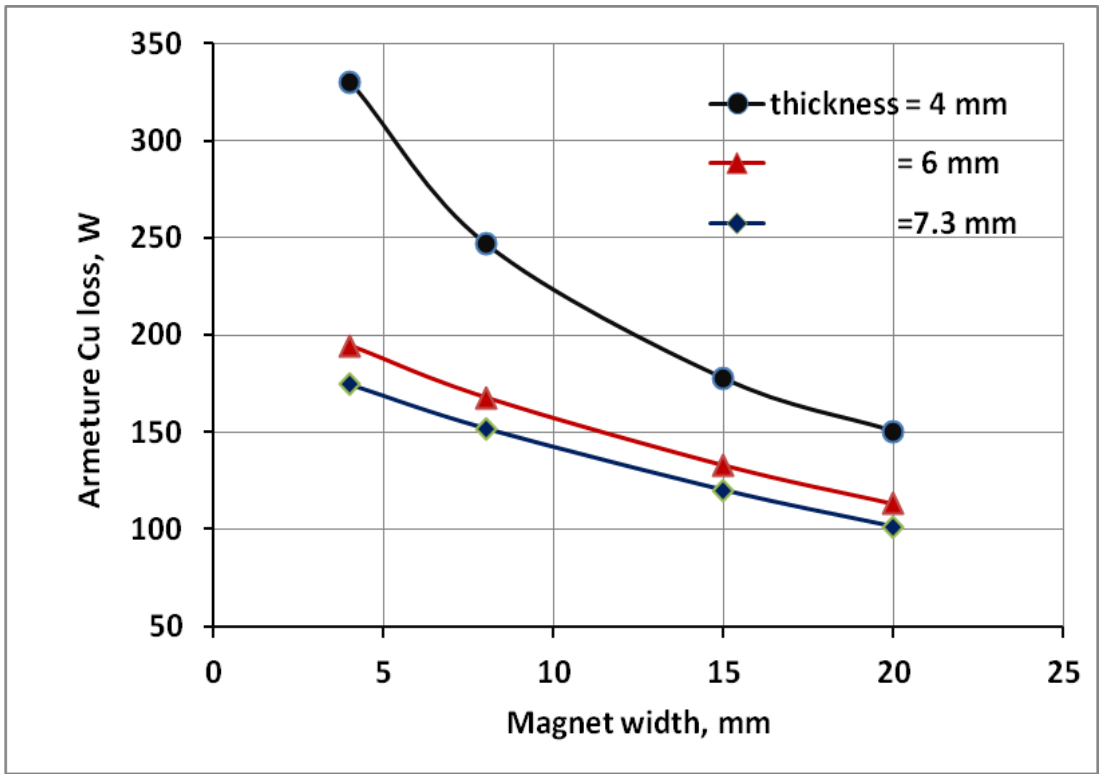

Fig. 4.10 Effect of magnet dimensions on the armature copper loss

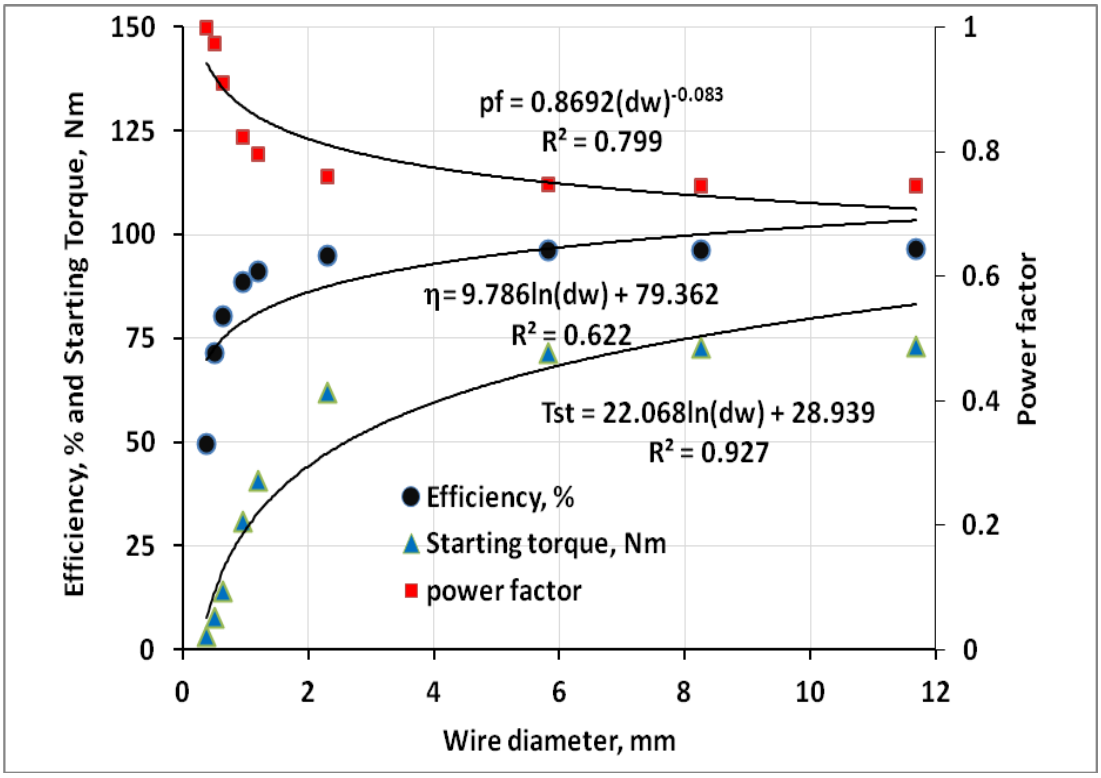

Fig. 4.11 Effect of wire diameter on power factor, efficiency and starting torque

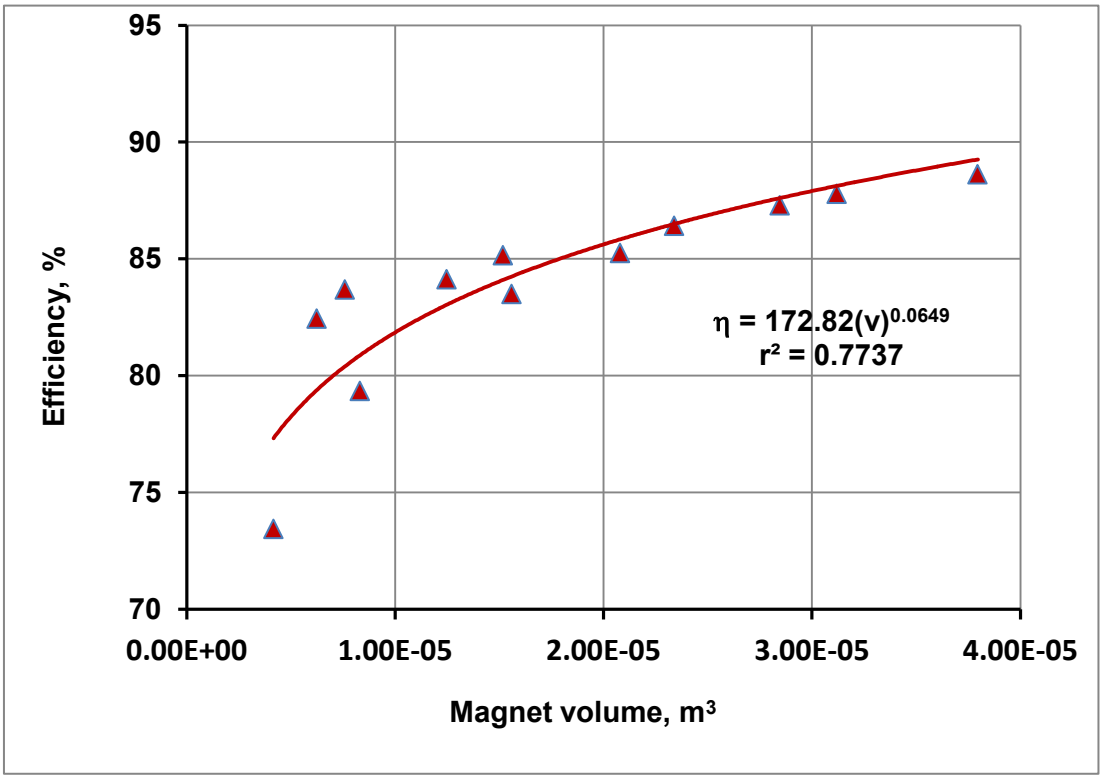

Fig. 4.12 Effect of magnet volume on the efficiency of PMSM

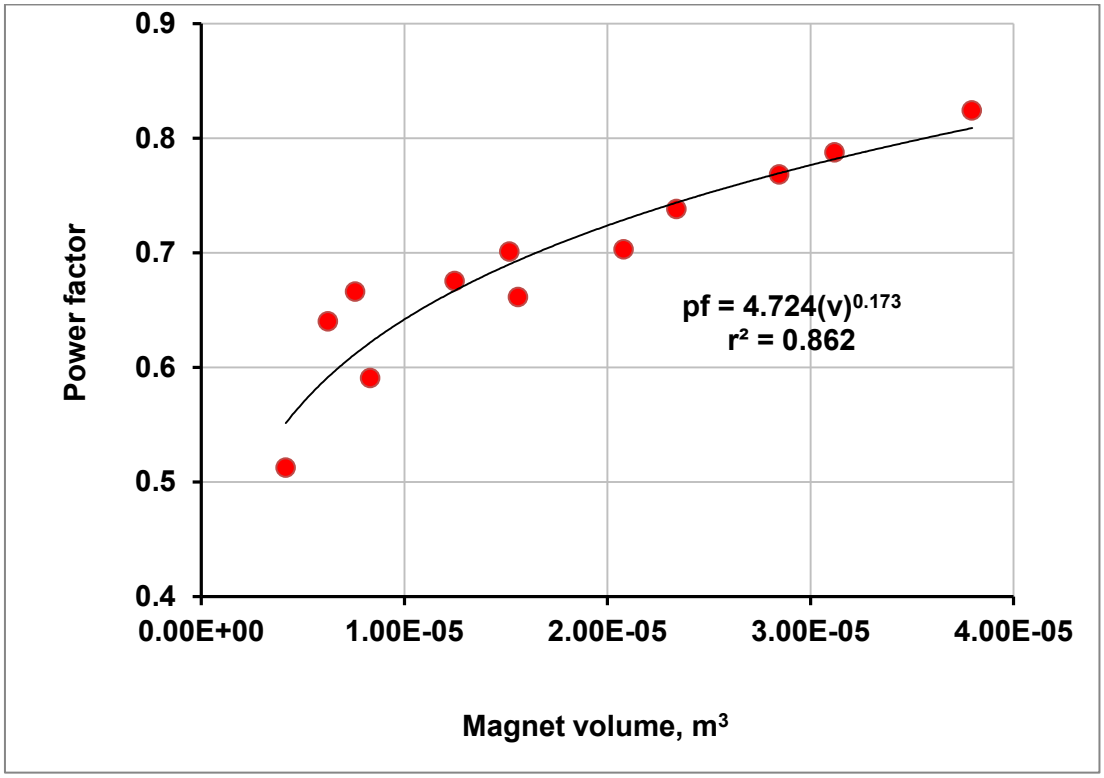

Fig. 4.13 Effect of magnet volume on the power factor of PMSM

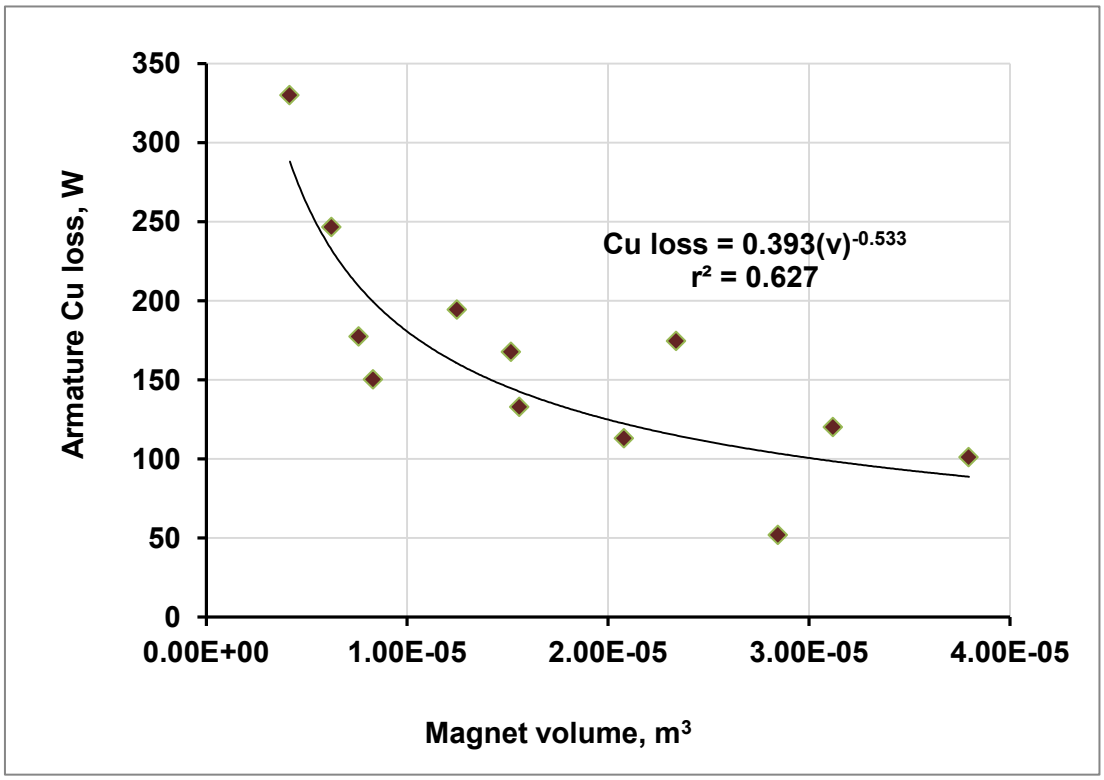

Fig. 4.14 Effect of magnet volume on the armature copper loss of PMSM

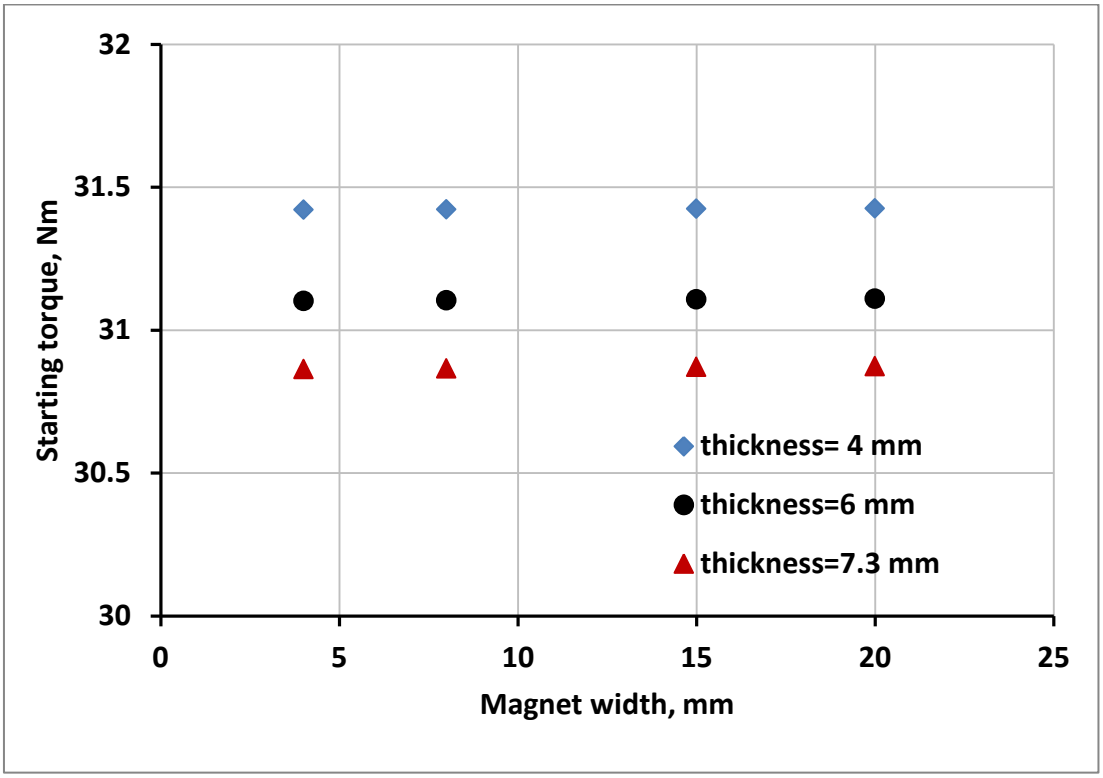

Fig. 4.15 Effect of magnet dimensions on the starting torque of PMSM

The effect of magnet volume on the PMSM performance parameters is presented in Figs. 4.11-4.14. These figures revealed that all performance parameters are significantly affected and there exists a non- linear relation with the magnet volume and the magnet dimensions. Hence, for optimal performance, proper selection of the magnet dimensions is of utmost importance in the design of PMSM.

A PMSM rotates by converting electrical energy to mechanical energy. The important parameters to study the performance of a motor are efficiency and power factor. The efficiency of the machine is directly related to the losses. In an electrical motor, general losses are iron loss and armature copper loss. In the present case, the iron loss was found to be varied between 1.05×10^{-5} W to 8.09×10^{-6} W whereas armature copper loss varies from 101.217 W to 330.1 W. The variance of copper loss was found to be 4774.7 W^2. Fig. 4.12 and Fig. 4.13 reveal that efficiency and power factor follows non linear relation with the magnet volume. These figures show that the rate of the increment of efficiency or power factor decreases with increase of magnet volume. The armature copper loss decreases rapidly with increase of magnet volume as depicted in Fig. 4.14.

The motor starting capability depends on the starting torque. The variation of motor starting torque with respect to magnet dimensions is shown in Fig. 4.15. This figure shows that the starting torque capacity remains between 30.85 N-m to 31.42 N-m. It also reveals that thickness is more prominent factor than width of a magnet for the starting torque capability of a PMSM. The results presented in Figs. 4.12-4.15 indicate that an optimal design of magnet volume is necessary for better performance of a PMSM.

A power law relation was found to be suitable between efficiency and volume of the magnet. The slope of two linear fitting between efficiency and volume of the magnet were found to be 7.94×10^5 and 2.26×10^5 for magnet volume $\leq 1.5\times10^{-05}$ m^3 and $>1.5\times10^{-05}$ m^3 respectively. Fig. 4.10 shows the armature copper loss as a function of magnet dimensions. This figure reveals that armature copper loss decreases as the magnet thickness and width were increasing. Similar trend was seen for iron loss but the magnitude of the iron loss is negligible as compared to Cu loss. From the above discussion, it is clear that different performance parameters depend on the magnet dimension. Hence, an optimum magnet dimension is desirable for better performance of the motor.

4.3 Taguchi Design Methodology

In Taguchi optimization method, different factors are selected with different levels to study the effect of these factors on the performance. The design of experiments (DoE) in Taguchi method uses specially created Orthogonal Arrays (OA) which allows reducing the number of experiments and time in conducting the experiments. In Taguchi method, a loss function is used to calculate the deviation between the experimental and the desired values. The Signal-to-Noise ratio (S/N) is obtained from the loss function. Three types of quality characteristics of S/N ratio are used in the analysis. These characteristics are the-lower-the-better, the-higher-the-better, and the-nominal-the-best. In the analysis, S/N ratio for each response is calculated as per response characteristics. In the present work, the motor efficiency, power factor, and starting torque were taken for maximization whereas armature copper loss was taken for minimization. Hence, for the first three responses, the-higher-the-better and for last response the-lower-the-better criteria were used. Equation 4.1 and Equation 4.2 describe the quality characteristics.

The-higher-the-better

$$\frac{S}{N} = -10log\left[\frac{1}{n}\sum_{i=1}^{n}\frac{1}{y_i^2}\right] \quad (4.1)$$

The-lower-the-better

$$\frac{S}{N} = -10log\left[\frac{1}{n}\sum_{i=1}^{n}y_i^2\right] \quad (4.2)$$

y_i is the i^{th} experimental data and n is the number of observations (Montgomery, 2009).

The selection of the arrays depends on the number of control factors and desired levels. The performance in terms of efficiency, power factor, starting torque etc. of PMSM depends on the several design parameters. As discussed earlier, the magnet size is one of the components which affect the performance of PMSM significantly.

4.3.1 Selection of factors and levels

The first step in the Taguchi method of optimization and analysis is the selection of factors and levels. In the present investigation, the magnet dimension such as width and thickness were taken as main factors with 4 levels.

Table 4.2 Design parameters and their levels

Parameters	**Levels**			
	1	2	3	4
Magnet Width (mm)	4	8	15	20
Magnet Thickness (mm)	4	6	7.3	7.38

Table 4.3 Details of the factors and responses

Expt No.	Magnet size		Response				S/N ratios (dB)		
	Width (mm)	Thickness (mm)	η (%)	pf	T_{st} (N-m)	Cu loss (W)	η	pf	Tst
1	4	4	73.427	0.512	31.421	330.091	37.317	-5.807	29.944
2	4	6	82.439	0.64	31.102	246.615	38.323	-3.876	29.856
3	4	7.3	83.687	0.666	30.864	177.486	38.453	-3.536	29.789
4	4	7.38	83.746	0.667	30.843	150.344	38.459	-3.519	29.783
5	8	4	79.341	0.591	31.422	194.397	37.99	-4.574	29.945
6	8	6	84.118	0.675	31.104	167.72	38.498	-3.411	29.856
7	8	7.3	85.147	0.701	30.867	132.895	38.603	-3.086	29.79
8	8	7.38	85.181	0.702	30.846	113.04	38.607	-3.075	29.784
9	15	4	83.493	0.661	31.424	174.52	38.433	-3.593	29.945
10	15	6	86.41	0.738	31.108	151.908	38.731	-2.639	29.857
11	15	7.3	87.282	0.768	30.871	120.143	38.818	-2.289	29.791
12	15	7.38	87.278	0.768	30.851	101.217	38.818	-2.291	29.785
13	20	4	85.242	0.703	31.426	173.601	38.613	-3.056	29.946
14	20	6	87.775	0.787	31.11	151.385	38.867	-2.075	29.858
15	20	7.3	88.61	0.824	30.874	12.198	38.95	-1.679	29.792
16	20	7.38	88.582	0.823	30.854	101.586	38.947	-1.693	29.786

The minimum and maximum dimensions (levels) were selected on the basis of several trial designs in the RMxprt design software. The levels and the associated parameters are presented in Table 4.2. The responses taken in this study were power factor, efficiency, and starting torque. In this study, there were two control factors each at four levels. Full factorial experiment with 2 factors and 4 levels require $4^2 = 16$ number of experiments (Montgomery, 2009). Hence, L16 array was selected and the details of the factors and responses are presented in Table 4.3.

4.3.2 Analysis of the Signal-to-Noise (S/N) ratio

The PMSM efficiency, power factor, and starting torque for different values of magnet width and thickness were used for optimization using Taguchi method. The optimization of the measured control factors are given by signal-to-noise (S/N) ratios. It is known that high values of power factor, efficiency, and starting torque are requirement of any motor for good performance. Hence, the-higher-the-better equation was used for these responses. Similarly, armature copper loss should be minimized for better efficiency. Hence, the-lower-the-better criterion was used for this response. Table 4.3 shows the values of S/N ratio (in dB) for these parameters. Analysis of the effect of each control factor, *i.e.,* magnet width and thickness on PMSM efficiency, power factor, starting torque, and armature copper loss was performed with S/N response in Table 4.4.

Table 4.4: S/N response table for PMSM efficiency, power factor, starting torque and armature copper loss

Levels	**Control factors**							
	Efficiency		**Power factor**		**Starting torque**		**Cu loss**	
	width	**thickness**	**width**	**thickness**	**width**	**thickness**	**width**	**thickness**
Level 1	38.14	38.09	-4.184	-4.258	29.84	**29.95**	-46.68	-46.44
Level 2	38.42	38.60	-3.536	-3.000	29.84	29.86	-43.45	-44.89
Level 3	38.70	**38.71**	-2.703	**-2.648**	29.84	29.79	-42.54	**-37.69**
Level 4	**38.84**	38.71	**-2.216**	-2.644	**29.85**	29.78	**-37.56**	-41.21
Delta	0.71	0.62	2.059	1.613	0	0.16	9.12	8.75
Rank	1	2	1	2	2	1	1	2

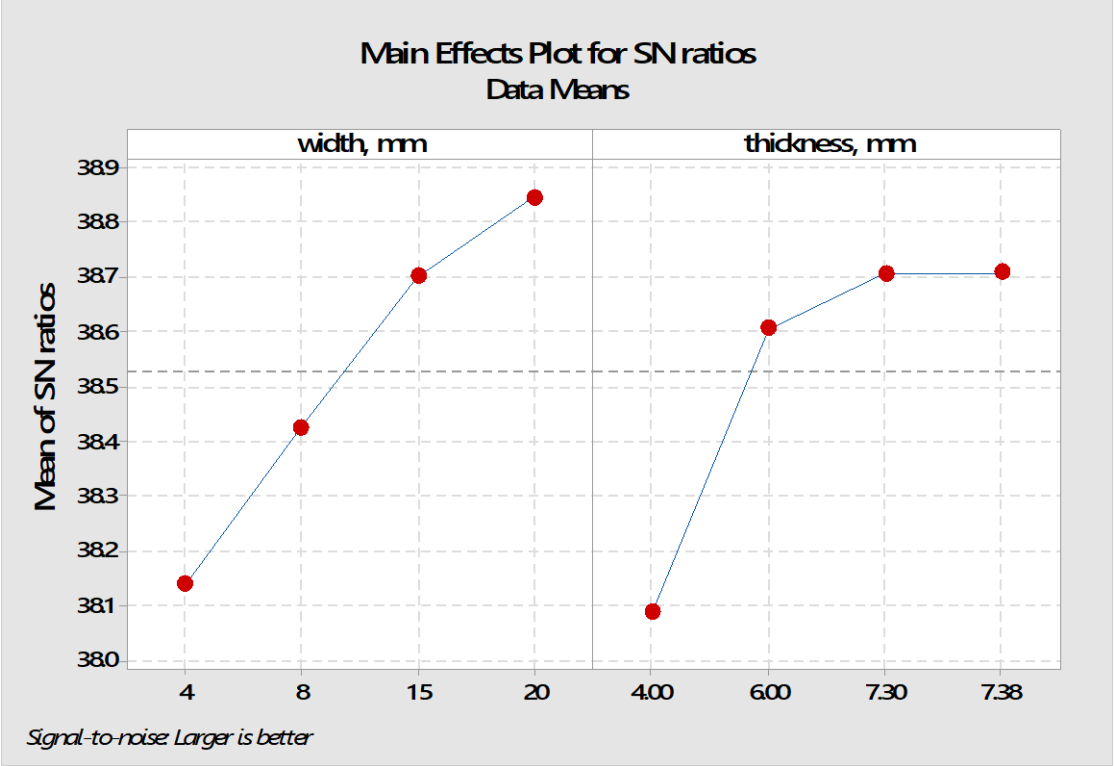

Fig. 4.16 Effect of magnet dimension on average S/N ratio for PMSM efficiency

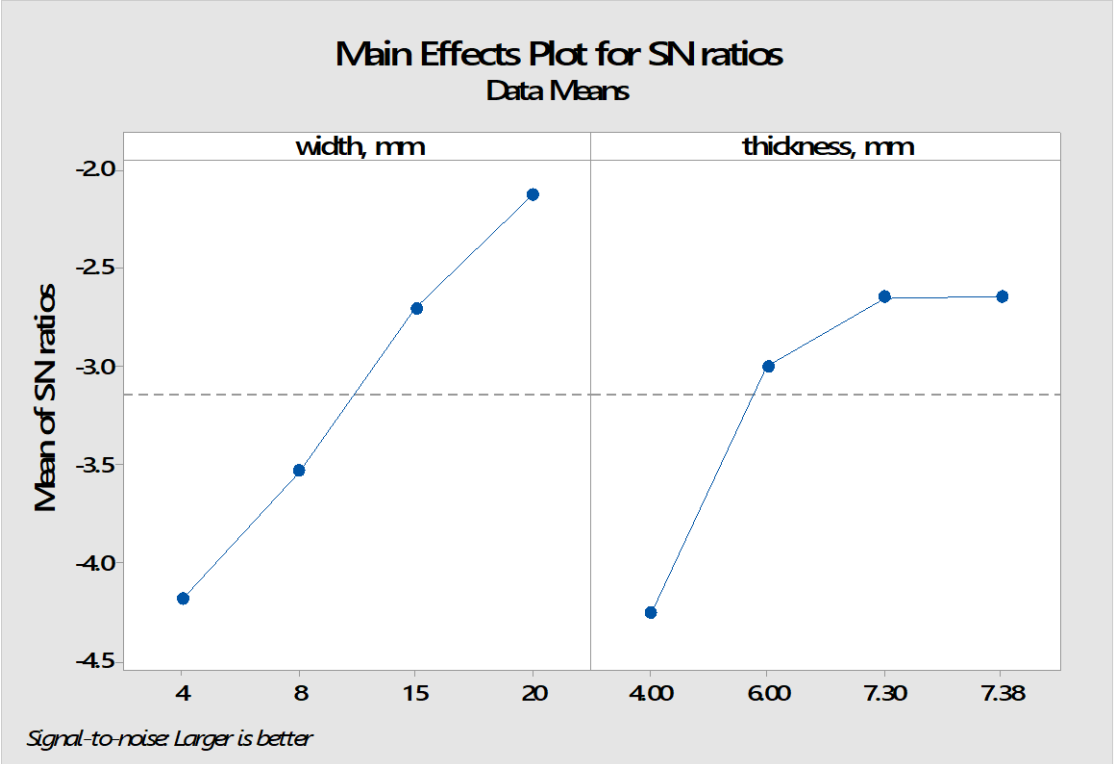

Fig. 4.17 Effect of magnet dimension on average S/N ratio for PMSM power factor

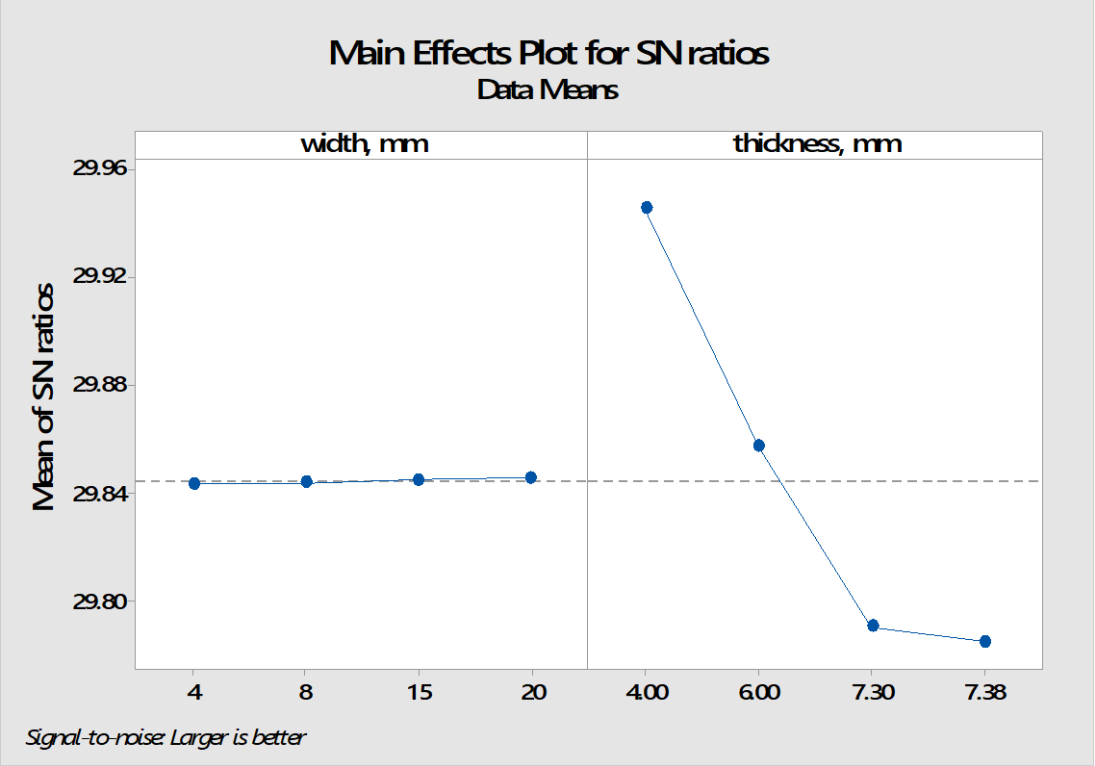

Fig. 4.18 Effect of magnet dimension on average S/N ratio for PMSM starting torque

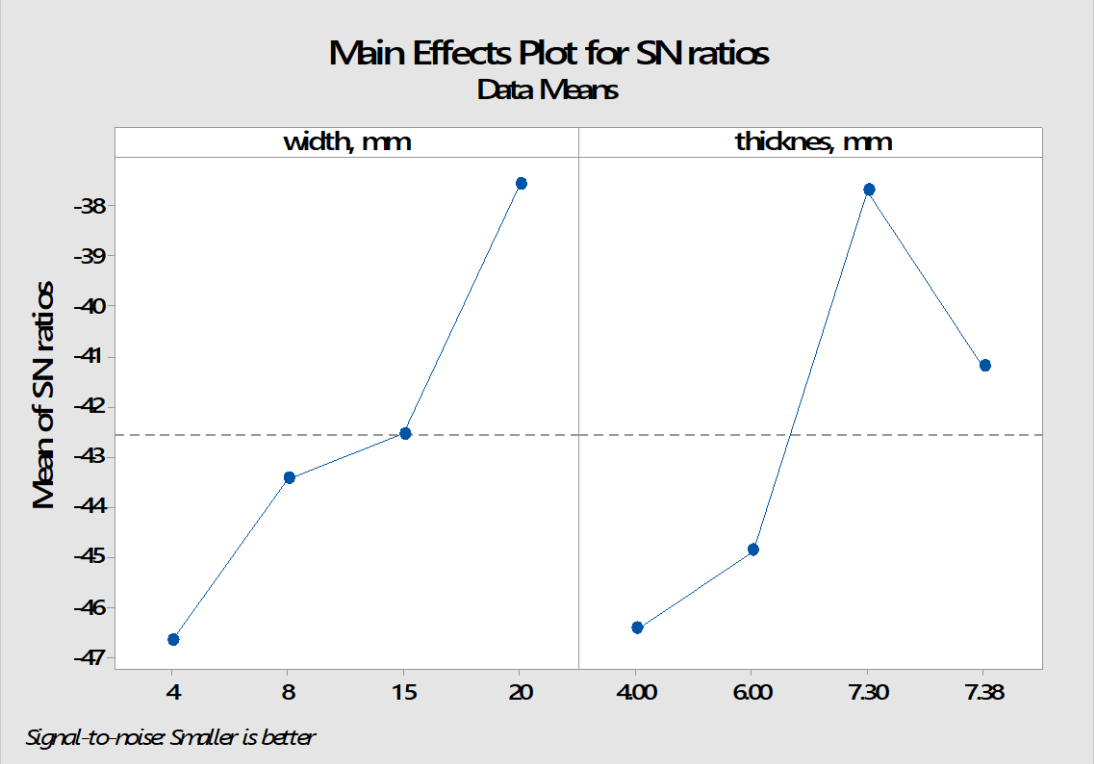

Fig. 4.19 Effect of magnet dimension on average S/N ratio for PMSM armature copper loss

In Table 4.4, the highest values of S/N ratio for each control factor are written in bold. The S/N ratio shown in Table 4.4 reveals that S/N ratios for the factors giving the best efficiency value are specified as factor A (Level 4, S/N = 38.84) and factor B (Level 3, S/N = 38.71). Hence, an optimum efficiency is obtained with magnet width of 20 mm and thickness of 7.30 mm. Similarly, optimum power factor are found for factor A (level 4, S/N = -2.216 and level 3, S/N = -2.648). Optimum value of stating torque is found for magnet width = 20 mm and thickness = 4 mm. The optimum value of S/N ratio for copper loss is obtained for level 4 and level 3 of factor A and factor B respectively. The value of delta is used to find the order of influence of various factors on the response. Based on the value of delta, rank of the factors for a particular response is assigned.

4.3.3 S/N ratio and analysis of magnet position in rotor

The effect of magnet size parameters i.e., *w* and *t*, and magnet position parameters i.e., *D1*, *O1,* and Rib on the S/N ratio for motor efficiency and power factor were investigated. Parametric values and their levels are presented in Table 4.5. A total of five control factors were considered in which two factors (magnet width and thickness) were at 4 levels and three factors (magnet position in the rotor i.e., *D1*, *O1,* and Rib) were at 2 levels. Mixed full factorial experiment with 2 factors at 4 levels and 3 factors at 2 levels requires $4^2 \times 2^3 = 128$ number of experiments which can be reduced to one-eighth of 128. Hence, L16 array was selected and the details of the factors are presented in Table 4.6.

Table 4.5: Design parameters and their levels

Parameters	**Levels**			
	1	2	3	4
Magnet Width, w (mm)	4	8	15	20
Magnet Thickness, t (mm)	4	6	7.3	7.38
D1 (mm)	63	64	-	-
O1 (mm)	21	23	-	-
Rib (mm)	0.5	4	-	-

Table 4.6: L16 array of magnet and position data

w	t	D1	O1	Rib
1	1	1	1	1
1	2	1	1	1
1	3	2	2	2
1	4	2	2	2
2	1	1	2	2
2	2	1	2	2
2	3	2	1	1
2	4	2	1	1
3	1	2	1	2
3	2	2	1	2
3	3	1	2	1
3	4	1	2	1
4	1	2	2	1
4	2	2	2	1
4	3	1	1	2
4	4	1	1	2

L16 Orthogonal Array (OA) was used in Taguchi method and the results of S/N ratio for power factor and efficiency are shown in Fig. 4.20 and Fig. 4.21, respectively. Fig. 4.20 and Fig. 4.21 reveal that S/N ratios for the factors giving the best power factor and efficiency are specified as w = 20 mm, t =7.38 mm, D_1 =64 mm, , O_1 =23 mm (all are factor 4, 4, 2, and 2) and Rib = 0.5 mm (factor 1).

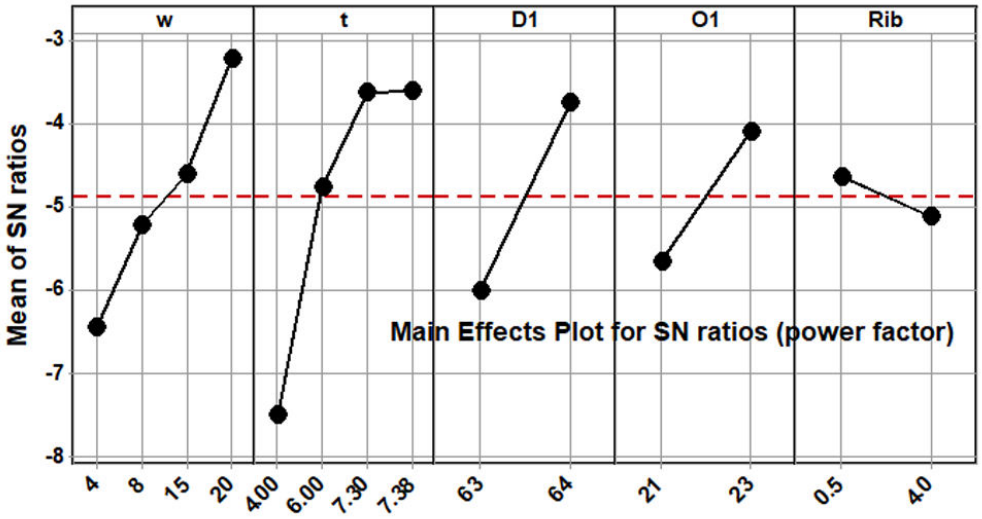

Fig. 4.20 Effect of magnet size and position on the S/N ratio for power factor

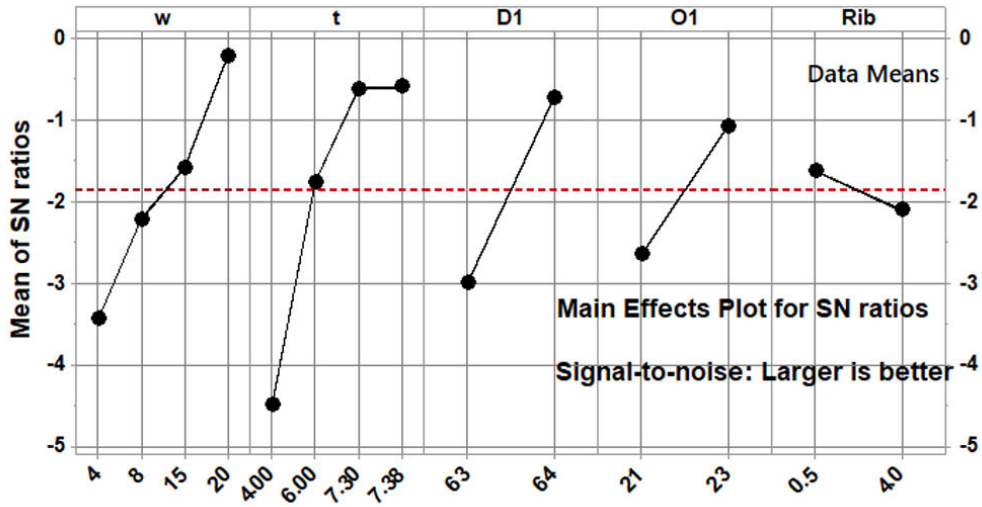

Fig.4.21 Effect of magnet size and position on the S/N ratio for efficiency

4.4 Objective Function and Optimization

PMSM design can be improved by using modern modeling, simulation, and optimization techniques. In optimal design of a product, it is important to identify the desirable quantity or measure that needed in the product. Hence, before looking for optimal design solution, it is important to identify characteristics which contribute the most to the overall value of the design. The magnet design of PMSM motor involves multiple criteria/objectives such as efficiency, power factor, rated torque, losses, starting torque, etc.. Therefore, the magnet size in a PMSM was optimized with

multiple objective functions. These objective functions may be conflicting in nature, but weighted approach can be used for minimizing the issue. In this work, multiple objective functions were derived from the 16 combinations of magnet dimension and the performance parameters of the PMSM. These objective functions are derived using multiple regression analysis. Here, the regression analyses are carried out for modeling and analyzing the effect of magnet dimension, width and thickness as dependent variables and efficiency, power factor, and starting torque as independent variables. Full quadratic models are developed on the basis of regression analysis, and the predictive equations are given in Equations 4.3 – 4.6.

$$\eta = 43.906 + 1.4997w + 8.741t - 0.0151w^2 - 0.4954t^2 - 0.1176wt \quad (4.3)$$

$$pf = 0.094 + 0.0143w + 0.1261t - 4.728 \times 10^{-5}w^2 - 7.354 \times 10^{-3}t^2 - 4.964 \times 10^{-4}wt \quad (4.4)$$

$$T_{st} = 31.873 - 2.073 \times 10^{-4}w - 8.235 \times 10^{-2}t - 5.147 \times 10^{-7}w^2 - 7.771 \times 10^{-3}t^2 - 1.21 \times 10^{-4}wt \quad (4.5)$$

$$Cu\ loss = 326.24 - 16.888w + 28.345t + 0.111w^2 - 6.407t^2 + 1.246wt \quad (4.6)$$

The corresponding r^2 values are 0.972, 0.992, 0.999, and 0.91 for efficiency, power factor, starting torque, and armature copper loss, respectively.

Usually, several solutions exist for multi-objective optimization problems. Therefore, different researchers have defined the term "solving a multi-objective optimization problem" in various ways. Many methods convert the multiple objective functions into a single objective function by assigning equal weightage or different weightage to each objective function. This is known as a scalarized problem. Proper scalarization of the functions ensures an optimal solution to a great extent.

The general formulation of multiple objective functions maximization is

$$max \quad g(f_1(x), f_2(x) \dots \dots \dots f_k(x)) \quad (4.7)$$

The commonly used scalarization is linear scalarization which is linear summation of weighted objective functions and is written as

$$max \sum_{i=1}^{k} \emptyset_i f_i(x) \quad (4.8)$$

where the weights $\emptyset_i$>0 .

Equation (4.8) can be converted into minimization problem considering inverse of the functions as

$$\sum_{i=1}^{k} \frac{\emptyset_i}{f_i(x)} \quad (4.9)$$

subjected to $l \ll x \ll u$

where *u* and *l* are upper and lower limits of *x,* respectively. The objective functions considered in the present investigation are given in Equations 4.3 – 4.6. The solution of the Equation 4.9 is made using MATLAB's $fminsearch$ subroutine. One set of the optimized dimensions of the magnet is *w* = 25.5 mm and *t* = 5.45 mm. It is seen that optimized solution greatly depends on the selection of proper weightage assigned to each objective function. Comparative solutions are shown in Table 4.7.

Table 4.7: Optimum solution of magnet width and thickness for PMSM with functions values

Method	**Width (mm)**	**Thickness (mm)**	**η (%)**	**pf**	**T_{st} (N-m)**
Optimization	28.54	5.45	89.13	0.855	31.168
RMxprt	28.54	5.45	89.611	0.877	31.145

The PMSM performance is compared with the commonly used induction motor of 1.07 kW capacity (**Niu *et al.,* 2015**). The average weight of a commercially available induction motor is about 26 kg whereas the present design of same capacity PMSM was found to be just one-fifth of the induction motor. The rated efficiency as per IE2 efficiency class for an induction motor is 81.5%. The PMSM with 20 mm width and 7.3 mm thick magnet size and 0.965 wire diameter shows 88.61% efficiency. The full load line current obtained for LSPMSM was 3.69 A. The starting torque of an induction motor having capacity of 1.07 kW is about 14 Nm whereas the

PMSM shows a variation between 30.87 Nm to 31.42 Nm for different magnet volumes. This shows that PMSM is more compact having a better performance than an induction motor of the same capacity.

4.4.1 Validation

The validation of the model was performed considering the different combination of the magnet size and estimating the performance in term of motor efficiency, power factor, starting torque, and armature copper loss. The different combination of magnet width and thickness considered were (20, 7.3), (20, 7), (25, 5.0), (28.67, 5.45), (28.54, 5.45), and (30, 5.45) in mm. The predicted and RMxprt simulated results are shown in Table 4.8 – Table 4.11. The percentage difference was found to be below 1%, 3%, 0.2%, and 5% for efficiency, power factor, starting torque, and armature copper loss, respectively. This indicates that correlations developed for efficiency and other factors with magnet dimensions are most suitable for the prediction and optimization of the magnet size.

Table 4.8: Comparison of predicted and RMxprt simulated efficiency

Magnet dimension, mm		Efficiency, %		% Difference
Width	**Thickness**	**RMxprt**	**Regression**	
20.00	7.30	88.610	88.180	0.485
20.00	7.00	88.606	88.392	0.241
25.00	5.00	88.524	88.656	0.149
28.67	5.45	89.639	89.133	0.564
30.00	5.45	89.902	89.101	0.890
28.54	5.45	89.611	89.133	0.533

Table 4.9 Comparison of predicted and RMxprt simulated power factor

Magnet dimension, mm		Power factor		% Difference
Width	Thickness	RMxprt	Regression	
20.00	7.30	0.834	0.817	2.009
20.00	7.00	0.824	0.814	1.220
25.00	5.00	0.820	0.807	1.640
28.67	5.45	0.879	0.856	2.575
30.00	5.45	0.895	0.868	3.006
28.54	5.45	0.877	0.855	2.484

Table 4.10 Comparison of predicted and RMxprt simulated starting torque

Magnet dimension, mm		Starting Torque, N-m		% Difference
Width	**Thickness**	**RMxprt**	**Regression**	
20.00	7.30	30.874	30.872	0.007
20.00	7.00	30.887	30.929	0.137
25.00	5.00	31.208	31.277	0.223
28.67	5.45	31.145	31.207	0.198
30.00	5.45	31.195	31.207	0.040
28.54	5.45	31.145	31.207	0.198

Table 4.11 Comparison of predicted and RMxprt simulated armature Cu loss

Magnet dimension, mm		Cu loss, W		
Width	**Thickness**	**RMxprt**	**Regression**	**% Difference**
20.00	7.30	101.217	98.718	2.46895
20.00	7.00	101.276	97.792	3.4401
25.00	5.00	102.422	101.715	0.69028
28.67	5.45	86.938	89.235	2.64211
30.00	5.45	83.4095	87.397	4.78103
28.54	5.45	87.3283	87.450	0.13936

4.5 Response Surface Method

The Response Surface Method (RSM) is a combination of mathematical and statistical techniques used for evaluation of a response or multiple responses. Generally, the response surface is described by polynomial equations and used for optimization of a required output called response. Polynomial representation was used for optimization of power factor and efficiency using RSM. These polynomials are given in Equation 4.11 and Equation 4.12, respectively. Using the D-optimal design criterion, 52 data points were selected. These data points were selected according to the Design of Experiments (DoE) available for five factors: two at four levels and three at two levels. The targets were power factor and efficiency. The ranges selected for different parameters were:

Parameters ranges

$$4\ mm \leq w \leq 30\ mm$$

$$4\ mm \leq t \leq 7.38mm$$

$$63mm \leq D1 \leq 64mm$$

$$21mm \leq O1 \leq 23mm$$

$$0.5mm \leq Rib \leq 4mm \tag{4.10}$$

Regression Equations

$$power\ factor = -12.66 - 0.0981 \times w + 0.401 \times t + 0.164D1 + 0.1092 \times O1 + 1.942 \times Rib + 0.00473 \times w \times O1 - 0.01561 \times t \times O1 - 0.0304 \times D1 \times Rib \tag{4.11}$$

$$efficiency(\%) = -2734 - 25.7w + 35.48t + 39.4D1 + 124.6O1 - 2.145 \times Rib - 0.1162 \times wt + 0.414w \times D1 + 0.206w \times Rib - 1.396t \times O1 - 1.758D1 \times O1 \tag{4.12}$$

The results of the analysis of variance of the regression coefficients and their interaction are shown in Table 4.12. Table 4.13 compares the results obtained from different methods with the ANSYS results.

The optimal solution is obtained by combining the Equations 4.11 and 4.12 with the range of the independent variables i.e., magnet width, thickness, *D1, O1* and Rib size as given in Equation 4.10. The optimum solutions are w =30 mm, t =5.45 mm, $D1$ =63 mm, $O1$ =23 mm, and Rib =0.5 mm as shown in Fig. 4.22.

Table 4.12: Analysis of variance (ANOVA) of regression coefficient of power factor model

Source	DF	Adj SS	Adj MS	F-Value	P-Value
Model	11	0.836538	0.076049	47.57	0.000
Linear	5	0.045357	0.009071	5.67	0.000
W	1	0.013869	0.013869	8.68	0.005
T	1	0.004153	0.004153	2.60	0.115
D1	1	0.017856	0.017856	11.17	0.002
O1	1	0.025609	0.025609	16.02	0.000
Rib	1	0.028227	0.028227	17.66	0.000
2-Way Interaction	6	0.072886	0.012148	7.60	0.000
w*D1	1	0.014238	0.014238	8.91	0.005
w*Rib	1	0.017262	0.017262	10.80	0.002
t*D1	1	0.009767	0.009767	6.11	0.018
t*O1	1	0.029185	0.029185	18.26	0.000
t*Rib	1	0.017225	0.017225	10.77	0.002
D1*O1	1	0.022621	0.022621	14.15	0.001
Error	40	0.063947	0.001599		
Lack-of-Fit	33	0.020955	0.000635	0.10	1.000
Pure Error	7	0.042992	0.006142		
Total	51	0.900485			
Critical $F_{11,51}$= 1.92 $F_{1,51}$=4.04					

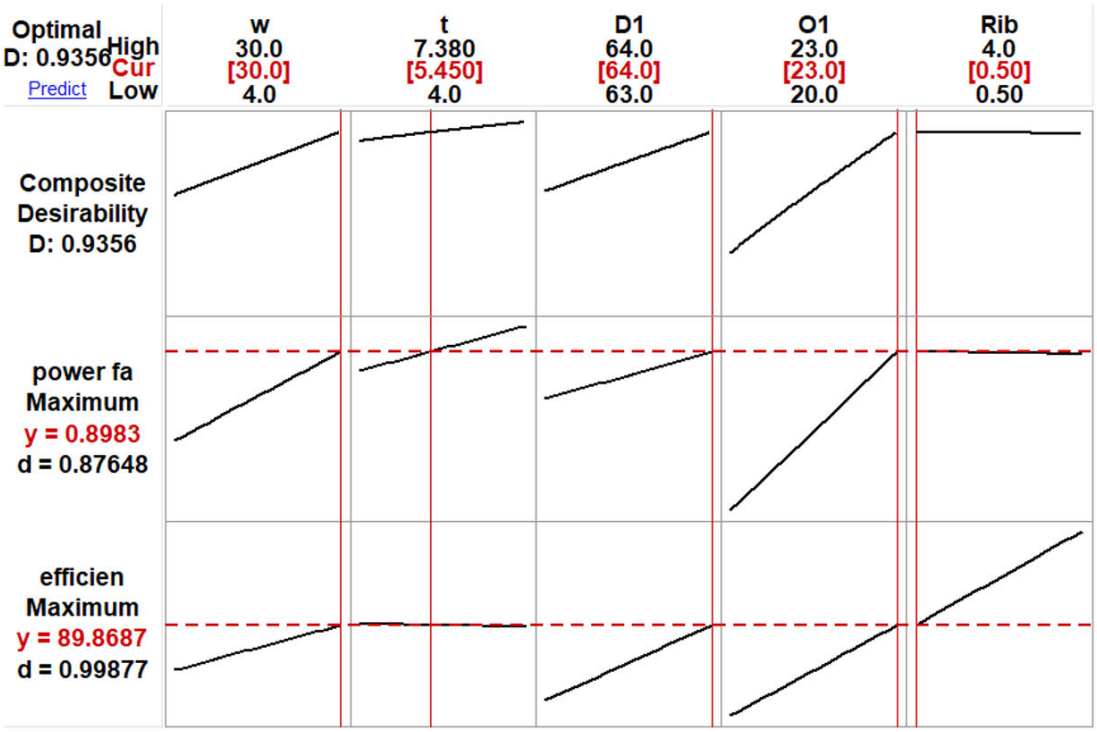

Fig. 4.22 Optimum parameters and corresponding efficiency and power factor

The predicted values of efficiency and power factor were 89.87 % and 0.898 respectively. The optimal D-value was 0.936. These optimum responses by RSM are compared with ANSYS Maxwell results in Table 4.13. It was found that the difference is less than 1%. It can be seen from Table 4.13 that the solution obtained from RSM and Taguchi methods are very close to ANSYS results and hence accepted for further performance studies of PMSM designed with optimum values of w =30 mm, t =5.45 mm, $D1$ =63 mm, $O1$ =23 mm, and Rib =0.5.

Table 4.13 Comparison of RSM, regression and ANSYS results

	RSM	ANSYS	% diff	Regression	% abs diff
Efficiency	89.868	89.902	0.038	89.870	0.036
Power Factor	0.898	0.895	0.335	0.897	0.223

The results shown in Fig. 4.22 and Table 4.12 reveal that the optimum parameters of 1.07 kW PMSM are w = 20 mm, t = 5.45 mm, D_1 =64 mm, O_1 =23 mm and *Rib*=0.5 mm. All the performance simulations were done using the optimum designed PMSM.

4.6 Performance Simulation

The result of the different performance parameters of designed PMSM is achieved in ANSYS Simplorer. The PMSM designed in ANSYS Maxwell was co-simulated with the drive system designed in ANSYS Simplorer. The complete drive system consists of IGBT inverter, PMSM coupled with DC Generator for electrical loading of the PMSM and a control circuit for switching of the IGBTs in the inverter circuit. In the control circuit, pulse width modulation (PWM) technique was used by comparing three sinusoidal signals having frequency of 50 Hz, each displaced from one another by 120 degrees, with a triangular carrier signal having frequency of 10 kHz. The complete drive system is shown in Fig. 4.23.

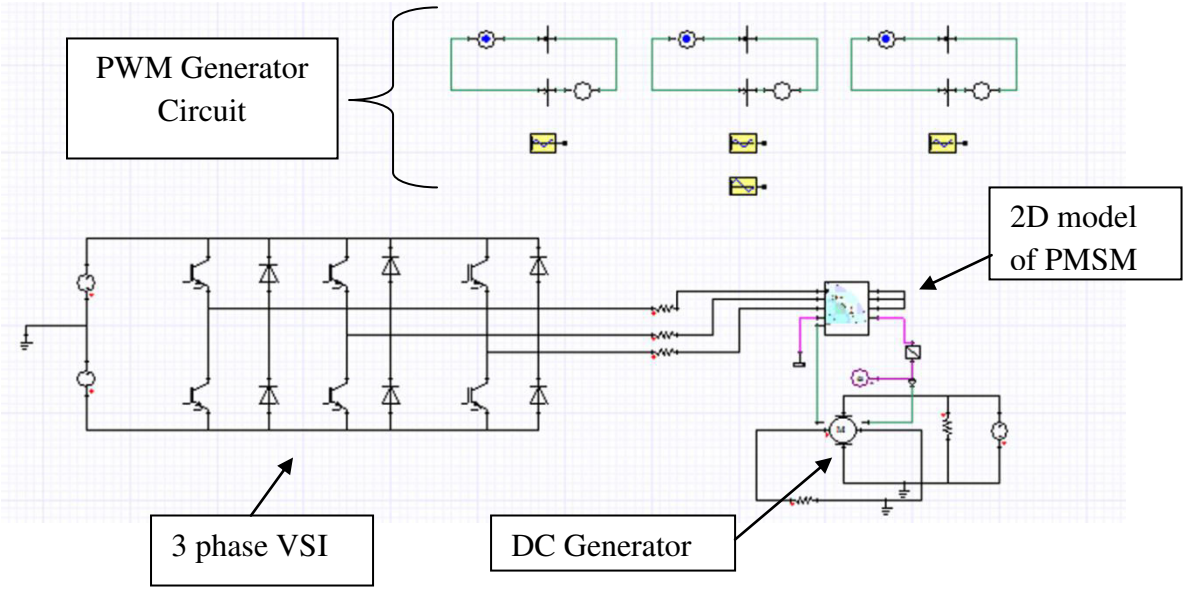

Fig. 4.23 Drive system for PMSM

4.6.1 Line current

The drive was run at different speeds *viz.,* 2700 rpm, 3000 rpm and 3300 rpm at full load condition. The input line current for the three phases were recorded for 1 second and the variation of line current for each phase, *i.e.,* I_a, I_b and I_c with time is presented in Fig. 4.24 to Fig. 4.26 for different speeds.

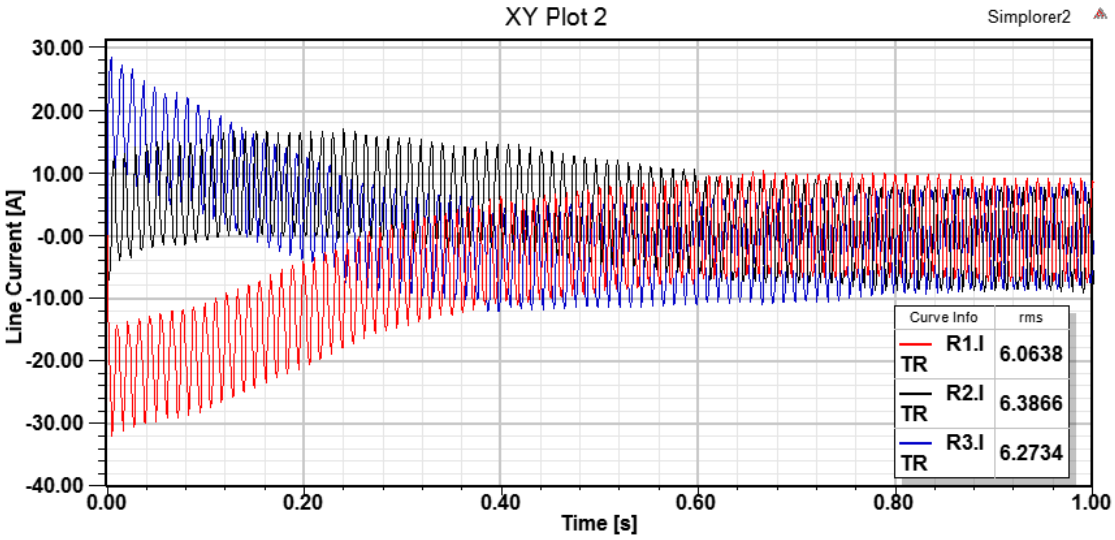

Fig. 4.24 Variation of three phase line currents with time at 2700 rpm

The simulation result shown in Fig. 4.24 indicates that the transient period remains for almost 0.6 second after which the line current reached a steady state condition. The steady state root mean square (RMS) line current for each phase is indicated in the Fig. 4.24. These values were $I_a = 6.064$ A, $I_b = 6.387$ A, and $I_c = 6.273$ A.

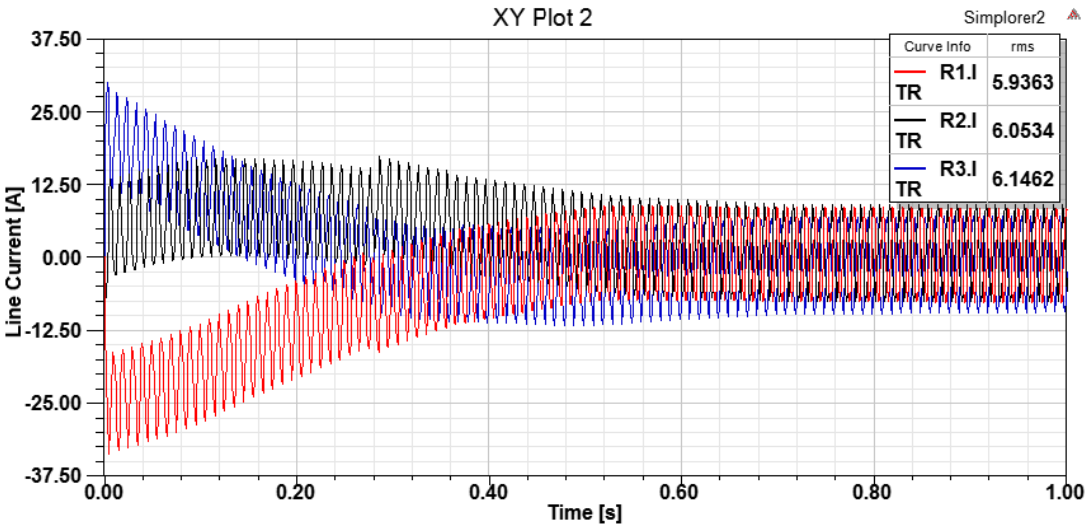

Fig. 4.25 Variation of line currents at 3000 rpm

The variation of line current at 3000 rpm is shown in Fig. 4.25. The steady state appears at 0.6 second in this case also. The steady state RMS input line currents for three phase of PMSM were $I_a = 5.936$ A, $I_b = 6.053$ A, and $I_c = 6.146$ A. Similarly, the RMS input line currents at 3300 rpm were found to be $I_a = 5.983$ A, $I_b = 5.954$ A, and $I_c = 5.893$ A as shown in Fig. 4.26.

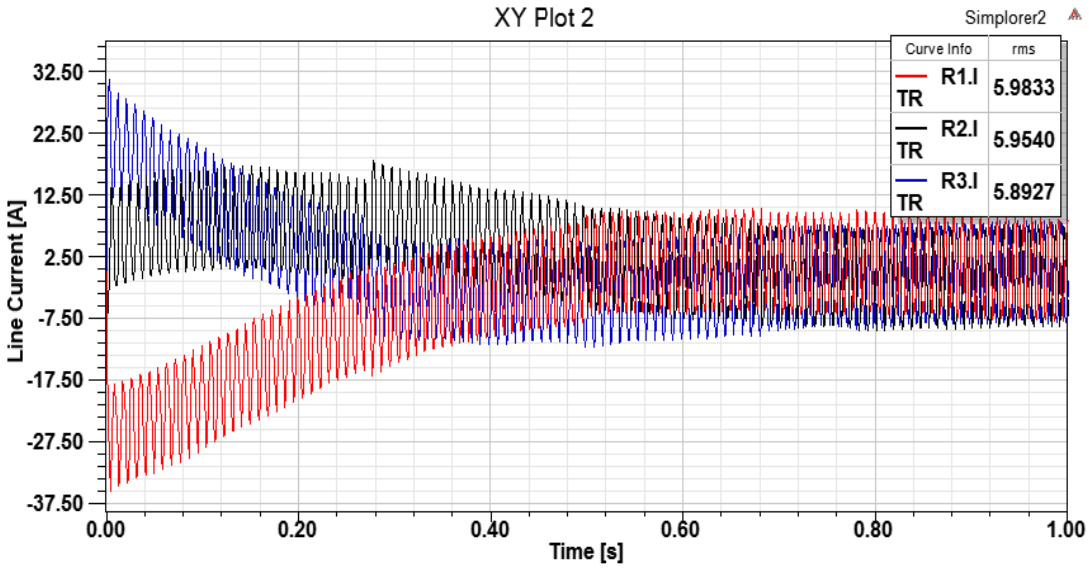

Fig. 4.26 Variation of line current at 3300 rpm

At around 0.28 second, a sudden increase in line current value can be seen when the machine was run at 3300 rpm. A similar increase in the line current value can also be seen when the machine was run at 3000 rpm. However, the magnitude of the peak that occurred in case of 3300 rpm was more than that of 3000 rpm. Any such peak is not seen when the machine was run at 2700 rpm. From the figures, it can be seen that magnitude of increase is very small and that occurs during the transient phase and hence it will not affect the performance parameters of PMSM.

4.6.2 Load Torque

Load torque is the torque measured at the load terminals. Load torque is the mechanical output of the electromagnetic torque generated in the armature of the motor and remains almost unchanged after the steady state is reached. The motor was run at three different speeds *viz.*, 2700 rpm, 3000 rpm, and 3300 rpm under full load condition. The load torque was recorded upto 1 second for each of the speeds at full load condition. The variation of load torque with time is shown in Fig. 4.27 to Fig. 4.29 for three different speeds.

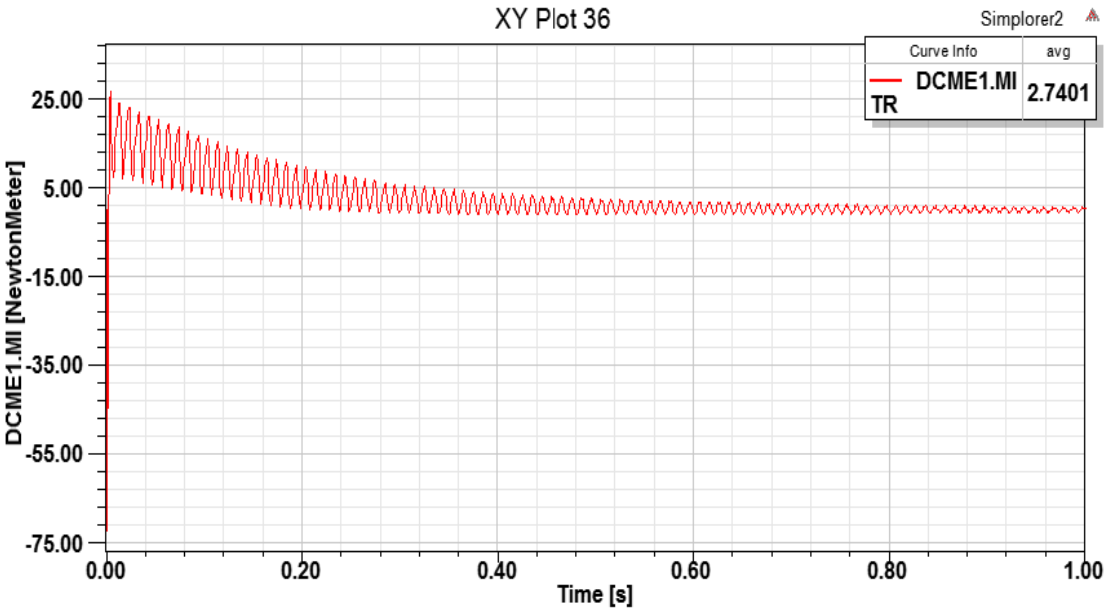

Fig. 4.27 Variation of load torque with time at 2700 rpm

Fig. 4.27 shows that the torque reaches a steady state value after 0.6 sec and an average load torque of 2.74 N-m is obtained at 2700 rpm during simulation.

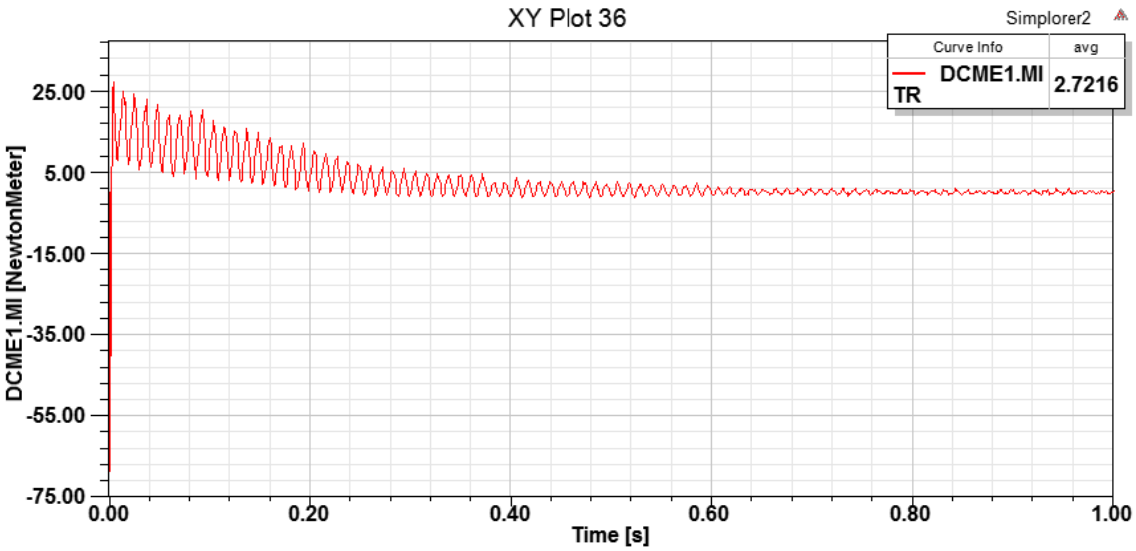

Fig. 4.28 Variation of load torque with time at 3000 rpm

Fig. 4.28 shows that as the speed of the PMSM was increased to 3000 rpm, the load torque at full load condition was decreased as compared to that of 2700 rpm. The average load torque at 3000 rpm was 2.722 N-m. In Fig. 4.29, it can be seen that on further increase of speed to 3300 rpm, the average load torque at full load was decreased to 2.566 N-m.

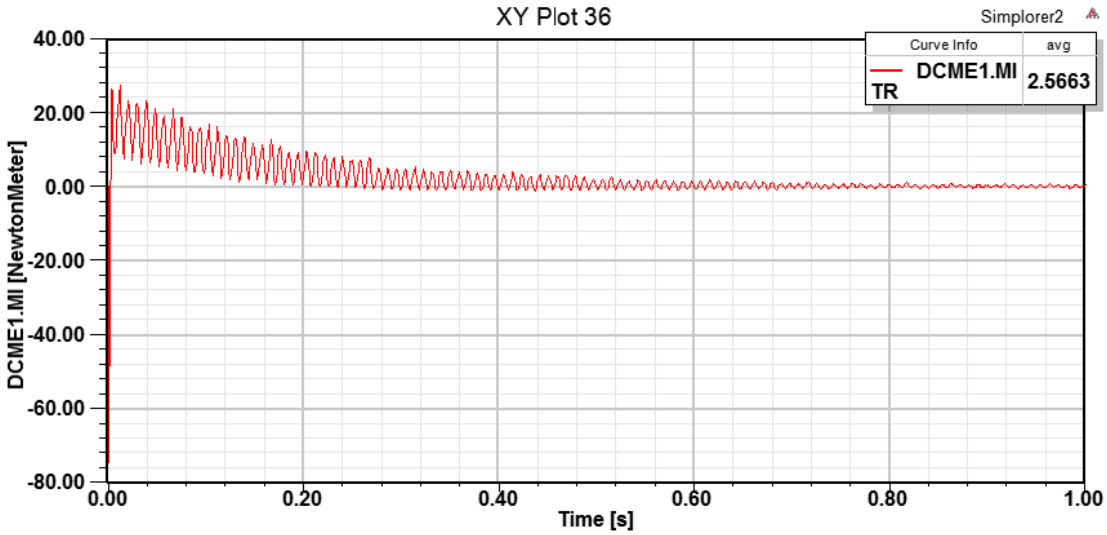

Fig. 4.29 Variation of load torque with time at 3300 rpm

4.6.3 Electromagnetic Torque

The torque produced over armature in the air gap is the electromagnetic torque. The motor was run at different speeds *viz*., 2700 rpm, 3000 rpm, and 3300 rpm, and the simulated electromagnetic torques for different speeds at full load condition were recorded for 1 second as shown in Fig. 4.30 to Fig. 4.32. Average electromagnetic torques of 2.87 N-m, 2.84 N-m, and 2.711 N-m were obtained at 2700 rpm, 3000 rpm, and 3300 rpm, respectively. This reveals that as the speed of operation increases the torque required to drive the full load is decreasing. This shows that the type of operation in this case is constant power operation.

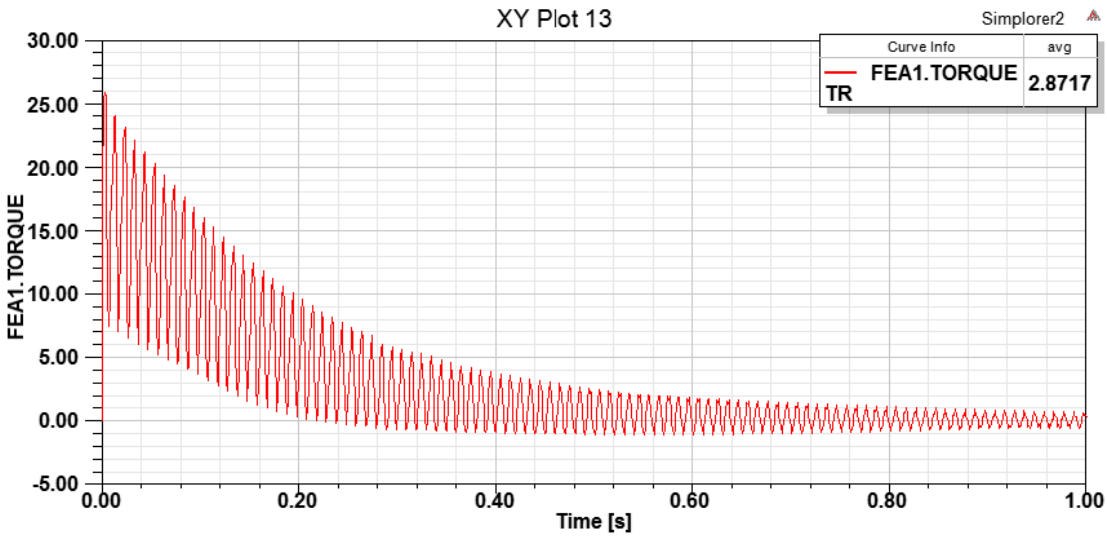

Fig. 4.30 Variation of electromagnetic torque with time at 2700 rpm

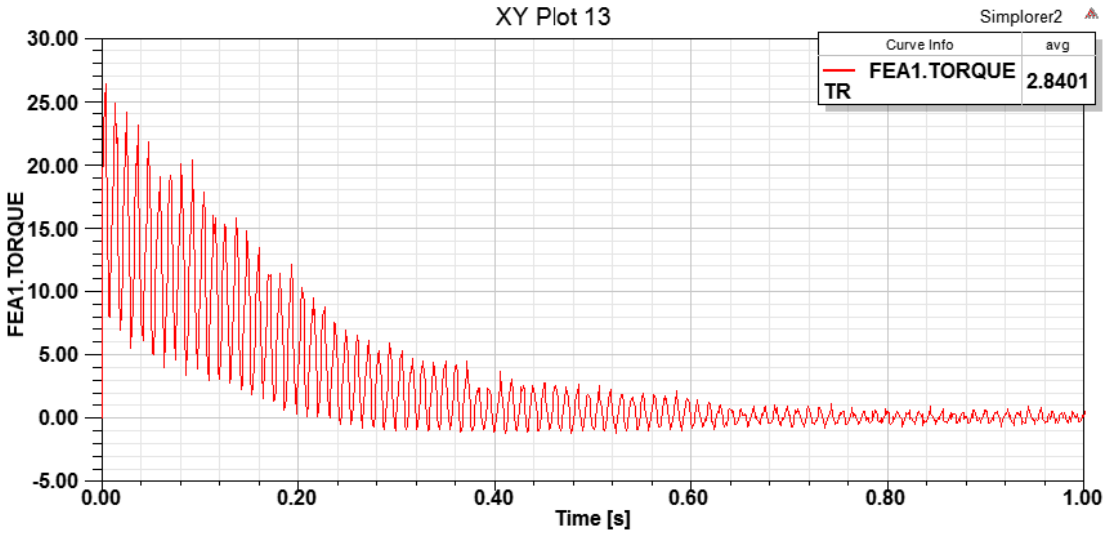

Fig. 4.31 Variation of electromagnetic torque with time at 3000 rpm

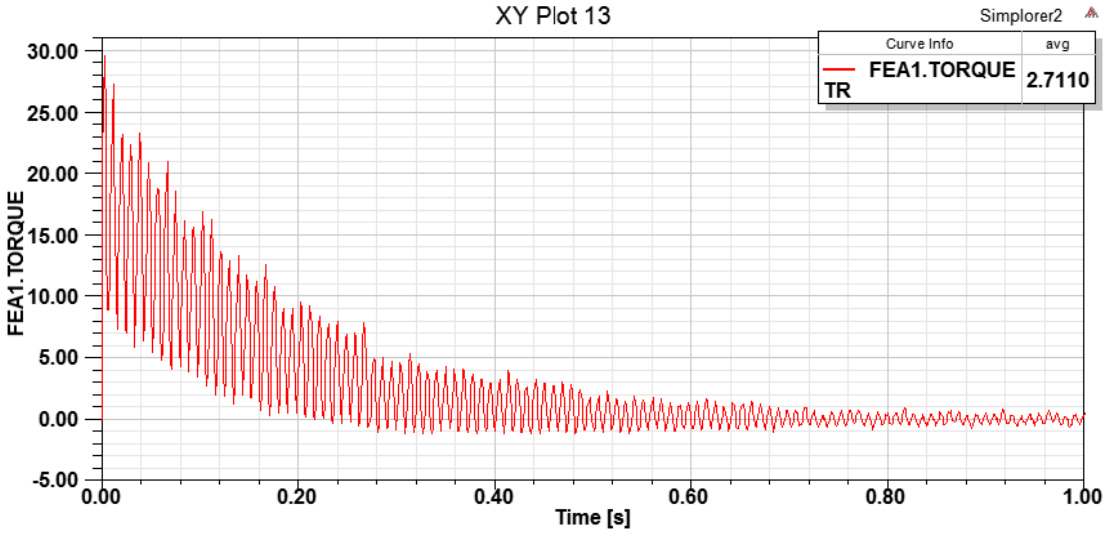

Fig. 4.32 Variation of electromagnetic torque with time at 3300 rpm

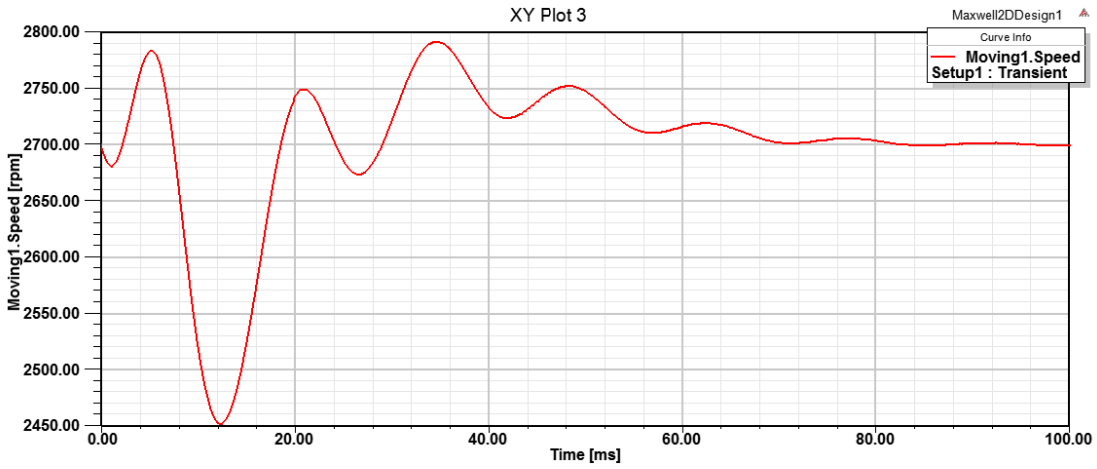

Fig. 4.33 Variation of speed with time for 2700 rpm

Fig. 4.33 shows that it takes about 80 ms to settle the speed at 2700 rpm finally. Large fluctuation was seen in the initial 20 ms time where the speed fell upto even 2450 rpm. Similar curves were observed for another speeds also *i.e.,* at 3000 rpm and 3300 rpm.

4.6.4 Induced voltage

The PMSM was run at different speeds *viz.*, 2700 rpm, 3000 rpm and 3300 rpm and the induced voltages were recorded upto 1 second. The induced voltage increases with increase in speed. The RMS values of induced voltages for each phase are shown in Fig. 4.34 to Fig. 4.36. It was observed that the induced voltages are varying sinusoidally with time.

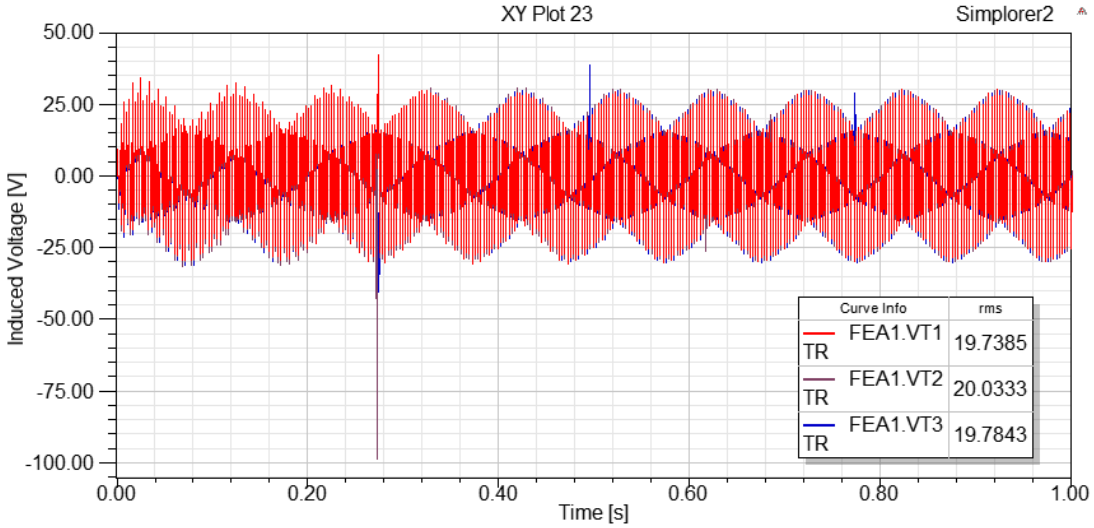

Fig. 4.34 Variation of induced voltage with time at 2700 rpm

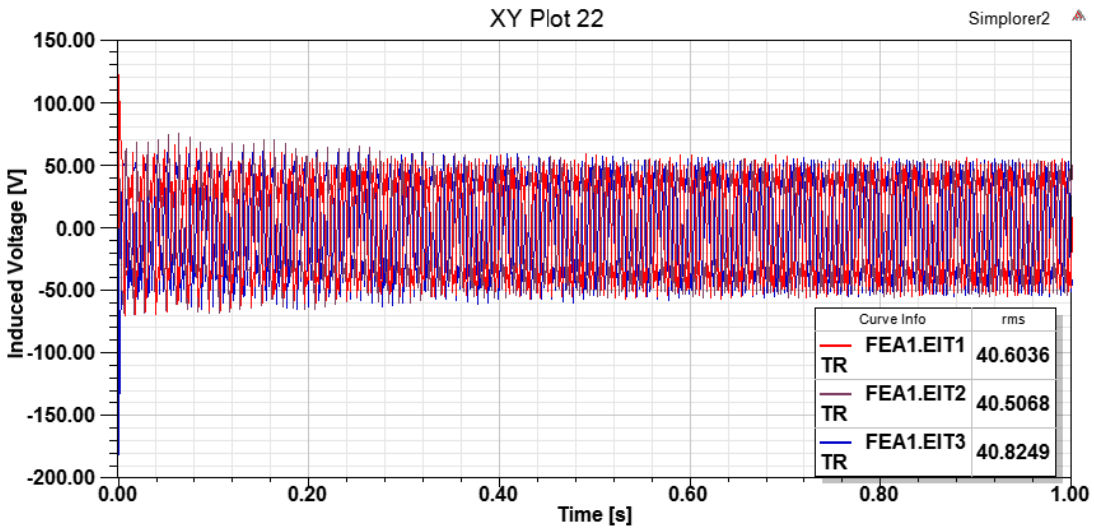

Fig. 4.35 Variation of induced voltage with time at 3000 rpm

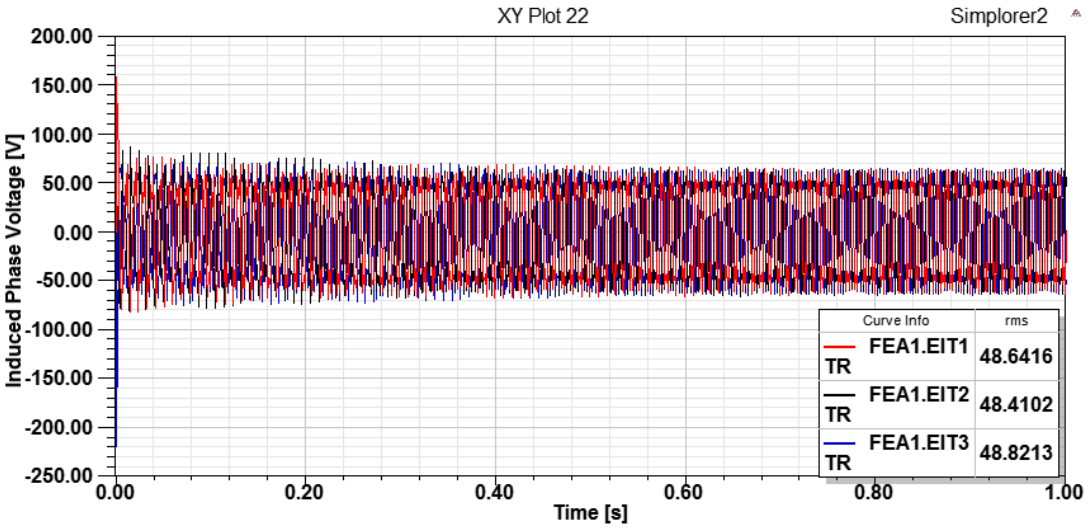

Fig. 4.36 Variation of induced voltage with time at 3300 rpm

4.6.5 Efficiency

The full load efficiency of PMSM was obtained after simulation of the designed model in RMxprt. The efficiency curve of the motor with respect to torque angle was found at four different speeds through simulation. The designed model of 1.07 kW capacity PMSM is having a rated speed of 4000 rpm. The model was simulated at 2700 rpm, 3000 rpm, 3300 rpm, and 4000 rpm, and the results are shown in Fig. 4.37 to Fig. 4.40. The efficiency achieved for the designed motor at 2700 rpm, 3000 rpm, 3300 rpm, and 4000 rpm were 81.47 %, 84.17 %, 87.31 %, and 91.27 %, respectively. The torque angle was seen to be reduced as the speed of operation increases. Initially at 2700 rpm, the torque angle for operation comes out to be 43.75°. It then reduces to 40.13°, 37.51°, and 31.35° at 3000 rpm, 3300 rpm, and 4000 rpm, respectively.

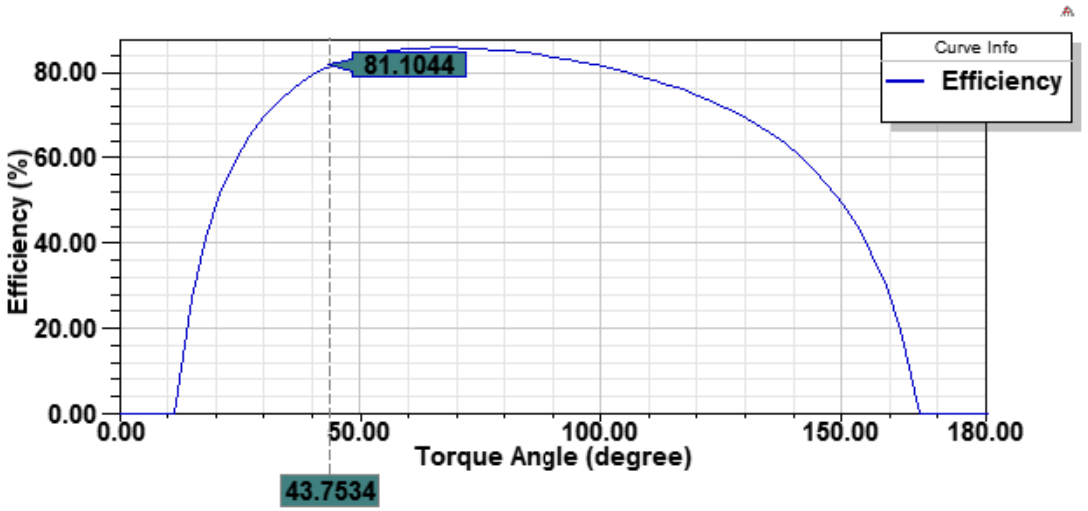

Fig. 4.37 Efficiency vs torque angle at 2700 rpm

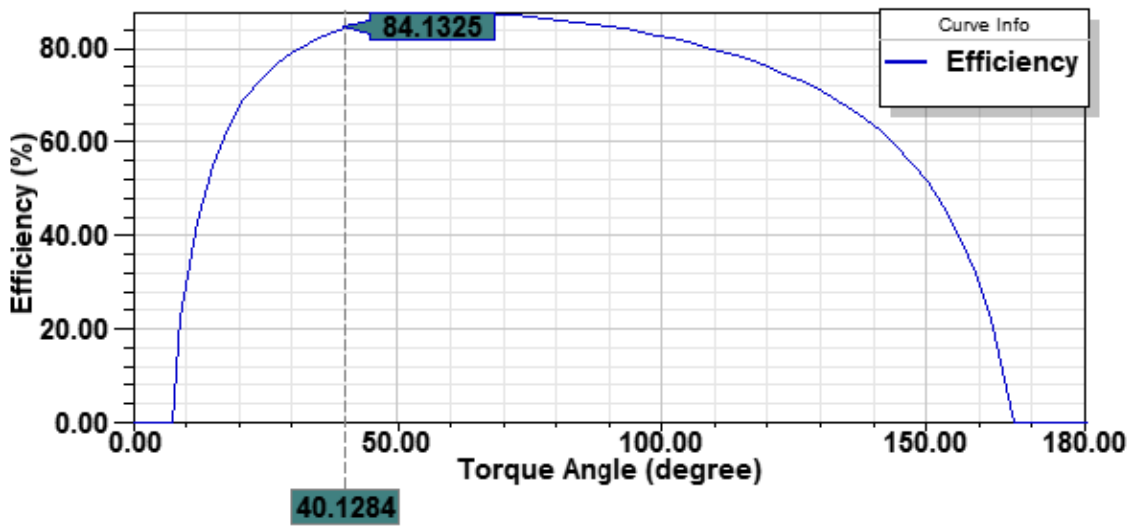

Fig. 4.38 Efficiency vs torque angle at 3000 rpm

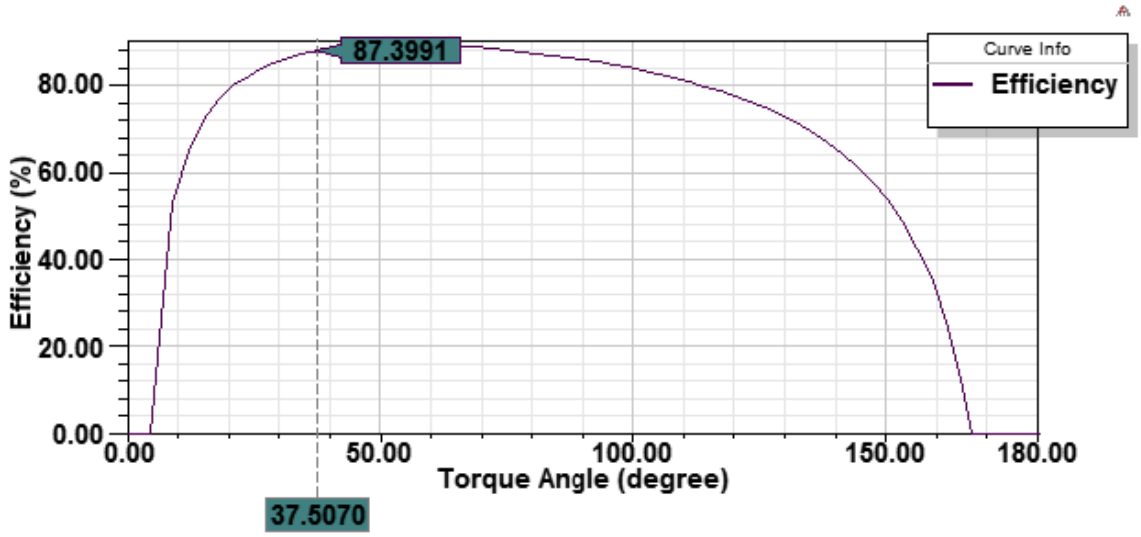

Fig. 4.39 Efficiency vs torque angle at 3300 rpm

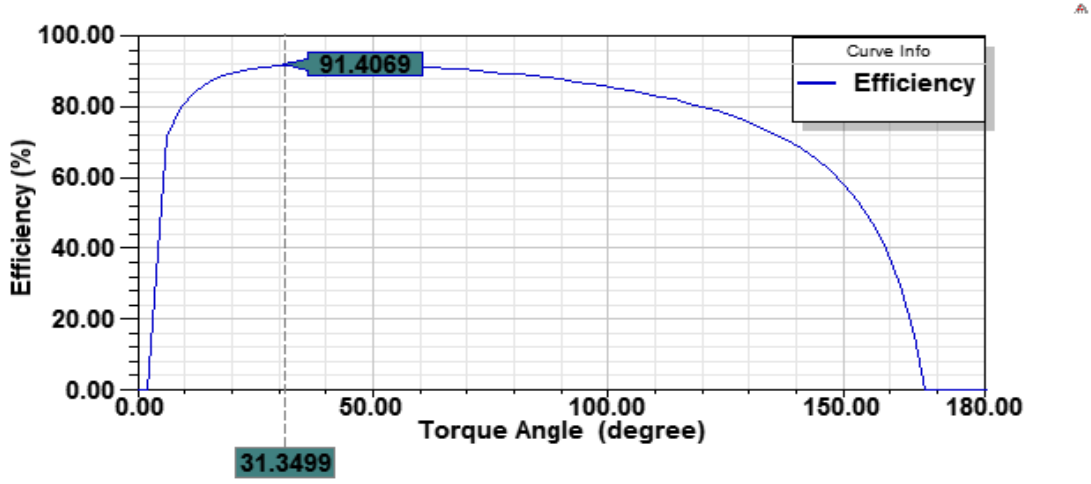

Fig. 4.40 Efficiency vs torque angle at 4000 rpm

4.7 Experiment and Validation

4.7.1 Experiment

The experiment on 1.07 kW PMSM having a rated speed of 4000 rpm, mechanically coupled with a DC generator was performed for validation of PMSM model designed in ANSYS Maxwell software. In the experiments, three speeds *viz.,* 2700 rpm, 3000 rpm, and 3300 rpm were selected and the corresponding line voltage, line current, and input power at 25% load, 50% load, 75% load, full load, and 110% load were measured. All the measurements of current, voltage, input power, and power factor were made using Fluke 1738 Power Logger. The variation of line current, line voltage, and power factor with different loading conditions for different speeds are shown in Appendices C-E. The PMSM is loaded indirectly by loading the mechanically coupled DC generator using lamp loads. The generated EMF and armature current of DC generator are also measured using voltmeter and ammeter, respectively and the results are shown in Appendices C-E. The generated emf and armature current values were used to calculate the output power. Performance parameters such as efficiency and torque were calculated using Equation 4.15 and Equation 4.16, respectively.

$$\eta = \frac{P_{out}}{P_{in}} \times 100 \tag{4.15}$$

$$T = P_{out} \frac{60}{2\pi N} \tag{4.16}$$

where P_{out} is the output power of PMSM and P_{in} is the input power to the PMSM. N is the speed of motor in rpm.

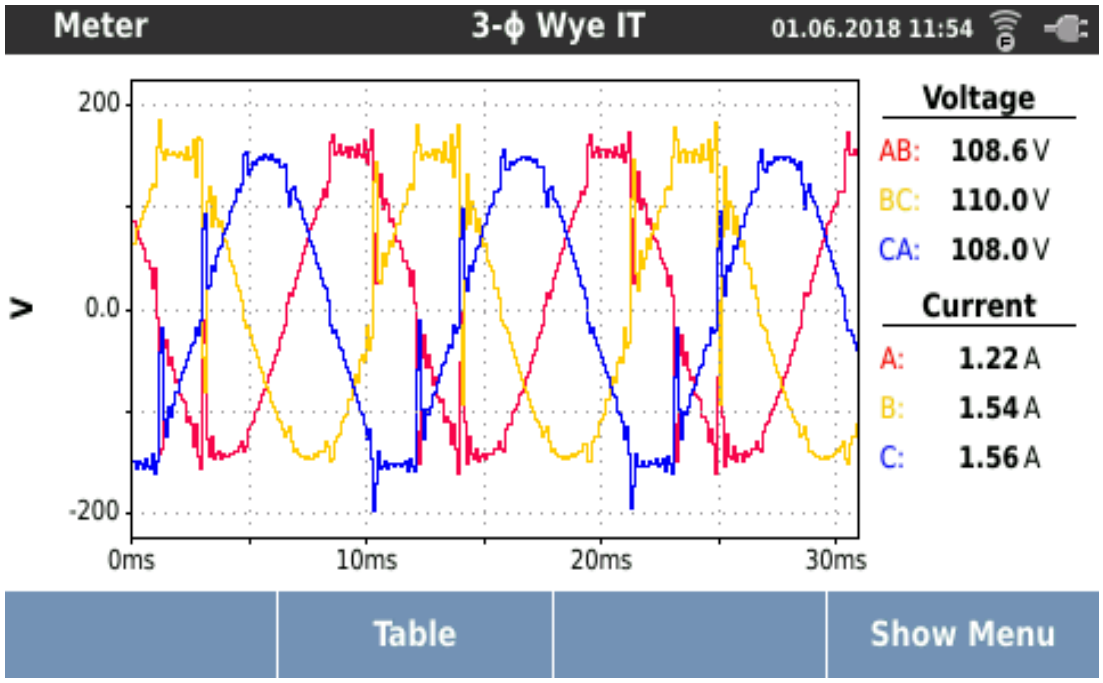

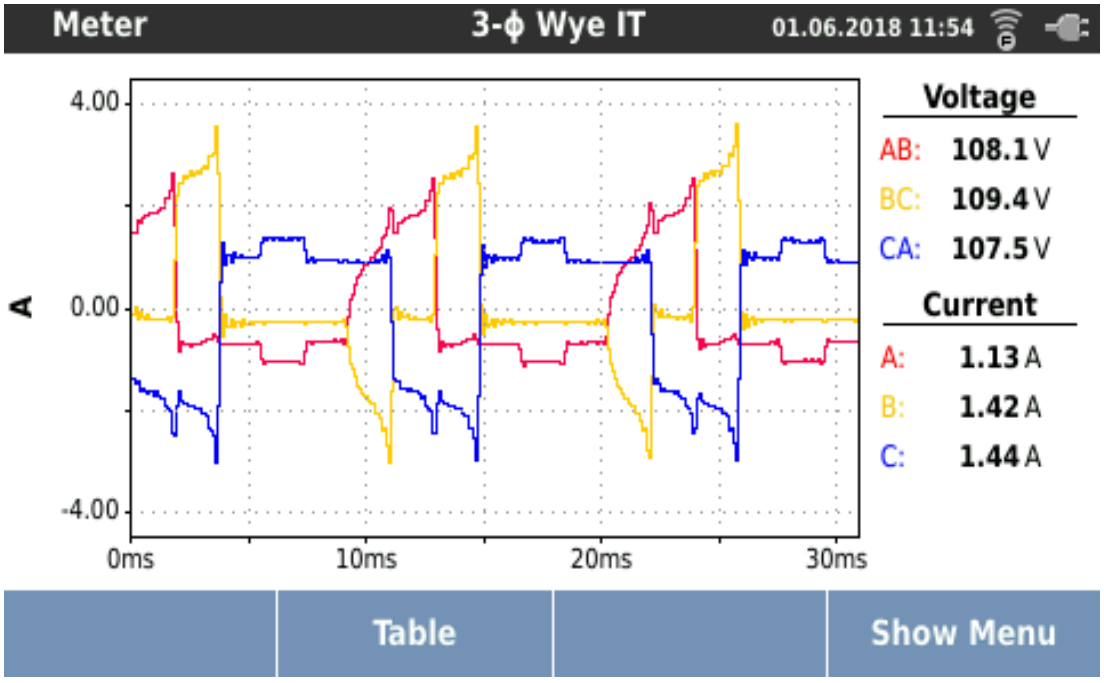

Fig. 4.41(a) Experimental curves of line voltage and line current for 25 % load at 2700 rpm

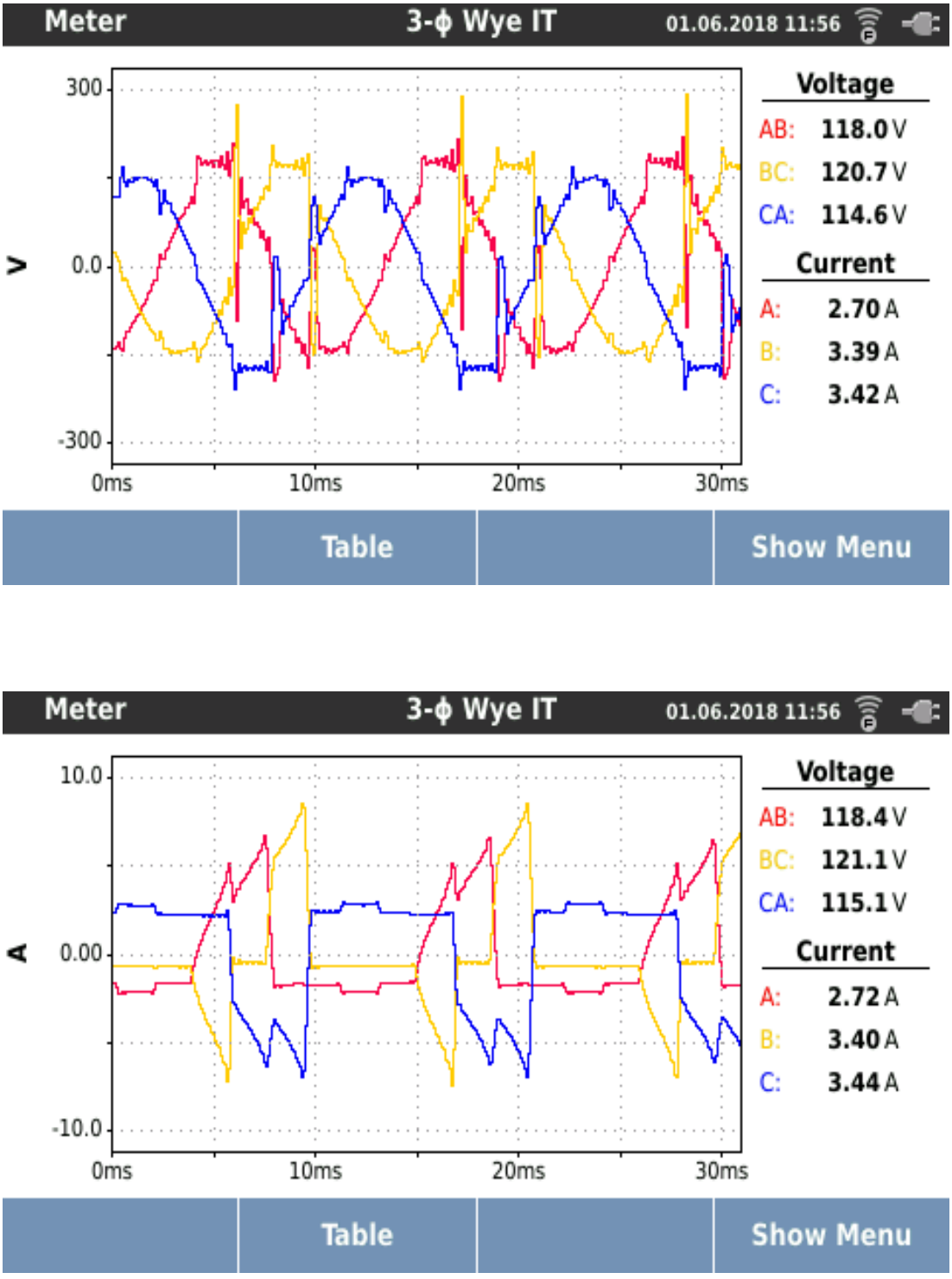

Fig. 4.41(b) Experimental curves of line voltage and line current for 50 % load at 2700 rpm

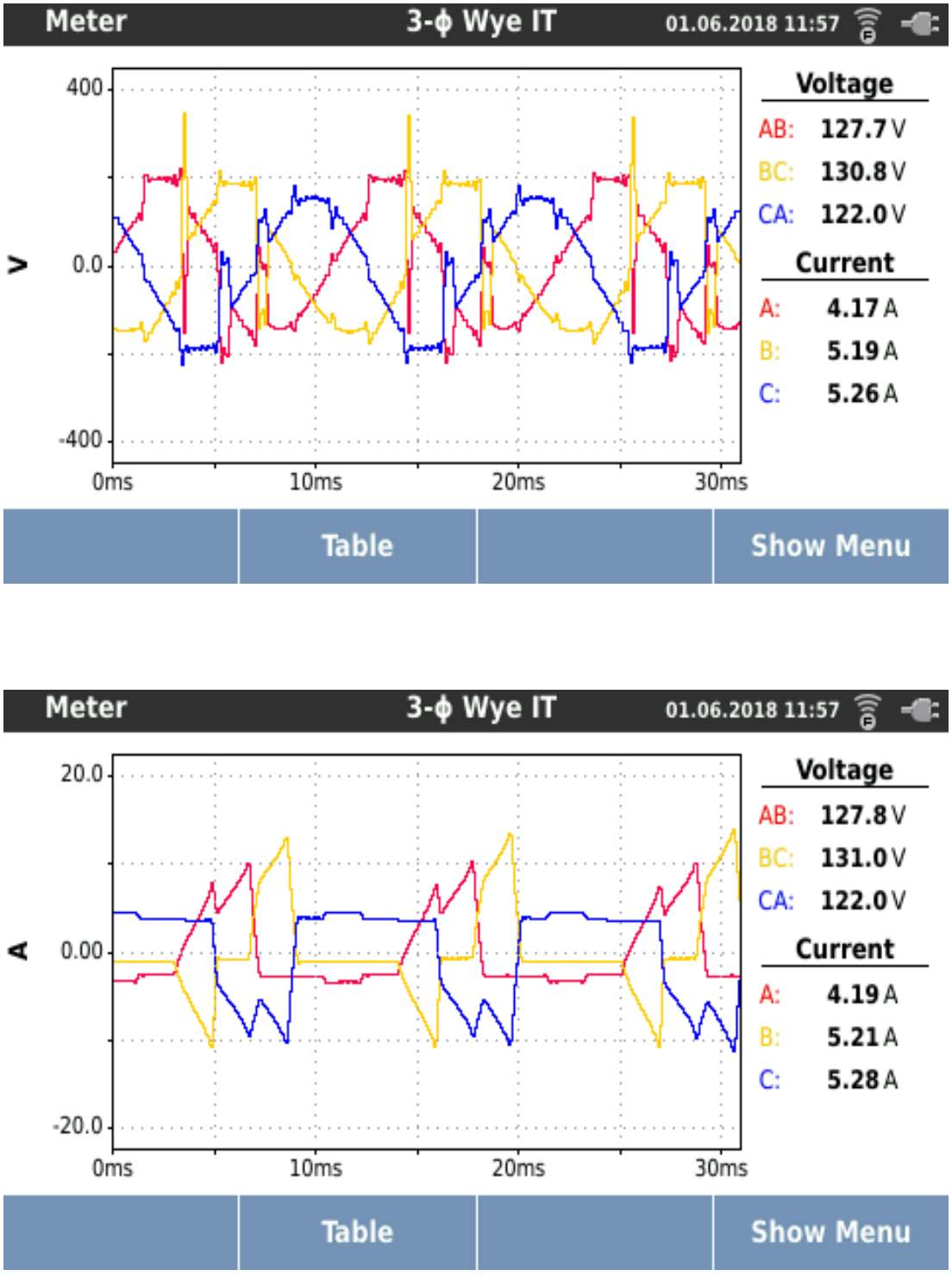

Fig. 4.41(c) Experimental curves of line voltage and line current for 75 % load at 2700 rpm

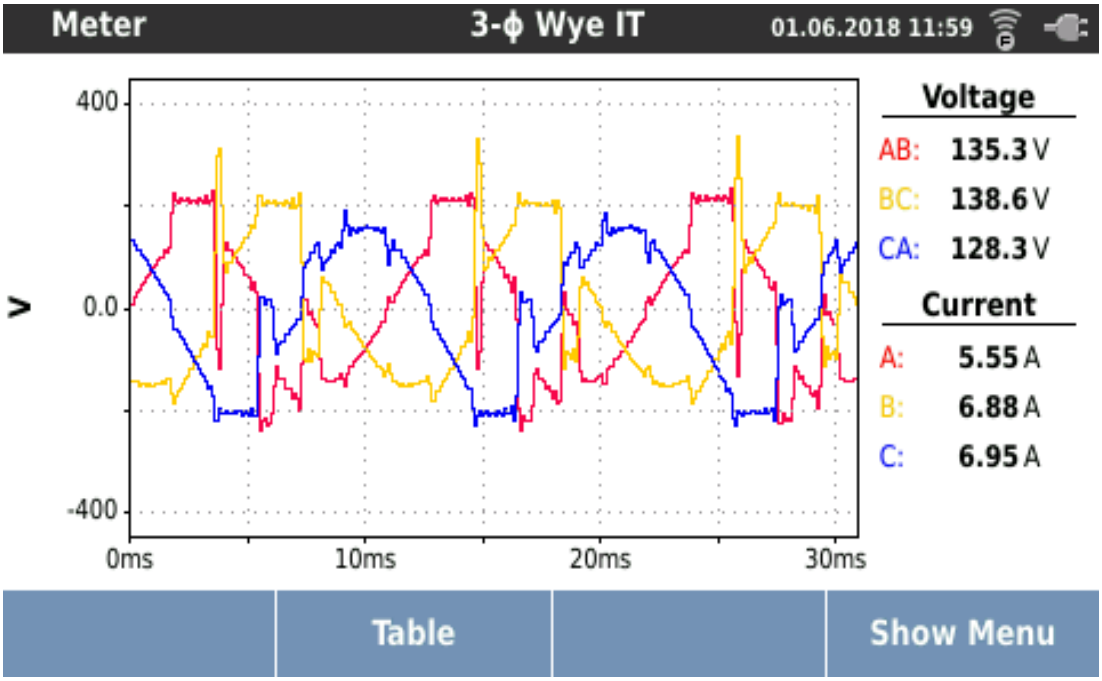

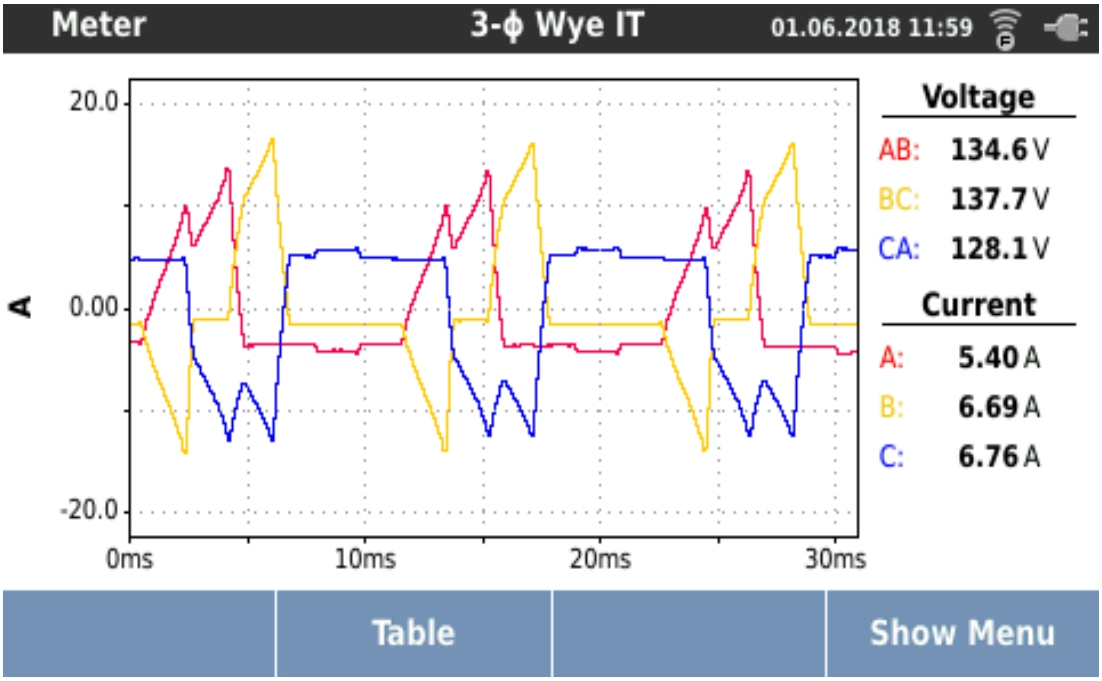

Fig. 4.41(d) Experimental curves of line voltage and line current for full load at 2700 rpm

Fig. 4.41(e) Experimental curves of line voltage and line current for 110 % load at 2700 rpm

Fig. 4.41(a) to Fig. 4.41(e) shows the experimental variation of line voltage and line current for different loading conditions at 2700 rpm. It can be observed that the line

voltage waveform is near to sinusoidal with distortions. The line voltage waveform is showing more distortions at higher loading conditions. However, the line current waveform does not show significant distortions with change in loading conditions.

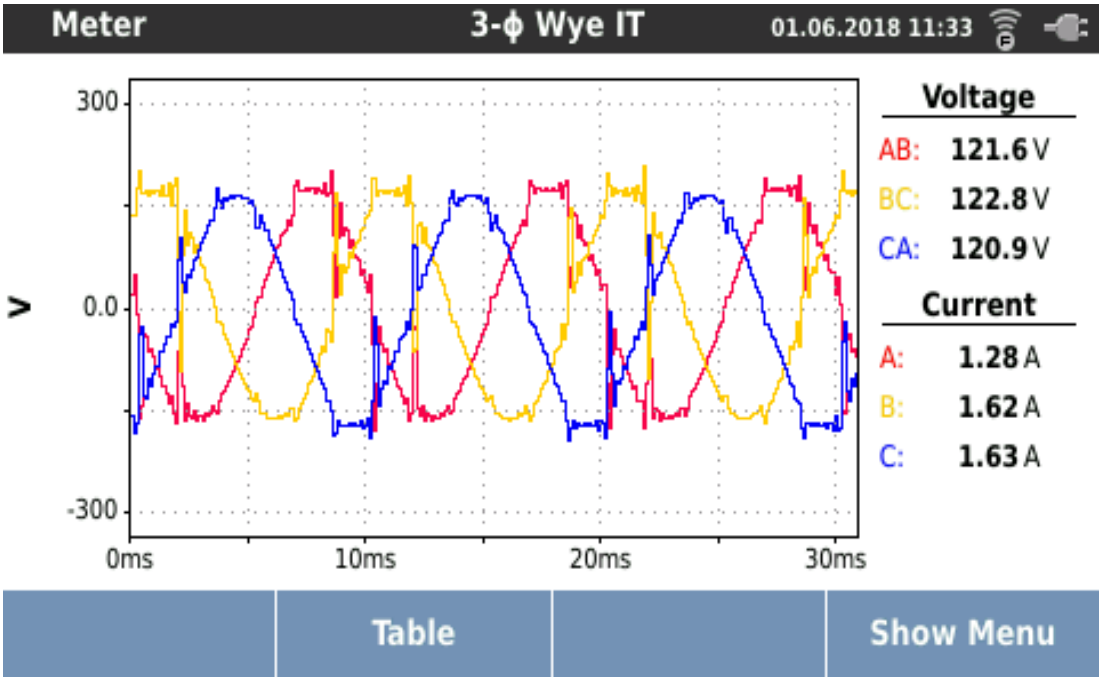

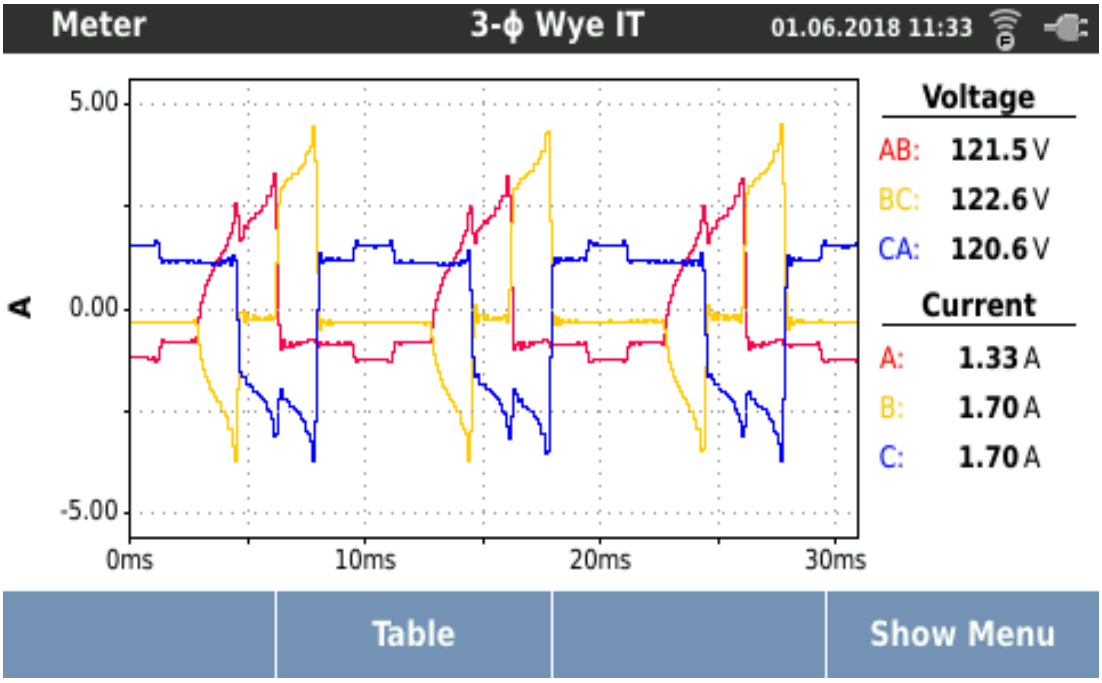

Fig. 4.42(a) Experimental curves of line voltage and line current for 25 % load at 3000 rpm

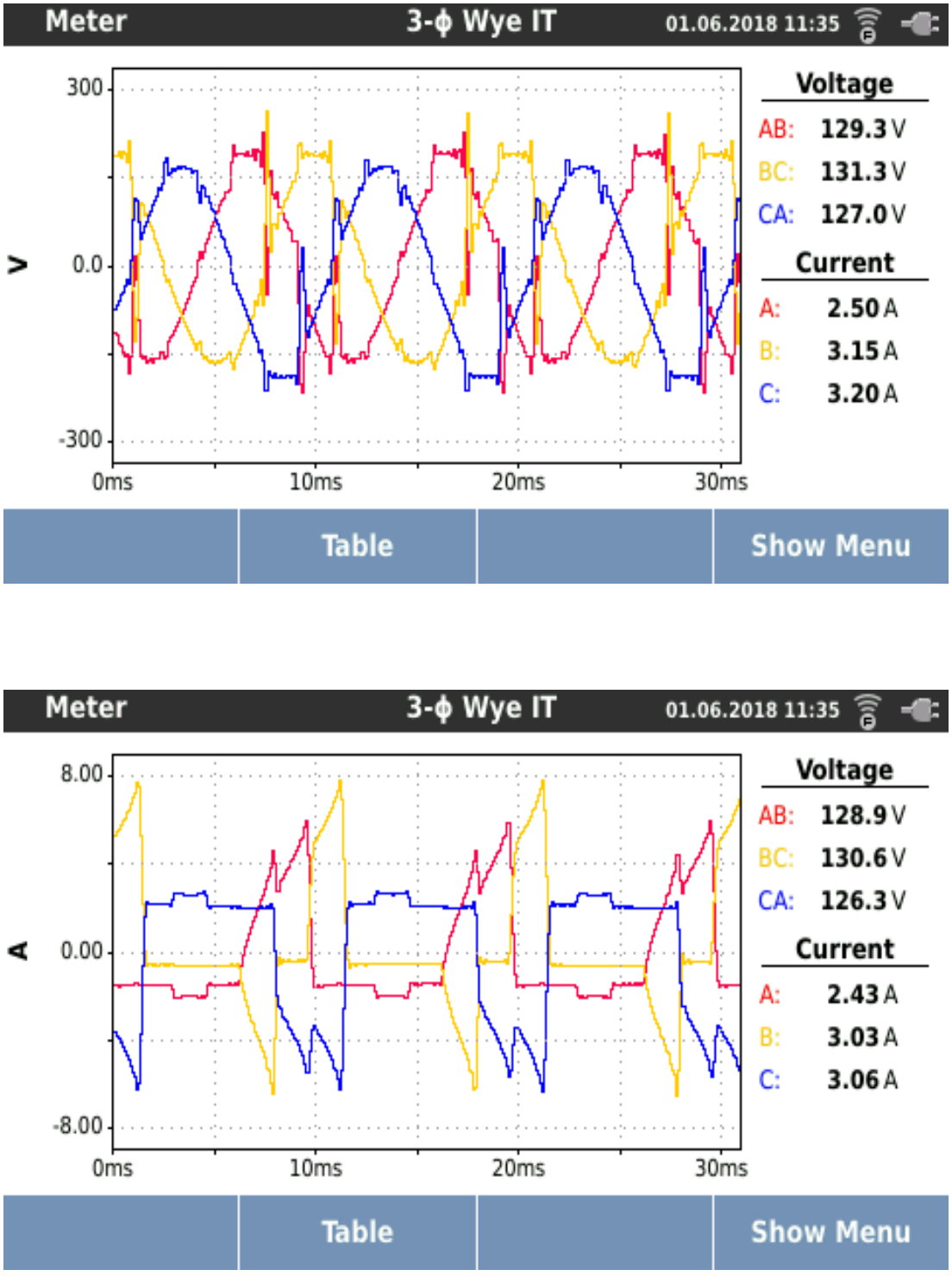

Fig. 4.42(b) Experimental curves of line voltage and line current for 50 % load at 3000 rpm

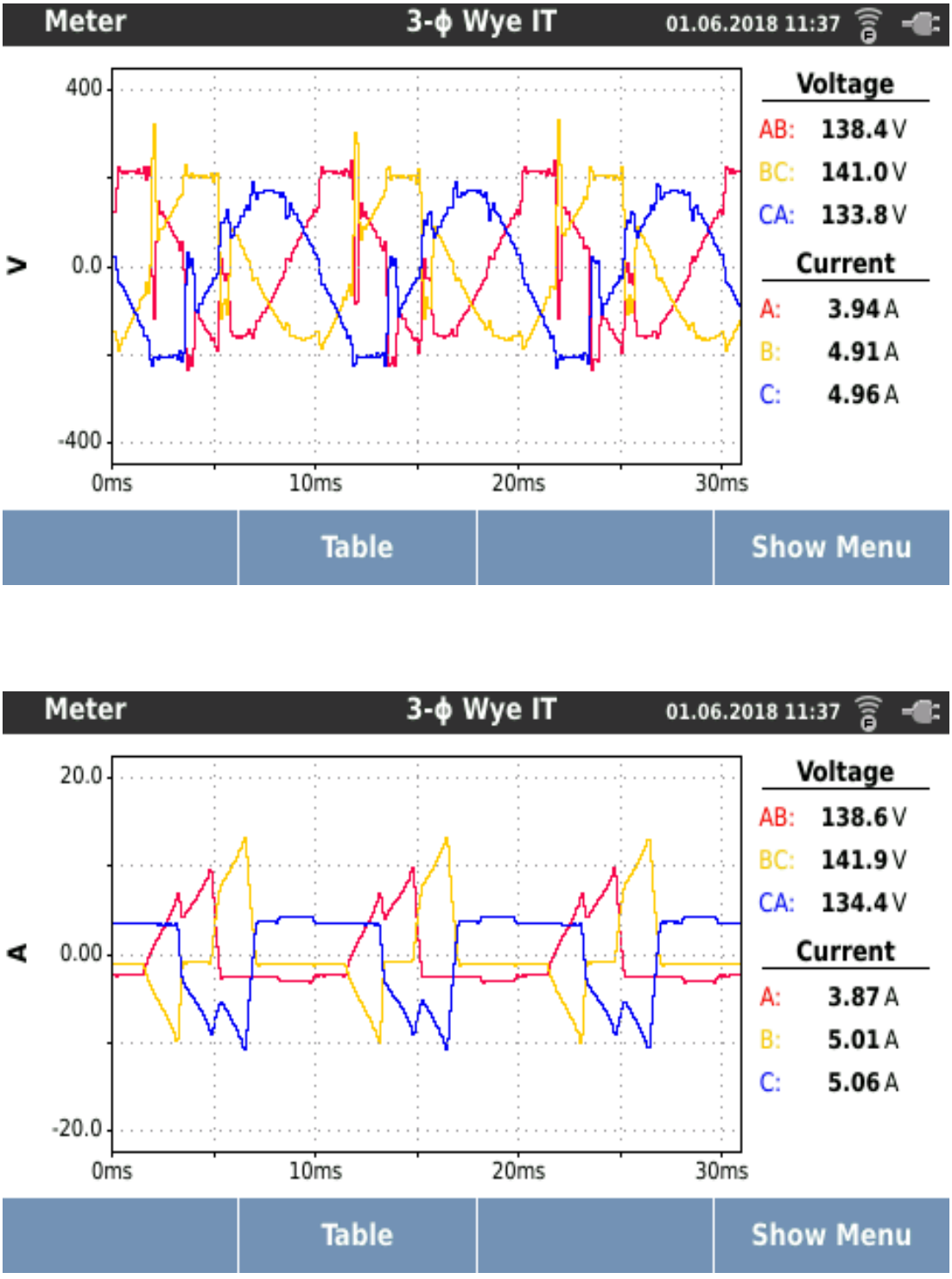

Fig. 4.42(c) Experimental curves of line voltage and line current for 75 % load at 3000 rpm

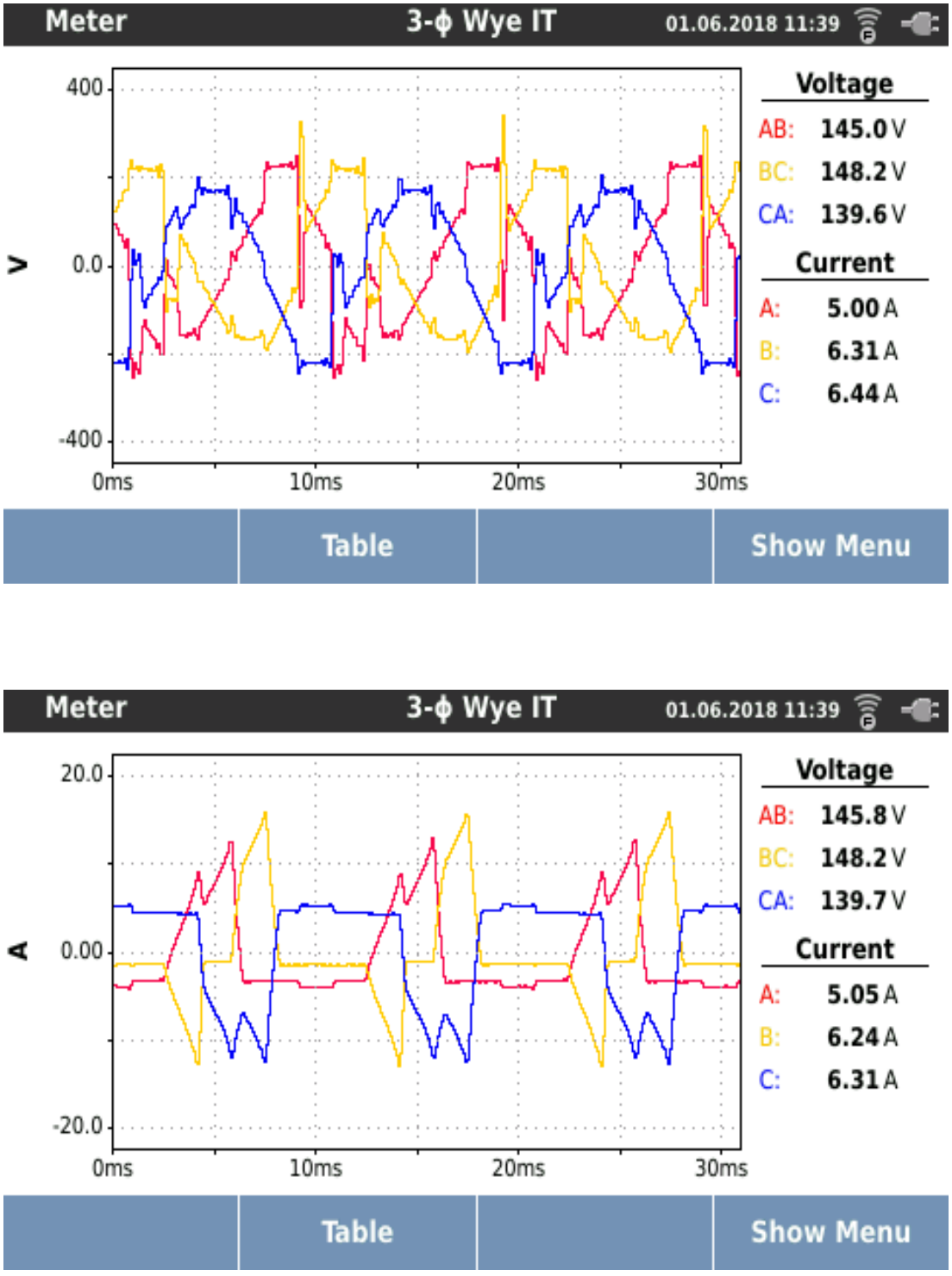

Fig. 4.42(d) Experimental curves of line voltage and line current for full load at 3000 rpm

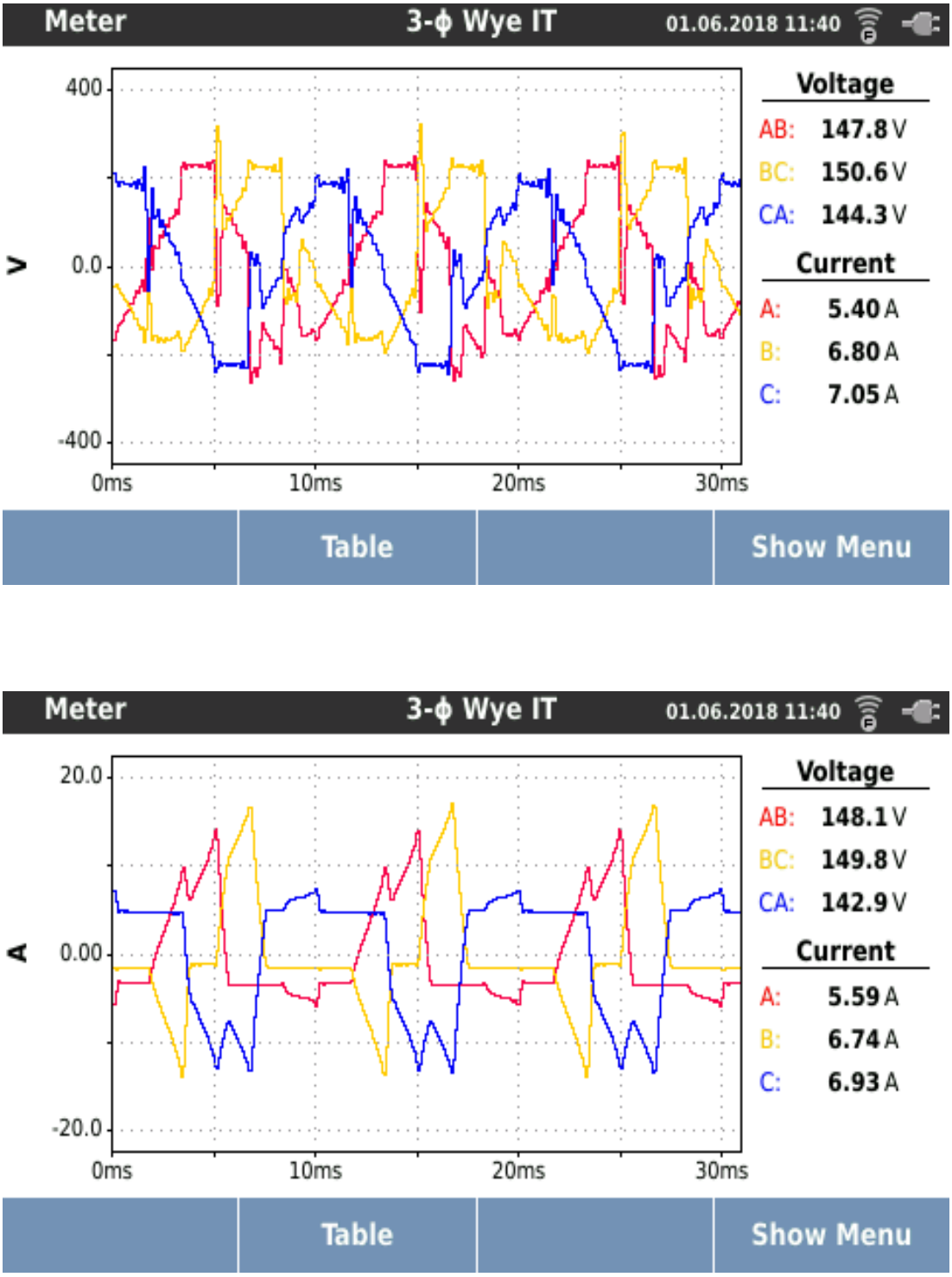

Fig. 4.42(e) Experimental curves of line voltage and line current for 110 % load at 3000 rpm

Fig. 4.42(a) to Fig. 4.42(e) shows the experimental variation of line voltage and line current for different loading conditions at 3000 rpm. In this case also, the line voltage is near to sinusoidal with some distortions. At higher loading levels, when the

line current demand is increased, more distortions can be seen in line voltage waveform.

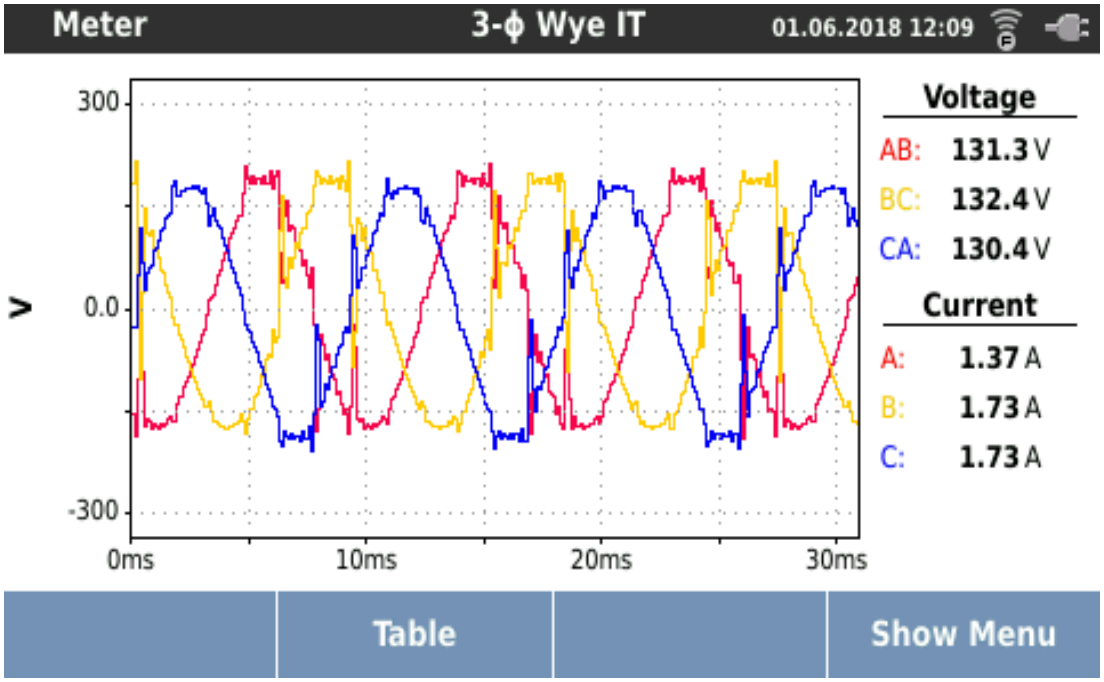

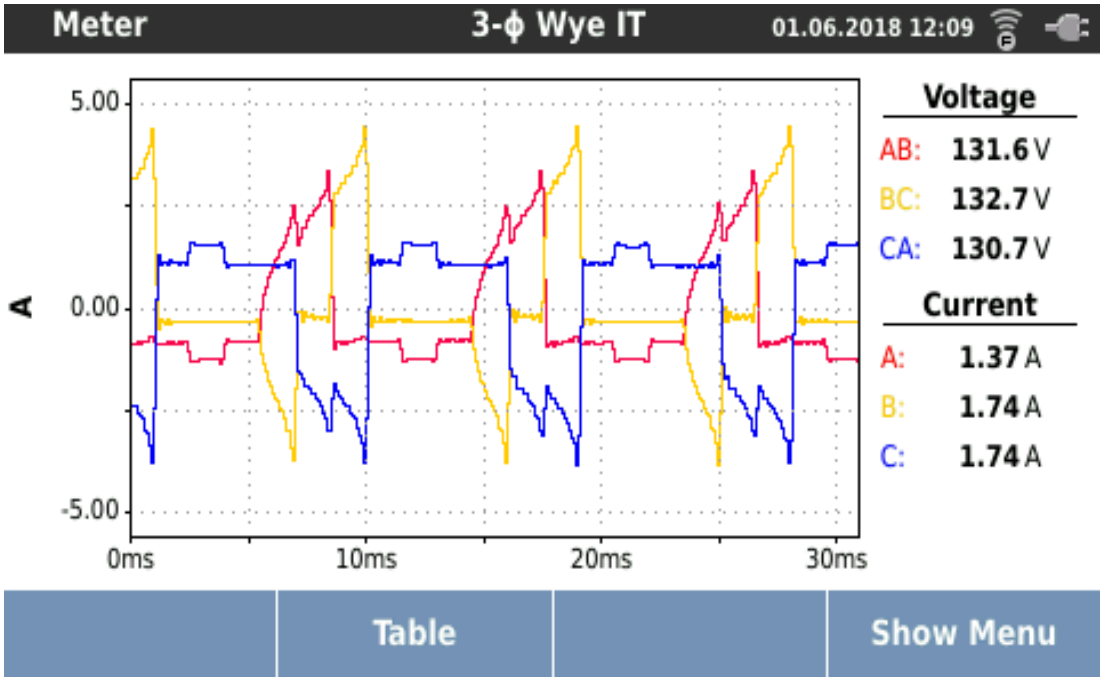

Fig. 4.43(a) Experimental curves of line voltage and line current for 25 % load at 3300 rpm

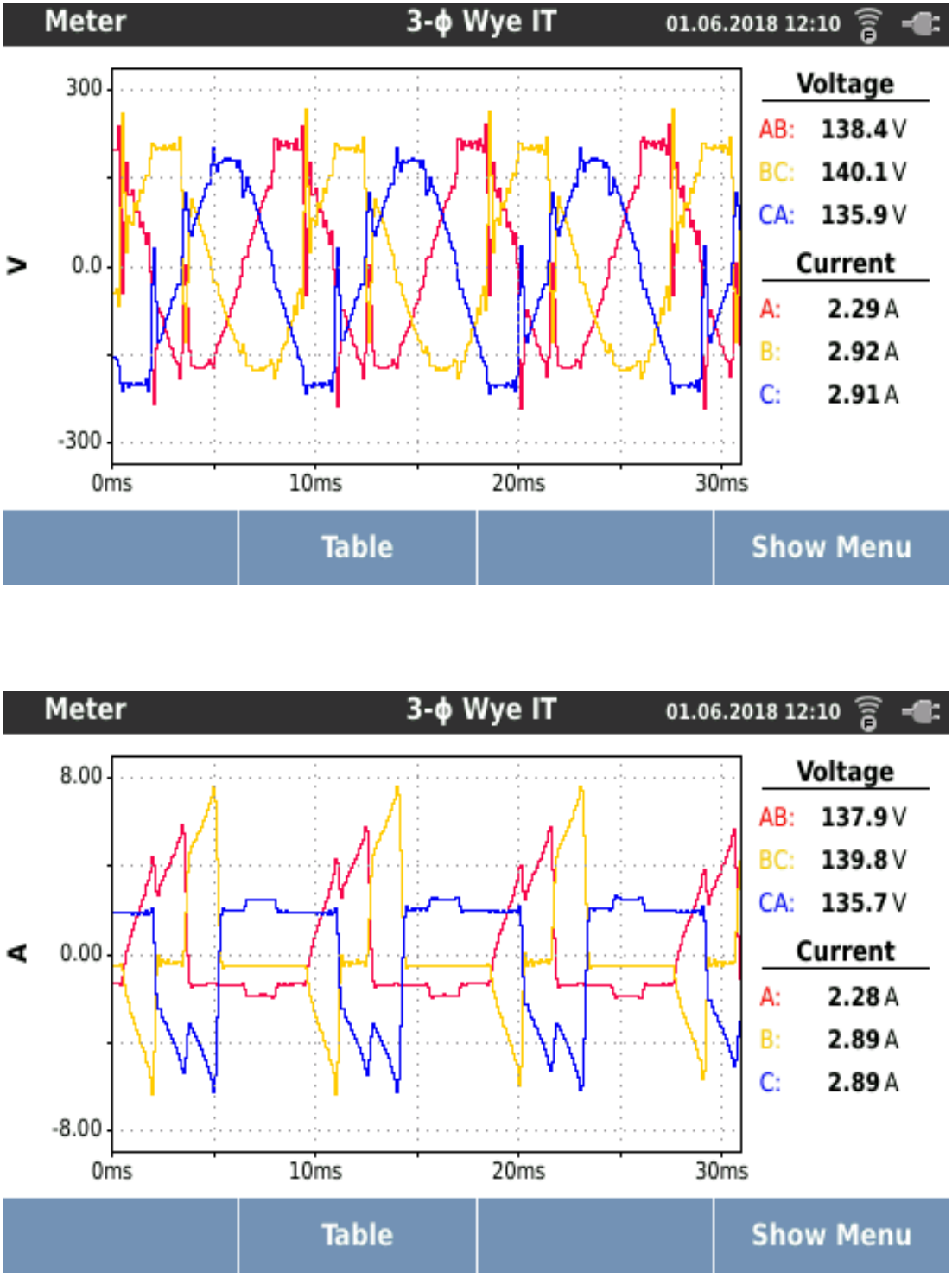

Fig. 4.43(b) Experimental curves of line voltage and line current for 50 % load at 3300 rpm

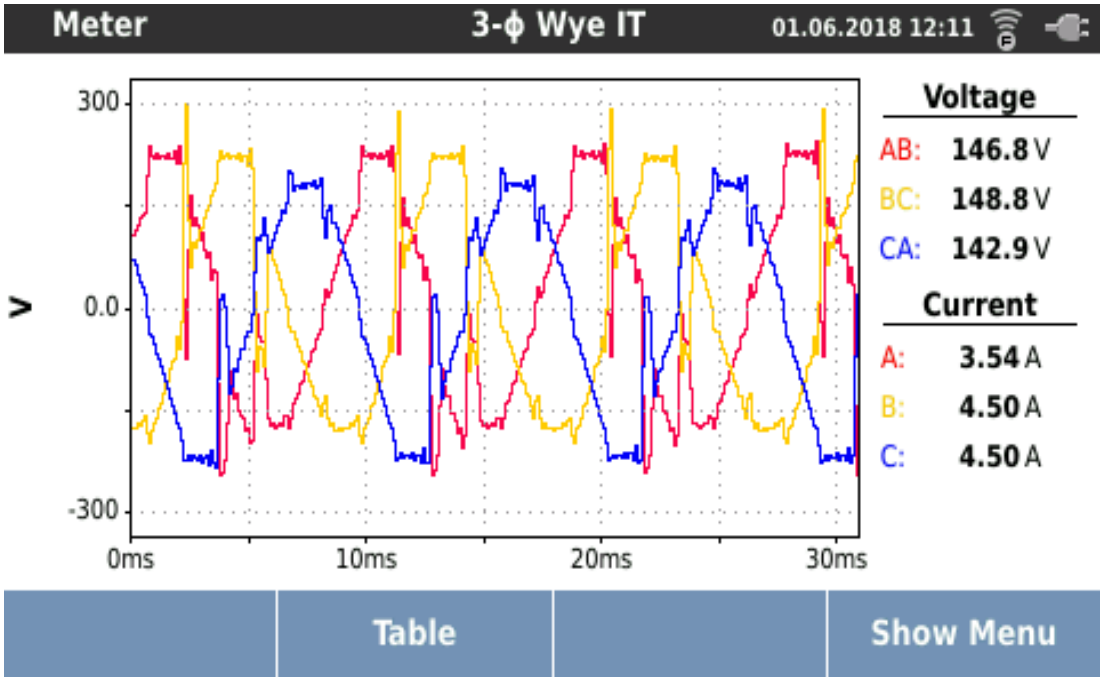

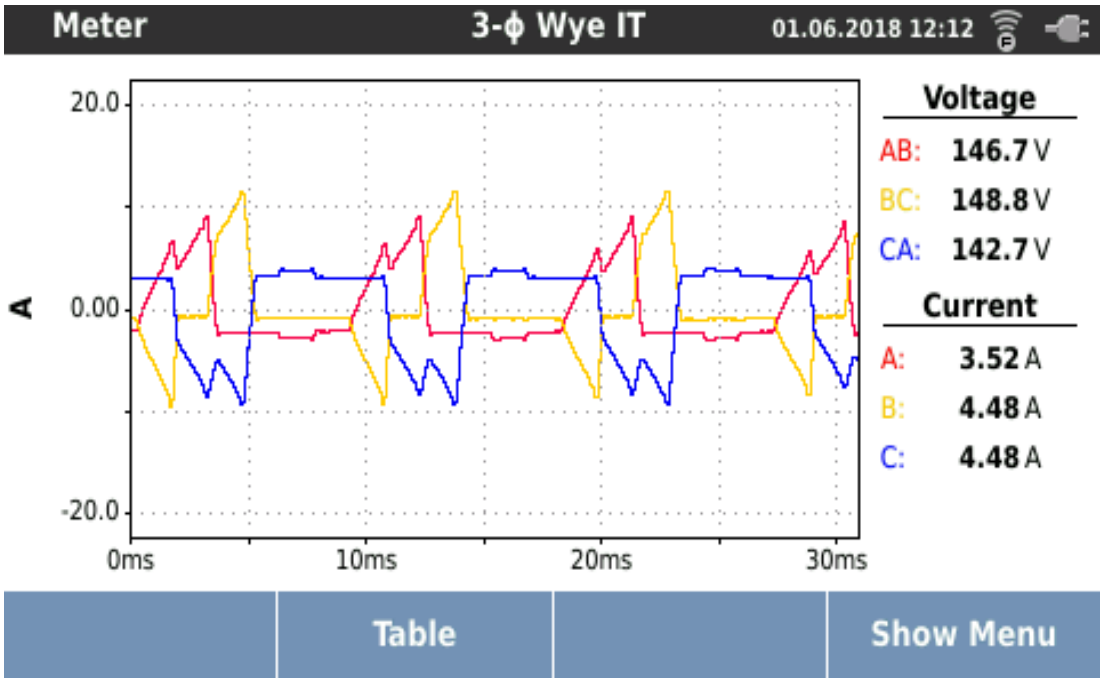

Fig. 4.43(c) Experimental curves of line voltage and line current for 75 % load at 3300 rpm

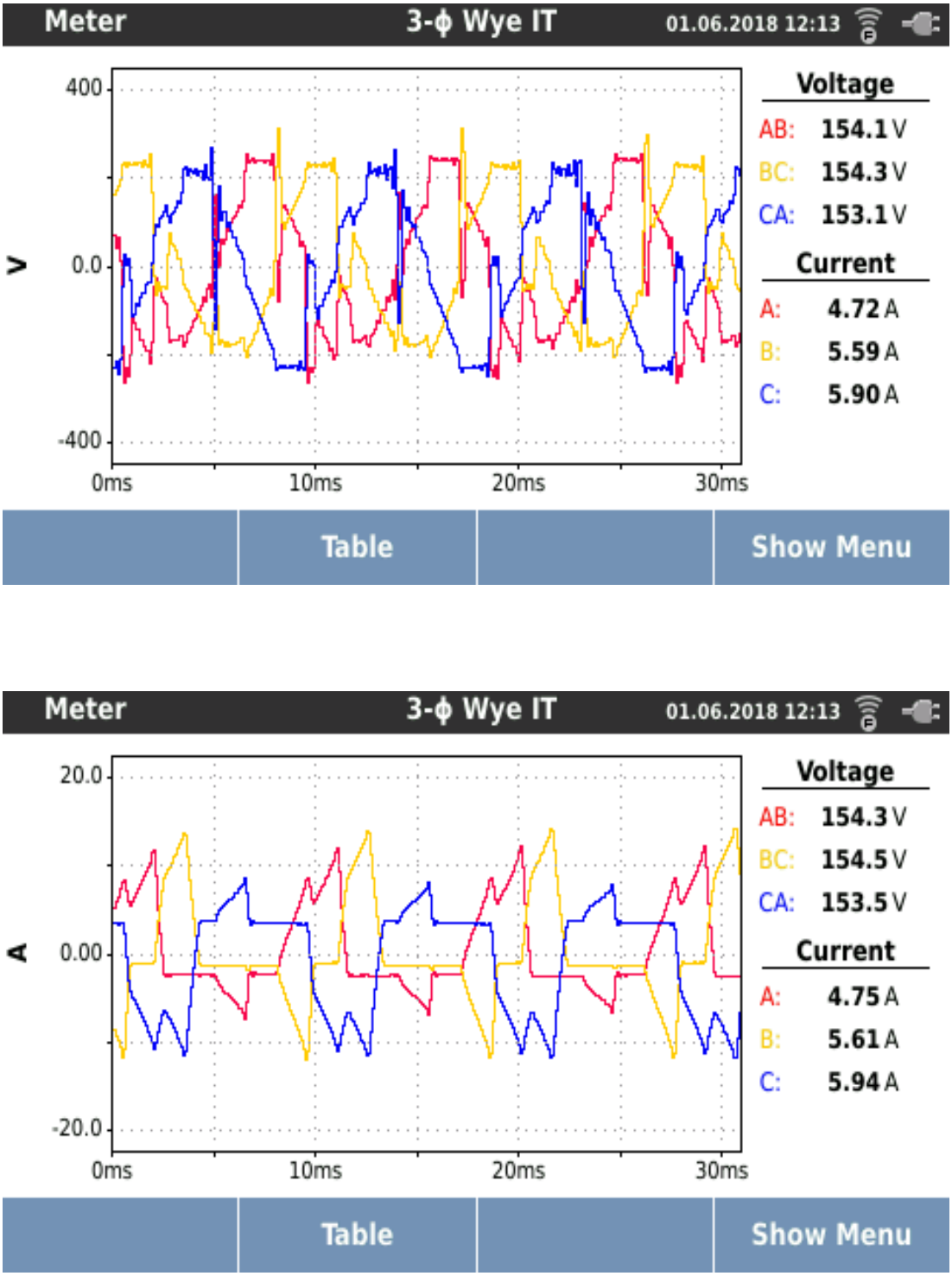

Fig. 4.43(d) Experimental curves of line voltage and line current for full load at 3300 rpm

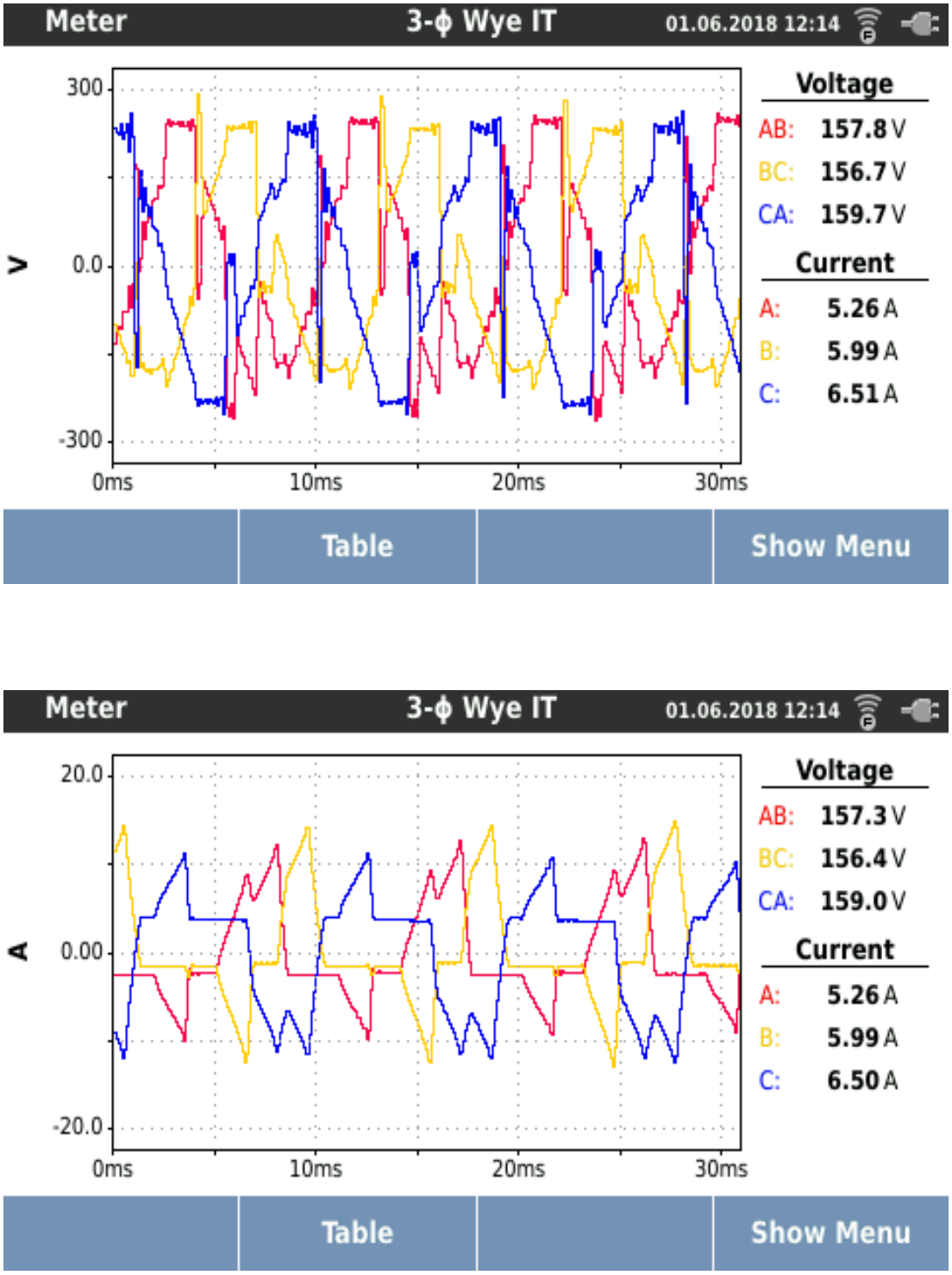

Fig. 4.43(e) Experimental curves of line voltage and line current for 110 % load at 3300 rpm

Fig. 4.43(a) to Fig. 4.43(e) represents the line voltage and line current for different loading conditions at 3300 rpm. The line voltage waveform can be seen near to sinusoidal. However, the line voltage waveform is more distorted when the motor

demands higher line currents at full load and overload conditions. The reason for distorted sinusoidal line voltage waveform is presence of harmonics.

For measurement of level of harmonic distortion, a term called Total Harmonic Distortion (THD) is used and it is defined as

$$THD\ (\%)\ = \frac{\sqrt{V_2{}^2+V_3{}^2+V_4{}^2+\cdots+V_n{}^2}}{V_1} \times 100\ \% \qquad (4.17)$$

where V_1 is the fundamental component of the waveform whereas V_2, V_3, V_4, and V_n are second, third, fourth, and n^{th} order harmonics.

The different harmonics present in the line is shown in Fig. 4.44 which was measured by the Fluke 1738 Power Analyzer.

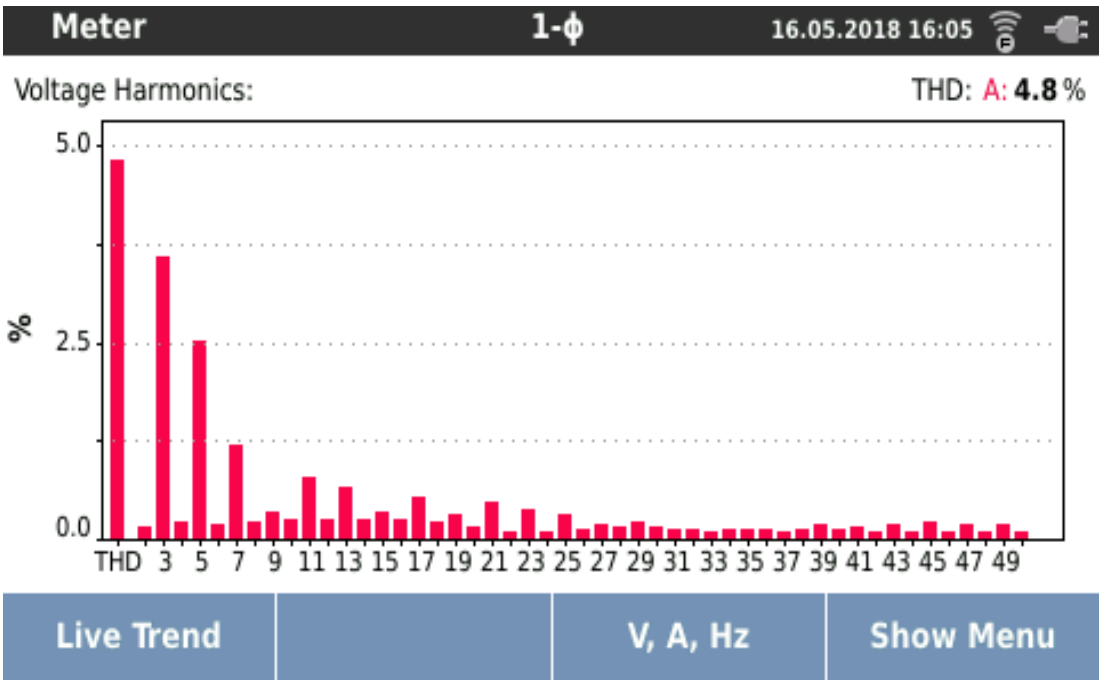

Fig. 4.44 Voltage Harmonics of different order with percentage

Fig. 4.44 shows that harmonics of different order are present in the supply voltage with third harmonics, fifth harmonics, and seventh harmonics being dominant. The total harmonic distortion (THD) was 4.8 %.

4.7.1.1 Line voltage

The PMSM was fed by a three phase VSI. The input line voltage for different loadings and at different speeds were measured using Fluke 1738 Power Logger. The

line voltage was seen to be increasing with increase in loading. Furthermore, on increasing the speed of motor, the line voltage for the same loading level increases. The experimental data for line voltage at different speeds for different loadings is shown in Appendices C-E.

4.7.1.2 Line current

The input line current to the PMSM for different loadings at different speeds were recorded using Fluke 1738 Power Logger. It was seen that input line current increases with increase in load. When the speed of motor increases, it was seen that the input line current for the same load decreases. Appendices C-E show the experimentally measured line currents for different loadings at different speeds.

4.7.1.3 Input power to PMSM

The power in an AC circuit is expressed in terms of active power, reactive power, and apparent power. The active, reactive, and apparent power input to the PMSM was recorded using Fluke 1738 Power Logger. The input power measurement of PMSM at different loading levels *viz.,* 25%, 50%, 75%, 100% and 110% by switching on the lamp loads connected to the DC generator which is coupled mechanically with the PMSM was done. The active, reactive and apparent power for different load and speed are shown in Appendix C - E.

4.7.1.4 Power factor

The power factor was seen to vary from 0.69 to 0.75. At lower speed of operation, such as at 2700 rpm and 3000 rpm, the power factor at full load and at 110% load condition is 0.69 which is quite low. However at 3300 rpm this improved to 0.71 at full load and at 110% load. However, the power factor was 0.75 when the motor is 25% loaded. The power factor at different speeds and loads are shown in Appendices C- E.

4.7.1.5 Output Power of PMSM

The PMSM was mechanically coupled with a DC generator. The DC generator was loaded using lamp loads and the load voltage and load currents for different loading levels *viz.,* 25%, 50%, 75%, 100%, and 110% of the PMSM were measured

using voltmeter and ammeter, respectively. The experiments were conducted at three different speeds *viz.,* 2700 rpm, 3000rpm, and 3300 rpm. Experimental data are given in Appendices C-E. The output power for each of the case was calculated using the Equation 4.18.

$$P_{out} = V_L \times I_L \tag{4.18}$$

where P_{out} is the output power of the DC generator, V_L is the voltage across the lamp loads, and I_L is the current flowing through the load.

4.7.1.6 No load losses in DC generator

The no load losses for 1 hp DC machine at three different speeds *viz.,* 2700 rpm, 3000 rpm, and 3300 rpm were calculated by conducting no load test of the DC machine. A supply voltage of 220 V DC was given to the DC motor and it was run at no load for each of the above stated speeds. A rheostat was added in series with the armature for speed control of the DC motor. A 3-point starter was also connected in series of the armature to limit the high initial starting current. The voltage across the armature and field were measured using multimeter. The field current and armature current were measured using ammeters. The no load losses comprises of armature copper loss, field copper loss and rotational losses. Rotational losses include friction and windage losses of the machine. The field losses and rotational losses are constant losses. The armature copper losses are variable losses which varies with the loading of PMSM. The armature copper loss, field copper loss and rotational loss are calculated using Equations 4.19 - 4.21.

$$P_{arm\_Cu} = {I_a}^2 \times R_a \tag{4.19}$$

$$P_{field\_Cu} = {I_f}^2 \times R_f \tag{4.20}$$

$$Rot\ loss = E_b \times I_a = (V - I_a.R_a) \times I_a \tag{4.21}$$

where P_{arm_Cu} is the armature copper loss, P_{field_Cu} is the field copper loss, and $Rot\ loss$ is the rotational loss in W. I_a, I_f denotes the armature current and field current of the DC motor respectively. The back emf generated by the DC motor is denoted by E_b and V denotes the applied voltage across the armature of the DC motor.

R_a denotes the armature resistance of the DC motor which was measured to be 1.9 Ω using a multimeter. R_f denotes the field resistance of the DC motor which was measured to be 207 Ω.

These constant losses were further used in efficiency calculations of the PMSM as they also act as a load to the PMSM. The calculated losses are shown in Appendix A.

4.7.2 Validation

The 1.07 kW PMSM is designed in ANSYS Maxwell software and the drive system for PMSM is designed in ANSYS Simplorer software. The final results were attained by co-simulating the model designed in ANSYS Maxwell with ANSYS Simplorer. These results were compared with the experimental results for validating the performance of the PMSM.

Table 4.14: Comparison of experimental line current with simulation line current under full load condition

Sl No.	Speed (rpm)	Phase	Simulation current (A)	Experimental Current (A)	% difference (absolute)
1	2700	A	6.064	5.55	9.261
2		B	6.387	6.88	7.166
3		C	6.273	6.95	9.741
4	3000	A	5.936	5.11	16.164
5		B	6.053	6.28	3.615
6		C	6.146	6.35	3.213
7	3300	A	5.983	4.75	25.958
8		B	5.954	5.61	6.132
9		C	5.893	5.93	0.624

Table 4.14 compares line currents for phase A (I_a), phase B (I_b), and phase C (I_c) obtained experimentally with simulation results. The percentage difference between experimental and simulation results of line current for phase A at 2700 rpm

was found to be 9.26% while at the same speed for phase B and C were 7.17% and 9.74%, respectively. The minimum difference of 0.624% was seen for a speed of 3300 rpm in phase C. In other cases except for phase A, the percentage difference lies below 8%. A higher percentage difference in experimental and simulation line currents is seen in phase A. This may be due to low current measured in phase A as compared to the current measured in phase B and phase C. As the same equipment was used for measuring current in all three phases, this difference was may be because of improper functioning of Current Transformer (CT) used in the equipment for measurement of current in phase A. This conclusion is made from repeated recording of experimental data for same speed, and a similar type of result was obtained each time. Another possible reason for difference in measured current and simulation current for phase A may be because of unbalanced loading. This conclusion is drawn after comparing the currents of the three phases for different load levels and different speed. The current in phase A is lesser in each case as compared to the current in phase B and phase C.

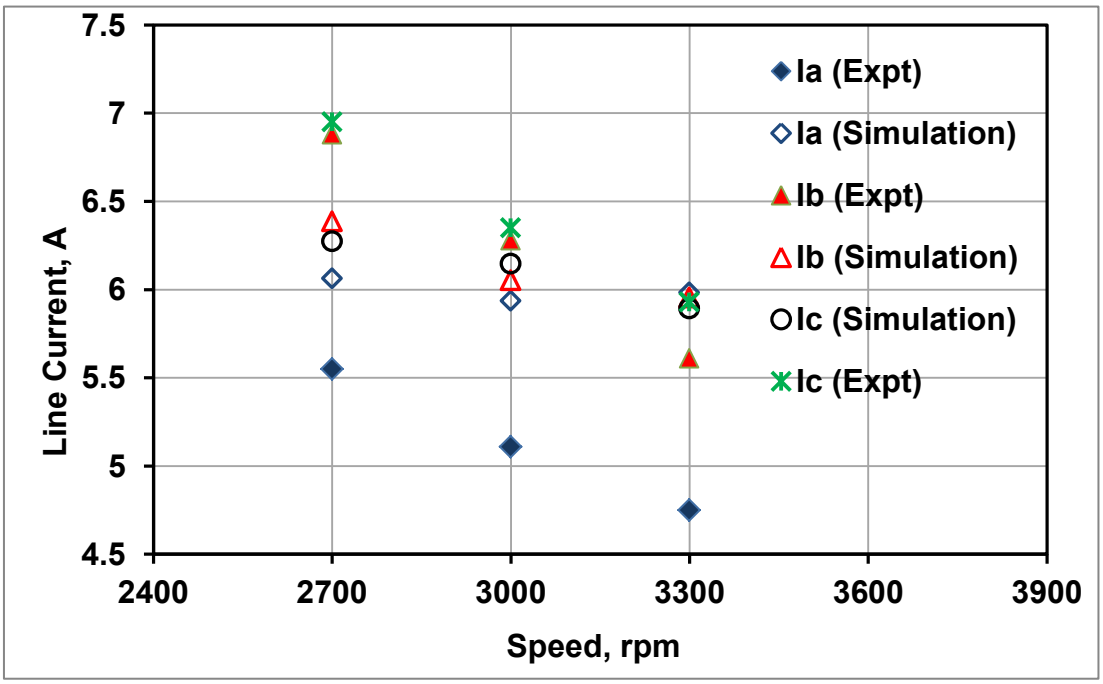

Fig. 4.46 Comparison of experimental and simulation line current at different speeds

The effect of speed on line current is shown in Fig. 4.46. Figure shows that both experimental and simulation line currents linearly decreases with speed. The

lowest current was seen in phase A both in experimental and simulation results. The line current in phase B and phase C were very close to each other both in experimental and simulation results.

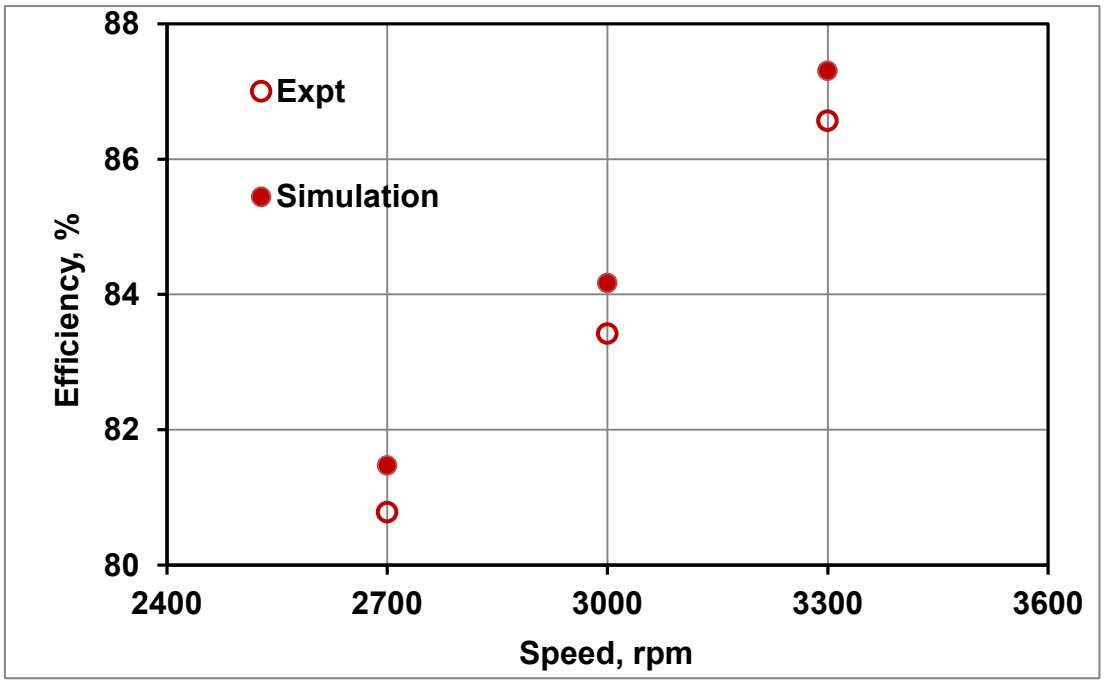

Fig. 4.47 Experimental and simulation efficiency of PMSM at different speeds

The efficiency of the PMSM was measured by experimental analysis and was compared with the efficiency results obtained in ANSYS Maxwell after simulation as shown in Fig. 4.47. The absolute percentage difference of experimentally calculated efficiency and simulation efficiency for 2700 rpm was 0.85 % whereas at 3000 rpm and 3300 rpm, the absolute percentage differences came out to be 0.89 % and 0.84 %, respectively. This shows the wide application of designed PMSM over a wide range of speed with efficiency much better than that of induction motor. This shows that PMSM can effectively be used in applications requiring higher efficiency over a wide range of speeds such as in electric vehicles, aircraft engine starter and even in cutters and grinders.

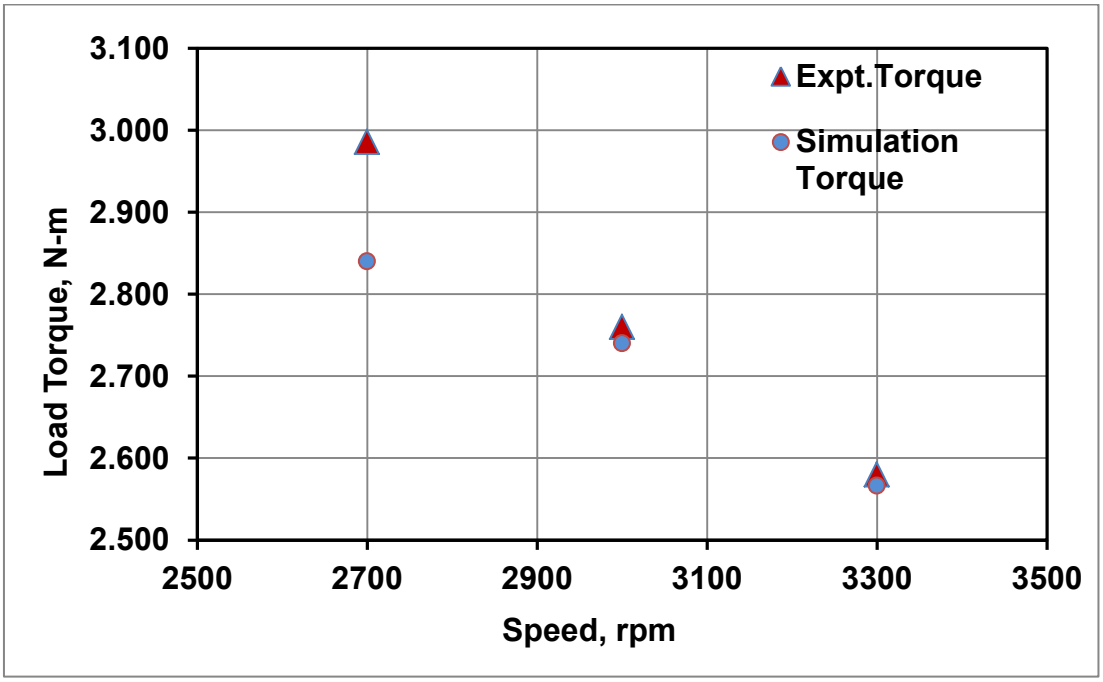

Fig. 4.48 Experimental and simulation load torque for different speeds under full load

The experimental and simulation load torque for different speeds under full load are compared in Fig. 4.48 which reveals that the difference between experimental and simulation load torques decreases as the speed increases. The maximum difference of 4.89% was observed at 2700 rpm while at other two speeds the percentage differences were less than 1%.

Chapter 5 SUMMARY AND CONCLUSION

A 1.07 kW permanent magnet synchronous motor having a rated speed of 4000 rpm was designed using ANSYS Maxwell software. Taguchi method and Response Surface Method (RSM) were used for optimal design of the motor in terms of efficiency and power factor. The magnet dimensions such as magnet width (w), magnet thickness (t) and magnet duct parameters *viz.,* diameter for magnet duct (D1), magnet duct dimension (O1) and width of the rib at the center of the two adjacent poles to support the bridge (Rib) were optimized. This ensures an optimum magnet size and position for placing the magnet inside the rotor so that high efficiency and power factor are attained. The optimized parameters were incorporated in the design, and optimal results in terms of efficiency and power factor were achieved. The results obtained from Taguchi, and RSM were compared with the simulation results. The results obtained from Taguchi and RSM were found to be reasonably accurate. Analysis of variance (ANOVA) was also performed to find out the effect of various design parameters and their interaction on the efficiency and power factor of the machine.

A drive system for studying the behavior of PMSM during transient as well as steady state is designed in ANSYS Simplorer. ANSYS Maxwell and ANSYS Simplorer were co-simulated to obtain the various simulation results. The study of line current, induced voltage, load torque, electromagnetic torque, and efficiency at different speeds was done.

The experimental analysis of 1.07 kW PMSM was done by loading the PMSM. The PMSM was run with the help of an FPGA controller. The PMSM mechanically coupled to a DC generator was loaded in steps and the corresponding line voltage, line current, input power requirement, and the power factor were recorded. The performance parameters such as efficiency and load torque at different loadings and speeds were calculated from the recorded data. A comparison between the experimental and simulated results was made and a good agreement was found between the results.

The results of the present study are concluded as follows:

1. A complete model was developed with the objective of examining the behavior of the PMSM using RMxprt tool of ANSYS Maxwell software, and the steady state results were used for optimization of different design parameters such as magnet width (w), magnet thickness (t), diameter for magnet duct (D1), magnet duct dimension (O1) and width of the rib at the center of the two adjacent poles to support the bridge (Rib).

2. In the present work, five factors, i.e., two magnet dimensions at 4 levels and three magnet duct position dimensions at 2 levels were used in Taguchi method and surface response method to optimize the magnet and rotor parameters. The optimum size were $w = 20$ mm, $t = 5.45$ mm, D_1 =64 mm, , O_1 =23 mm and Rib=0.5 mm.

3. The results of analysis of variance (ANOVA) show that Rib dimension has the highest effect on power factor, followed by O1, D1, w and t in descending order. Similarly, magnet thickness is having the highest effect on efficiency, followed by Rib dimension, O1, D1 and width of the magnet in descending order. A significant interaction between different dimensions was also seen in ANOVA results.

4. It can be concluded that magnet and its positional dimensions play an important role in improving the efficiency and power factor of the motor. An efficiency of 91.27% and a power factor of 0.75 were achieved after simulation of 1.07 kW PMSM having a rated speed of 4000 rpm.

5. The proposed methodology made use of efficient computational resource, i.e., RMxprt tool of the ANSYS Maxwell software for obtaining the real time solutions. Designing the machine in RMxprt saves a lot of simulation time as compared to other tools. The model designed in RMxprt can be easily converted to 2D model in ANSYS.

6. The drive system for the PMSM can be designed in ANSYS Simplorer which helps in obtaining the real time results and performance study of the motor designed by co-simulating the PMSM modeled in ANSYS Maxwell.

7. The performance of 1.07 kW PMSM in terms of line current, load torque, and efficiency has been verified with the experimental results obtained and they were found to be in a good agreement.

FUTURE SCOPE OF STUDIES

The design and optimization procedure used in the present study can be further extended to design PMSM having more power capacity for applications such as in hybrid electric vehicles. The optimization process can further be extended to design other electrical machines available in ANSYS. Various control techniques can be included in the design and a comparative analysis of the techniques can be done using ANSYS Simplorer. Fault analysis of the PMSM using Artificial Neural Network (ANN) can also be done in future works. Torque pulsation minimization is another field of work in PMSM which can be included in future studies.

LITERATURE CITED

Aliabad A. D., M. Mirsalim, and N. F. Ershad (2010). "Line-Start Permanent-Magnet Motors: Significant Improvements in Starting Torque, Synchronization, and Steady-State Performance," IEEE Transactions on Magnetics, Vol. 46, No. 12, Page 4066-4072.

Araujo R. E., A. V. Leite, and D. S. Freitas (1997), "The Vector Control Signal Processing blockset for use with Matlab and Simulink," 1997

Box, G. E. P. and Wilson, K.B. (1951). On the Experimental Attainment of Optimum Conditions (with discussion). *Journal of the Royal Statistical Society* Series B 13(1):Pages 1–45.

Cavagnino A., M. Lazzari, F. Profumo, and A. Tenconi, (2002), A Comparison between the Axial Flux and the Radial Flux Structures for PM Synchronous Motors," IEEE Transaction on Industrial Applications, Vol. 38, No. 6, Page 1517-1524.

Chabchoub Mourad, Ibrahim Ben Salah, Guillaume Krebs, Rafik Neji and Claude Marchand (2012), PMSM Cogging Torque Reduction: Comparison between different shapes of magnet , 2012 First International Conference on Renewable Energies and Vehicular Technology (REVET), 26-28 March 2012, Hammamet, Tunisia,Page 206-211, **DOI:** 10.1109/REVET.2012.6195272

Chaudhari B.N., B.G. Fernandes and S.K.Pillai (1998), A New Hybrid Rotor Geometry for Permanent Magnet Synchronous Motor, 1998 International Conference on Power Electronic Drives and Energy Systems for Industrial Growth, Proceedings, 1-3 Dec, 1998, Perth, WA, Australia , Vol 1, Page 260-263

Chaudhari, B. N.Fernandes, B. G. (1999), Synchronous motor using ferrite magnets for general purpose energy efficient drive, TENCON 99.

Chikouche Brahim L., Kamel Boughrara, R. Ibtiouen (2015), Cogging Torque Minimization of Surface-Mounted Permanent Magnet Synchronous Machines

Using Hybrid Magnet Shapes, Progress In Electromagnetics Research, Vol B 62, No. 1, Page 49-61, DOI: 10.2528/PIERB14112302

Cvetkovski Goga and Lidija Petkovska (2008), Efficiency Maximisation in Structural Design Optimisation of Permanent Magnet Synchronous Motor, Proceedings of the 2008 International Conference on Electrical Machines, 6-9 Sept. 2008, Vilamoura, Portugal, Paper ID 891, **Page 1-6, DOI:** 10.1109/ICELMACH.2008.4799866

Demir Uğur, Mustafa Caner Aküner (2017), Using taguchi method in defining critical rotor pole data of lspmsm considering the power factor and efficiency, tehnički vjesnik 24, 2(2017), 347-353 doi: 10.17559/tv-20140714225453

Dinh Bui Minh (2017), Optimal Rotor Design of Line Start Permanent Magnet Synchronous Motor by Genetic Algorithm, Advances in Science, Technology and Engineering Systems Journal, Volume 2, Issue 3, Page No 1181-1187, DOI: 10.25046/aj0203149

Duan Yao and Dan M. Ionel (2011), A review of recent developments in electrical machine design optimization methods with a permanent magnet synchronous motor benchmark study Energy Conversion Congress and Exposition (ECCE), 2011 IEEE, 17-22 Sept. 2011, Phoenix, AZ, USA, **DOI:** 10.1109/ECCE.2011.6064270

Duan Yao and Dan M. Ionel (2013), A Review of Recent Developments in Electrical Machine Design Optimization Methods With a Permanent-Magnet Synchronous Motor Benchmark Study, IEEE Transactions on Industry Applications, Volume: 49, Issue: 3, May-June 2013, **Page** 1268 – 1275. **DOI:** 10.1109/TIA.2013.2252597

Duan Yao and Dan M. Ionel. (2013), A Review of Recent Developments in Electrical Machine Design Optimization Methods With a Permanent-Magnet Synchronous Motor Benchmark Study, IEEE Transactions on Industry Applications , Volume: 49, Issue: 3, **Page(s):** 1268 – 1275. **DOI:** 10.1109/TIA.2013.2252597

Fang L., J. Jung, J. Hong, and J. Lee, (2008), "Study on High-Efficiency Performance in Interior Permanent-Magnet Synchronous Motor With Double-Layer PM Design," IEEE Trans. Magn., vol. 44, no. 11, Pages 4393–4396.

Fei W., P. Luk, J. Ma, J. X. Shen, and G. Yang, (2009), "A High-Performance Line-Start Permanent Magnet Synchronous Motor Amended From a Small Industrial Three-Phase Induction Motor," IEEE Transactions on Magnetics, Vol. 45, No. 10, Pages 4724 – 4727.

Fujishima Y., S. Wakao, A. Yamashita, and T. Katsuta (2002), Design optimization of a permanent magnet synchronous motor by the response surface methodology , Journal of Applied Physics 91, Page 8305 ; https://doi.org/10.1063/1.1456045

Hong D. , B. Woo, D. Koo, and D. Kang (2008), "Optimum Design of Transverse Flux Linear Motor for Weight Reduction and Improvement Thrust Force Using Response Surface Methodology," IEEE Trans.Magn., vol. 44, no. 11, pp. 4317–20, Nov. 2008.

Hong Guo, Xu Jinquan, Kuang Xiaolin (2015), "A novel fault tolerant permanent magnet synchronous motor with improved optimal torque control for aerospace application", Chinese Journal of Aeronautics Volume 28, Issue 2, April 2015, Pages 535-544. **DOI:** https://doi.org/10.1016/j.cja.2015.01.008

Hung P.W, S.H Mao, M.C Tsai (2008), "Investigation of Line Start Permanent Magnet Synchronous Motors with Interior-Magnet Rotors and Surface-Magnet Rotors." International Conference on Electrical Machines and Systems, February 2008

Ilya Petrov and Juha Pyrhönen (2013) Performance of Low-Cost Permanent Magnet Material in PM Synchronous Machines IEEE Transactions on Industrial Electronics, Vol. 60, No. 6,

Isfahani A.H., S.V. Zadeh, M.A. Rahman (2011) Evaluation of Synchronization Capability in Line Start Permanent Magnet Synchronous Motor. IEEE International Electric Machines & Drives Conference.

Jacobs Sigrid, Dietrich Hectors, Francois Henrotte, Martin Hafner, Mercedes Herranz Gracia, Kay Hameyer, Patrick Goes (2009), Magnetic material optimization for hybrid vehicle PMSM drives, World Electric Vehicle Journal Vol. 3 page 875-883.

Jolly L., M. Jabbar, and L. Q. (2005), "Design Optimization of Permanent Magnet Motors Using Response Surface Methodology and Genetic Algorithms," IEEE Trans. Magn., vol. 41, no. 10, pp. 3928–30, oct. 2005.

Jolly L., M. Jabbar, and L. Qinghua (2006), "Optimization of the Constant Power Speed Range of a Saturated Permanent-Magnet Synchronous Motor," IEEE Trans. Ind. Appl., vol. 42, no. 4, pp. 1024–30, July-Aug. 2006.

Kalluf F, C Pompermaier, M Ferreira, N Sodowski (2010), "Braking torque analysis of the single phase line-start permanent magnet synchronous motor", 2010 International conference on electrical machines, September 2010

Kim Mi-Jung, Ik-Sang Jang, Ki-Doek Lee, Jae-Jun Lee, Won-Ho Kim, Ju Lee (2012), Torque Density Elevation of Interior PM Synchronous Motor with Minimized Magnet Volume, 2012 IEEE Vehicle Power and Propulsion Conference, 9-12 Oct. 2012, Seoul, South Korea, Page 51-55, DOI: 10.1109/VPPC.2012.6422573

Knight A. M., and C. I. McClay, "The Design of High-Efficiency Line-Start Motors (2000)," IEEE Transactions on Industry Applications, Vol. 36, No.36, 1555-1562, November-December 2000.

Lee Kab-jae and KiChan Kim, Sol Kim, Joon-Seon Ahn, SeongYeop Lim, and Ju Lee (2005), Optimal magnet shape to improve torque characteristics of interior permanent magnet synchronous motor, Journal of Applied Physics, Vol **97**, 10Q505 (2005); https://doi.org/10.1063/1.1852411

Lee Liangfang, B. H. Lee, J. J.Kim, H. J.Jungpyohong (2009), Study on high-efficiency characteristics of interior permanent magnet synchronous motor with different magnet material, Electrical Machines and Systems (2009), ICEMS 2009.

Li J, J Song, Y Cho (2010), "High Performance Line Start Permanent Magnet Synchronous Motor for Pumping System", 2010 IEEE International Symposium on Industrial Electronics (ISIE), pp.1308-1313,4-7 July 2010

Luo D, B Cheng, S Huang, J Gao (2009), "Method for optimizing the air gap flux density of permanent magnet synchronous motor.", International Conference on Electrical Machines and Systems, November 2009

Lv Changzhi, Ting Gao, Guozhi Xin, Yuanyuan Zhou (2013), Three-phase AC Variable Frequency Speed Adjustment Controller Based on FPGA, Applied Mechanics and Materials, Vols. 260-261 Page: 532-536, doi:10.4028/www.scientific.net/AMM.260-261.532

Macbahi H., A. Ba-razzouk, J. Xu, A. Cheriti, and V. Rajagopalan 2000 "A unified method for modeling and simulation of three phase induction motor drives."

Mahmoudi A., N. A. Rahim, and W. P. Hew (2010), "Analytical Method for Determining Axial-Flux Permanent-Magnet Machine Sensitivity to Design Variables," International Review of Electrical Engineering (IREE), Vol. 5, No. 5, 2039-2048, September-October 2010.

Mahmoudi A., N. A. Rahim, and W. P. Hew (2011) "Axial-Flux Permanent-Magnet Machine Modeling, Design, Simulation, and Analysis," Scientific Research and Essay (SRE), Vol. 6, No. 12, 2525-2549, June 2011.

Mahmoudi A., N. A. Rahim, and W. P. Hew (2011), "An Analytical Complementary FEA Tool for Optimizing of Axial-Flux Permanent-Magnet Machines," International Journal of Applied Electromagnetics Machines (IJEAM), Vol. 37, No. 1, 19-34, September 2011.

Mahmoudi A., N. A. Rahim, and W. P. Hew (2012) "Axial-Flux Permanent-Magnet Motor Design for Electric Vehicle Direct Drive using Sizing Equation and Finite Element Analysis" Progress In Electromagnetics Research (PIER), Vol. 122, 467-496, 2012.

Manko Roman, Mykhaylo Zagirnyak, Mario Vukotiü, Martin Mavriþ, Selmaýoroviü, MihaŠrekl, Damijan Miljavec (2017), Design of Experiment in Optimization of Permanent Magnet Synchronous Motor Performance, 2017 International Conference on Modern Electrical and Energy Systems (MEES), 15-17 Nov. 2017 , Kremenchuk, Ukraine, **DOI:** 10.1109/MEES.2017.8248932

Martin Floran, Anouar Belahcen, Mohammed El Hadi Zaïm (2015), Electrical Machines and Systems (ICEMS), 18th International Conference on Electrical Machines and Systems (ICEMS) 25-28 Oct. 2015, Pattaya City, Thailand, Page 661-667, DOI: 10.1109/ICEMS.2015.7385117

Meeker D. (2005), "Finite Element Method Magnetics - FEMM", User's Manual, Ver. 4.0, Foster-Miller, MA, USA, 2005.

Montgomery, D.C. (2009), Design and analysis of experiments, 7th edn., John Wiley, New York.

Niu S., S. L. Ho, W. Fu (2015), Fast computation of torque-speed characteristics of induction machines 2015 IEEE International Magnetics Conference (INTERMAG) DOI:10.1109/INTMAG.2015.7156783

Ong C.M. (1998), Dynamic Simulation of Electric Machinery using Matlab/Simulink:Prentice Hall, 1998.

Park J., S. Kim, J. Hong, and J. Lee (2006), "Rotor Design on Torque Ripple Reduction for a Synchronous Reluctance Motor With Concentrated Winding Using Response Surface Methodology," IEEE Trans. Magn., vol. 42, no. 10, pp. 3479–81, oct. 2006.

Petkovska L., and G. Cvetkovski (2006), FEM Based Simulation of a Permanent Magnet Synchronous Motor Performance Characteristics, Power Electronics and Motion Control Conference, 2006. IPEMC 2006. CES/IEEE 5th International, 14-16 Aug. 2006 ,Shanghai, China, **DOI:** 10.1109/IPEMC.2006.4777986 Page 1-5.

Product Manual, Toshiba Infrastructure Systems & Solutions Corporation

Pyrhnen J, V Ruuskanen, J Nerg, J Puranen, H Jussila (2010), "Permanent-Magnet Length Effects in AC Machines", IEEE Transactions on Magnetics, Vol. 46, no. 10, October 2010

Richter, E. Neumann, T. (2014): Line start permanent magnet motors with different material, IEEE Trans. Magnetics 20, 1762–1764.

Sebastian T., G. Slemon, and M. Rahman (1986), "Modelling of permanent magnet synchronous motors," Magnetics, IEEE Transactions on, vol. 22, pp. 1069-1071, 1986.

Seker´ak Peter, Val´eria Hrabovcov´a, Juha Pyrh¨onen, Luk´aˇs Kalamen, Pavol Rafajdus, Mat´uˇs Onufer (2012), Ferrites and Different Winding Types in Permanent Magnet Synchronous Motor, Journal of Electrical Engineering, Vol. 63, No. 3, Page 162–170.

Sergeant P., and A. Van den Bossche, (2012), "Reducing the permanent magnet content in fractional-slot concentrated-windings permanent magnet synchronous machines," International Conference on Electrical Machines (ICEM), Marseille, France, 2-5 September, 2012, Page1403-1409, paper FF-001201.

Sergeant Peter and Alex Van den Bossche (2013), Influence of the amount of permanent magnet material in fractional-slot permanent magnet synchronous machines, IEEE Transactions on Industrial Electronics (Volume: 61, Issue: 9, Sept. 2014) Page(s): 4979 – 4989 DOI: 10.1109/TIE.2013.2258310

Si Jikai, Suzhen Zhao, Haichao Feng, Ruiwu Cao, and Yihua Hu (2018), Multi-Objective Optimization of Surface-Mounted and Interior Permanent Magnet Synchronous Motor Based on Taguchi Method and Response Surface Method, Chinese Journal of Electrical Engineering, Vol.4, No.1, Page:67-73

Singh B., B.P Singh, S Dwivedi (2006), "A State of art on Different Configurations of Permanent Magnet Brushless Machines.", Journal of IE , vol 87, pp.63-73. June 2006.

Sorgdrager Albert J. , Andre J. Grobler (2013) , Influence of Magnet Size and Rotor Topology on the Air-gap Flux Density of a Radial Flux PMSM, 2013 IEEE International Conference on Industrial Technology (ICIT), 25-28 Feb. 2013, Cape Town, South Africa, Page 337-343, DOI: 10.1109/ICIT.2013.6505695

Tarimer Ilhan (2009), "Investigation of the Effects of Rotor Pole Geometry and Permanent Magnet to Line Start Permanent Magnet Synchronous Motor's Efficiency", Muğla Turkey.

Todorov George and Bozhidar Stoev (2015), Analytical Model for Sizing the Magnets of Permanent Magnet Synchronous Machines, Journal of Electrical Engineering Vol.3, Page 134-141, DOI: 10.17265/2328-2223/2015.03.004

Wang Jing, Jianhua Wu, Qingguo Sun (2017), Field-circuit coupled design and analysis for permanent magnet synchronous motor system used in electric vehicles, Published in: 2017 20th International Conference on Electrical Machines and Systems (ICEMS), **DOI:** 10.1109/ICEMS.2017.8055981

Wang Lingling, Xin Wang, Yihui Zheng, Lixue Li, Wei Wang and Hao Wu (2015), Finite Element Analysis of Permanent Magnet Synchronous Motor of Electric Vehicle, International Conference on Advances in Energy and Environmental Science (ICAEES 2015), page 1127-1130.

Zhao C., S. Li, Y. Yang (2006) "Influence Factor Analysis of PMSM Air Gap Flux Density.", Proceedings of the Eighth International Conference on Electrical Machines and Systems. January 2006.

Zheng Ping, Jing Zhao,Jianqun Han, Jie Wang, Zhiyuan Yao, Ranran Liu (2007), Optimization of the Magnetic Pole Shape of a Permanent-Magnet Synchronous Motor ,IEEE Transactions on Magnetics Vol.43 No(6) Page:2531 – 2533, DOI: 10.1109/TMAG.2007.893631.

Appendix A

Measurements during no-load test of DC machine

Sl No	Speed (rpm)	V_f (V)	V_a (V)	I_f (A)	I_a (A)
1	2700	214	167.8	0.22	1.02
2	3000	210.3	180.7	0.22	1.12
3	3300	210.8	198.7	0.22	1.2

where V_f, V_a , I_f , and I_a are voltage across field winding of DC machine, voltage across armature winding of DC machine, field current, and armature current respectively.

No load losses

Sl No	Speed (rpm)	P_{cu_arm} (W)	$P_{cu\text{-}field}$ (W)	P_{rot} (W)
1	2700	1.976	10.018	181.175
2	3000	2.383	10.018	200
3	3300	2.736	10.018	235.704

where P_{cu_arm}, P_{cu_field}, and P_{rot} are the armature copper loss, field copper loss, and rotational loss of the DC machine.

Appendix B

Load torque and efficiency calculated for different loadings at different speeds.

Sl No	Speed (rpm)	Load (%)	Torque (N-m)	Efficiency (%)
1(a)	2700	25%	0.64	90.58
1(b)		50%	1.56	93.692
1(c)		75%	2.34	86.923
1(d)		100%	2.986	80.78
1(e)		110%	3.188	80.106
2(a)	3000	25%	0.67	84.96
2(b)		50%	1.34	90.07
2(c)		75%	2.17	88.62
2(d)		100%	2.76	83.42
2(e)		110%	3.013	82.26
3(a)	3300	25%	0.719	85.67
3(b)		50%	1.28	94.26
3(c)		75%	1.97	89.69
3(d)		100%	2.58	86.57
3(e)		110%	2.803	84.19

Appendix C

Experimental data measured at 2700 rpm

Sl No	Line to line voltage (V)			Line to line current (A)			Input Power			pf	V_L (V)	I_L (A)
	V_{ab}	V_{bc}	V_{ca}	I_a	I_b	I_c	P (kW)	Q (kVar)	S (kVa)			
1	108.6	110.0	108.0	1.22	1.54	1.56	0.20	0.18	0.27	0.75	161	0
2	118.0	120.7	114.6	2.70	3.39	3.42	0.46	0.45	0.65	0.72	159.5	1.55
3	127.7	130.8	122.0	4.17	5.19	5.26	0.75	0.77	1.07	0.70	157.5	2.9
4	135.3	138.6	128.3	5.55	6.88	6.95	1.03	1.09	1.51	0.69	153.5	4.05
5	136.9	140.0	129.9	5.86	7.21	7.31	1.11	1.18	1.62	0.69	153	4.4

"P" is the active power measured in kW, "Q" is the reactive power measured in kVar, and "S" is the apparent power measured in kVa. $V_{ab,}$ $V_{bc,}$ and V_{ca} are the three input line to line voltages of PMSM. $I_{a,}$ $I_{b,}$ and I_c the three input line currents of PMSM.

Appendix D

Experimentally measured data at 3000 rpm

Sl No	Line to line voltage (V)			Line to line current (A)			Input Power			pf	V_L (V)	I_L (A)
	V_{ab}	V_{bc}	V_{ca}	I_a	I_b	I_c	P (kW)	Q (kVar)	S (kVa)			
1	121.6	122.8	120.9	1.33	1.70	1.70	0.25	0.22	0.33	0.75	185	0
2	129.3	131.3	127.0	2.43	3.03	3.06	0.47	0.44	0.65	0.73	183.3	1.15
3	138.4	141.0	133.8	3.87	5.01	5.06	0.77	0.78	1.10	0.71	180.4	2.55
4	145.0	148.2	139.6	5.11	6.28	6.35	1.04	1.09	1.50	0.69	178.5	3.55
5	147.8	150.6	144.3	5.59	6.74	6.93	1.15	1.19	1.65	0.69	176.4	4

Appendix E

Experimentally measured data at 3300 rpm

Sl No	Line to line voltage (V)			Line to line current (A)			Input Power			pf	V_L (V)	I_L (A)
	V_{ab}	V_{bc}	V_{ca}	I_a	I_b	I_c	P (kW)	Q (kVar)	S (kVa)			
1	131.3	132.4	130.4	1.37	1.73	1.73	0.29	0.26	0.39	0.75	196.4	0
2	138.4	140.1	135.9	2.29	2.92	2.91	0.47	0.44	0.64	0.73	195.4	1
3	146.8	148.8	142.9	3.54	4.50	4.50	0.76	0.75	1.06	0.71	194.0	2.2
4	154.1	154.3	153.1	4.75	5.61	5.93	1.03	1.02	1.46	0.71	192.6	3.25
5	157.8	156.7	159.7	5.26	5.99	6.51	1.15	1.15	1.62	0.71	191.0	3.65

Appendix F

DC Generator parameters measured using multimeter,

Armature resistance, R_a= 1.9 Ω

Field resistance, R_f = 207 Ω

Stator resistance per phase of PMSM used in experimental analysis = 2.6 Ω

The stator windings are connected in star.

Appendix G

No load induced emf of DC generator at different speeds

Sl No	Speed (rpm)	Induced EMF (V)
1	1500	92.5
2	1800	111.0
3	1900	116.8
4	2000	122.3
5	2100	128.7
6	2200	135.0
7	2300	140.2
8	2400	146.0
9	2500	153.0
10	2600	159.2
11	2700	166.2
12	2800	172.0
13	2900	177.7
14	3000	184.8
15	3100	190
16	3200	196.8
17	3300	201.6
18	3400	207.8
19	3500	212.9

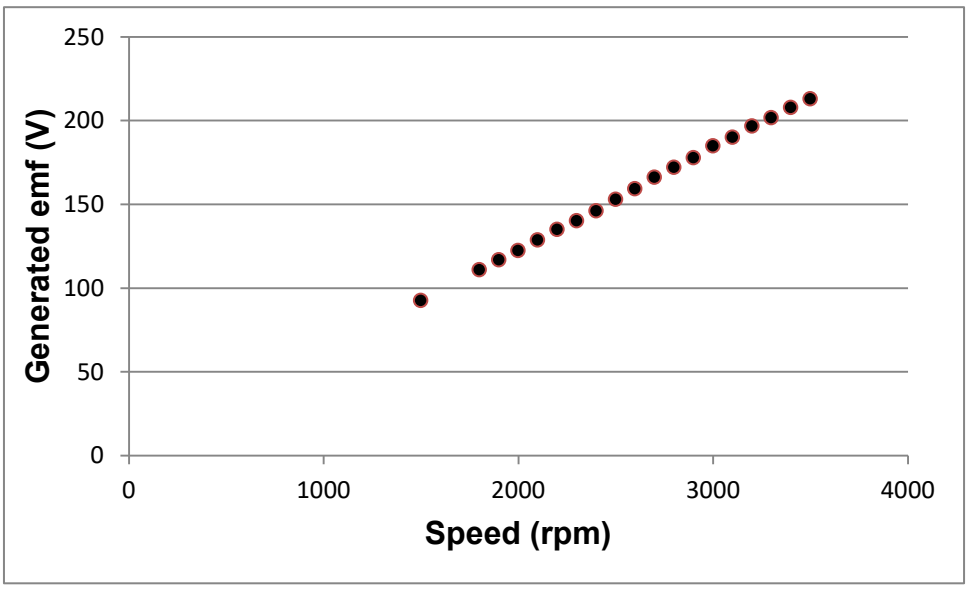

Fig. A DC generator generated emf vs speed

At around 2500 rpm, appropriate emf was generated for loading of DC generator upto 1.07 kW. So, the experiments were conducted for 2700 rpm, 3000 rpm, and 3300 rpm. However, the rated speed of PMSM coupled with DC generator was 4000 rpm, but the rated speed of DC generator was only 3000 rpm and it was not possible to conduct experiments at speeds much above than 3000 rpm. So, the experimental investigation was restricted to 3300 rpm.

Appendix H

At 3000 rpm, when the PMSM coupled with DC generator was run at no load. The input power to the PMSM measured was 250 W. This power is required to supply the no load losses of the PMSM which are stator copper losses, friction and windage losses. This power also supplies the no load losses of DC generator which include the armature copper loss, field copper loss, and rotational losses.

P_{in} = 250 W

$P_{dc\_losses} = P_{cu\_arm} + P_{Cu\_field} + P_{rot}$ = 212.4028 W

P_{stator_losses} = 17.78 W

$P_{fric+windage} = P_{in} - P_{dc\_losses} - P_{stator\_losses}$ = 19.84 W

Name of the student	: Deepayan Gope
ID No	: 50889
Semester and year of admission	: 2016
Degree	: M.Tech
Major	: Electrical Energy Systems
Minor	: Nil
Department	: Electrical Engineering
Advisor	: Dr. S.K Goel
Thesis Title	: DESIGN OPTIMIZATION AND PERFORMANCE SIMULATION OF PERMANENT MAGNET SYNCHRONOUS MOTOR

Abstract

A 1.07 kW permanent magnet synchronous machine having a rated speed of 4000 rpm is designed using ANSYS Maxwell software and magnet dimension and position parameters of the magnet inside the rotor are optimized for efficiency and power factor using Taguchi and surface response methods. ANOVA was conducted to analyze the effect and interaction of various parameters. A drive system for studying the behavior of PMSM during transient as well as steady state is designed in ANSYS Simplorer. ANSYS Maxwell and ANSYS Simplorer were co-simulated to obtain the various results and their variation with time. The study of line current, induced voltage, load torque, electromagnetic torque and efficiency at different speeds is done.

The experiments are conducted in 1.07 kW PMSM at different loading and speed. The PMSM is run with the help of a FPGA controller. The PMSM is coupled to a DC generator which is loaded in steps and the corresponding line voltage, line current and power requirements and the power factor were recorded. The performance parameters such as efficiency and load torque at different loadings and speed are calculated from the recorded data. A comparison between the experimental and simulated results is made and a good agreement is seen between the results. A higher efficiency and power factor have been obtained with the optimized magnet dimension and positional parameters as compared to experimental efficiency of 91.27% and a power factor of 0.75 of 1.07 kW PMSM.

(S. K. Goel)
Professor & Advisor

Deepayan Gope.
(Deepayan Gope)
Author

विषय सार

छात्र का नाम	: दीपायन गोप
आईडी संख्या	: 50889
सेमेस्टर और प्रवेश का वर्ष	: 2016
डिग्री	: एम.टेक
मेजर	: इलेक्ट्रिकल एनर्जी सिस्टम्स
माइनर	: -
विभाग	: इलेक्ट्रिकल इंजीनियरिंग
सलाहकार	: डॉ. एस के गोयल

थीसिस शीर्षक: निष्पादन मैग्नेट सिंकोनस मोटर का डिज़ाइन ऑप्टिमाइज़ेशन और सिमुलेशन प्रदर्शन

विषय सार

एक 1.07 किलोवाट स्थायी चुंबक सिंक्रोनस मशीन जिसमें 4000 आरपीएम की रेटेड गति है, ANSYS मैक्सवेल सॉफ़्टवेयर और चुंबक आयाम का उपयोग करके डिज़ाइन किया गया है और रोटर के अंदर चुंबक के स्थिति पैरामीटर को टैगुची और सतह प्रतिक्रिया विधियों का उपयोग करके दक्षता और पावर फैक्टर के लिए अनुकूलित किया गया है। एनोवा को विभिन्न मानकों के प्रभाव और परस्पर प्रभाव का विश्लेषण करने के लिए आयोजित किया गया था। क्षणिक और स्थिर स्थिति के दौरान पीएमएसएम के व्यवहार का अध्ययन करने के लिए एक ड्राइव सिस्टम ANSYS Simplorer में डिज़ाइन किया गया है। ANSYS मैक्सवेल और ANSYS Simplorer को विभिन्न परिणामों और समय के साथ उनकी विविधता प्राप्त करने के लिए सह-अनुकरण किया गया था। लाइन विद्युत, प्रेरित वोल्टेज, भार टोक़, विद्युत चुम्बकीय टोक़ और विभिन्न गति पर दक्षता का अध्ययन किया गया है।

विभिन्न लोडिंग और गति पर 1.07 किलोवाट पीएमएसएम में प्रयोग किए गए थे। पीएमएसएम एक एफपीजीए नियंत्रक की मदद से चलाया गया है। पीएमएसएम डीसी जनरेटर के साथ जोड़ा गया था। रेखा वोल्टेज, विधुत धारा, बिजली की आवश्यकताओं और बिजली कारक मापा गया था। विभिन्न लोडिंग और गति पर दक्षता और लोड टोक़ जैसे प्रदर्शन मानकों को मापा मानों से गणना की गई थी। प्रयोगात्मक और सिमुलेशन परिणामों के बीच तुलना की जाती है और परिणामों के बीच एक अच्छा समझौता देखा जाता है। 91.27% की प्रयोगात्मक दक्षता और 0.75 के पावर फैक्टर की तुलना में अनुकूलित चुंबक आयाम और स्थितित्मक मानकों के साथ उच्च दक्षता और पावर फैक्टर प्राप्त किया गया है।

एसगोयल

(एस के गोयल)
प्रोफेसर और सलाहकार

दीपायन गोप

(दीपायन गोप)
लेखक

VITA

The author of this manuscript, Deepayan Gope was born on 24th June 1993 at Baripada, Mayurbhanj, Odisha. He passed his High School from Campus School, Pantnagar, Udham Singh Nagar in 2009 from CBSE Board and Intermediate from Campus School, Pantnagar, Udham Singh Nagar in 2011 from CBSE Board. He completed his B.Tech. in Electrical Engineering from Veer Surendra Sai University of Technology, Burla, Odisha in 2015. He took admission in the College of Post Graduate Studies in G.B. Pant University of Agriculture and Technology, Pantnagar, Uttarakhand, in 2016 for the degree of Master of Technology with major in Electrical Energy Systems.

Address for Communication:

Deepayan Gope
Qr. No. VI/1919
TA- Colony, Pantnagar
Udham Singh Nagar, Uttarakhand- 263145
Mobile No. – 9411159916
Email – deepayangope@gmail.com